NANO · MICRO small
www.small-journal.com

MXene-Based Flexible Memory and Neuromorphic Devices

Yan Li, Guanglong Ding, Yongbiao Zhai, Ziyu Lv, Yan Yan, Shuangmei Xue, Kui Zhou, Meng Zhang, Yutong Zhang, Qi-Jun Sun, Yi Liu, Vellaisamy A. L. Roy, Ye Zhou,* and Su-Ting Han**

As the age of the Internet of Things (IoTs) unfolds, along with the rapid advancement of artificial intelligence (AI), traditional von Neumann-based computing systems encounter significant challenges in handling vast amounts of data storage and processing. Bioinspired neuromorphic computing strategies offer a promising solution, characterized by features of in-memory computing, massively parallel processing, and event-driven operations. Compared to traditional rigid silicon-based devices, flexible neuromorphic devices are lightweight, thin, and highly stretchable, garnering considerable attention. Among the materials utilized in these devices, transition metal carbides/nitrides (MXenes) are particularly noteworthy materials with their excellent flexibility, exceptional conductivity, and hydrophilicity, which confer remarkable properties upon these devices. Herein, a comprehensive discussion is provided on the applications of MXenes in flexible memory and neuromorphic devices. This review covers the basic principles and device structures of memory and neuromorphic devices, common parameters and emerging materials of flexible devices, as well as the common synthesis, functionalization methods, and distinct properties of MXenes. The remaining challenges and future opportunities of MXenes in relevant devices are also presented. This review can serve as a valuable reference and lay a cornerstone for the practical and feasible implementation of MXenes in flexible memory and neuromorphic technologies.

1. Introduction

The advancement of the IoTs, Big data, and AI technologies has raised great requirements for enormous data storage and energy-efficient information processing.[1] The rapid advancement of the information industry drives the exploration of novel intelligent architectures capable of low power consumption, high-density integration, and fast speed.[2] However, traditional von Neumann-based computing architecture faces challenges such as relatively low information processing efficiency alongside high power consumption because of the separation between memory and central processing units (CPUs),[3] a limitation named the von Neumann bottleneck.[4] Consequently, developing new-generation data storage and computing technology is becoming imperative and challenging.[5] In contrast to traditional computers, the human brain exhibits simultaneous information storage and processing capabilities while being significantly more energy-efficient by several orders of magnitude,[6]

Y. Li, Y. Zhou
Institute for Advanced Study
Shenzhen University
Shenzhen 518060, P. R. China
E-mail: yezhou@szu.edu.cn

G. Ding, Y. Yan, S. Xue, M. Zhang, Y. Zhou
State Key Laboratory of Radio Frequency Heterogeneous Integration
Shenzhen University
Shenzhen 518060, P. R. China
E-mail: dinggl@szu.edu.cn

G. Ding, Y. Zhai, Z. Lv, Y. Yan, S. Xue, M. Zhang
College of Electronics and Information Engineering
Shenzhen University
Shenzhen 518060, P. R. China

The ORCID identification number(s) for the author(s) of this article can be found under https://doi.org/10.1002/smll.202410914

DOI: 10.1002/smll.202410914

K. Zhou
The Construction Quality Supervision and Inspection Station of Zhuhai
Zhuhai 519000, P. R. China

Y. Zhang
Meta Platforms
Inc.
1 Meta Way, Menlo Park, CA 94025, USA

Q.-J. Sun
School of Physics and Optoelectric Engineering & Guangdong Provincial Key Laboratory of Sensing Physics and System Integration Applications
Guangdong University of Technology
Guangzhou 510006, P. R. China

Y. Liu
Department of Materials
Loughborough University
Loughborough LE11 3TU, UK

V. A. L. Roy
School of Science and Technology
School of Science and Technology
Hong Kong Metropolitan University
Ho Man Tin, Hong Kong SAR 999077, P. R. China

S.-T. Han
Department of Applied Biology and Chemical Technology
The Hong Kong Polytechnic University
Hung Hom, Hong Kong SAR 999077, P. R. China
E-mail: suting.han@polyu.edu.hk

thereby inspiring researchers to explore novel hardware architectures. Memory devices with high-density data storage capacities are a fundamental building block in electronics, particularly in the era beyond Moore's Law. Neuromorphic devices with excellent nonvolatile features can also offer programmable information recording via switching adjustable resistance when they are in response to external stimuli, thereby enabling applications in data storage and intelligent perception.[7]

With the developments of novel device concepts and manufacturing technologies, various memory and neuromorphic devices have been investigated, based on different architectural structures (two- and three-terminal devices).[8] In addition to low energy consumption, two-terminal devices (mainly memristors) offer advantages such as simple construction and high compatibility with complementary metal oxide semiconductors (CMOS) technology.[9] By contrast, three-terminal devices (mainly transistor-based devices) can perform programming and reading operations simultaneously, similar to the learning process in biological synapses, enabling significant potential for constructing advanced neuromorphic engineering and intelligent systems.[10] A wide range of functional materials have been explored for fabricating memory and neuromorphic devices. Critical parameters such as retention, endurance, and variability have been thoroughly investigated.[11] In terms of neuromorphic functions, various short/long-term plasticity (STP/LTP), including pair pulse facilitation/depression (PPF/PPD), long-term potentiation/depression, and spike-timing/spike-rate dependent plasticity (STDP/SRDP), have been implemented successfully.[12] Furthermore, advanced neuromorphic computing functions have also been achieved, including pattern classification and recognition,[13] in-memory logic,[14] and data preprocessing,[15] enabling their applications in the fields of robotics, machine vision, and autonomous systems.[16]

Flexible devices have garnered intense interest owing to their potential applications in modern electronics like health monitoring,[17] biomimetic systems, and implantable technologies.[18] High-performance flexible memory and neuromorphic devices are expected to be competitive in applications like intelligent wearable electronics and smart medical, due to their advantages of thin, lightweight, and conformability.[19] The mechanical flexibility of neuromorphic devices is also important in emulating synaptic functions because the real biological neurons and synapses are generally soft and exhibit adaptability to various mechanical deformations.[20] Conventional silicon materials are typically rigid, which limits the development of flexible devices. To achieve superior properties, it is imperative that every functional component of flexible devices, including substrates, electrodes, as well as intermediate/dielectric and semiconductor layers, should demonstrate remarkable mechanical flexibility. Therefore, the exploration of novel materials becomes indispensable.

Various materials have been utilized in multifunctional flexible electronic devices, such as semiconducting polymers and two-dimensional (2D) materials.[21] Typically, 2D materials provide rich platforms for advanced flexible memory and neuromorphic devices owing to their excellent flexibility, atomic-scale thickness, and distinctive physico-chemical properties.[22] MXenes, first discovered in 2011 and possessing 2D graphene-like structures,[23] offer unique advantages, including high hydrophilicity,[24] excellent conductivity,[25] favorable bio-compatibility, superior flexibility,[26] and good optical properties.[27] To date, MXenes have gained growing attention across multiple fields, including batteries,[28] supercapacitors,[29] sensors,[30] water purification,[31] electrocatalysis,[32] photocatalysts,[33] and electromagnetic interference shielding.[34] In recent years, 2D MXenes have garnered intense interest in high-performance memory devices and neuromorphic systems, endowing these devices with remarkable features like a large ON/OFF ratio and high recognition accuracy.[35] Moreover, the interest in their flexible applications stems from their superior electronic and mechanical properties, along with the hydrophilic surface with feature tunable functional groups, they are also suitably applied in flexible electronics.

Up to now, several reviews discussing the common synthesis, distinct properties, and diverse applications of MXenes have been published.[24,36] For instance, Ding et al. reviewed the common structural features and synthetic processes of MXenes, particularly highlighting their applications in memristors and their operational mechanisms.[36a] Lian et al. discussed the advances in MXene-based memristors for neuromorphic intelligence applications.[36d] However, these reviews have provided limited coverage of MXene-based flexible applications. This review is centered on the most recent reports of flexible memory and neuromorphic devices based on MXenes (**Figure 1**). It begins in Section 2 with some basic principles about flexible memory and neuromorphic devices, involving device structures, operation mechanisms, synaptic plasticity, parameters of flexible devices, and common flexible materials. In Section 3, the structures, synthesis methods, as well as properties of 2D MXenes are introduced. Section 4 provides recent developments in MXene-based flexible memory and neuromorphic devices. Finally, Section 5 summarizes the remaining challenges of MXenes in relevant devices and outlines their prospects.

2. Flexible Memory and Neuromorphic Devices

2.1. Device Structures and Mechanisms

2.1.1. Two-Terminal Devices

Two-terminal structure-based devices, primarily memristors, possess active layers sandwiched between two electrodes.[37] Memristor, also referred to as resistive switching random access memory (RRAM), is classified as one of the fundamental passive circuit components, alongside resistors, capacitors, and inductors.[38] They offer merits like low power consumption, simple structure,[39] and excellent miniaturization.[40] The structure of the memristor closely resembles that of a biological synapse,[41] where top electrodes (TEs) and bottom electrodes (BEs) can be likened to pre- and postsynaptic membranes respectively, while the active layer functions as synaptic cleft. Therefore, memristors are suitable for simulating the functions of biological synapses and biological neural networks (BNNs),[42] exhibiting significant potential to advance the semiconductor field and provide data storage for high-throughput computing.[43]

The underlying switching mechanisms of memory devices have been explored through filamentary- and interface-type mechanisms, which explain specific memristive behaviors based on given theoretical calculation and experimental analysis

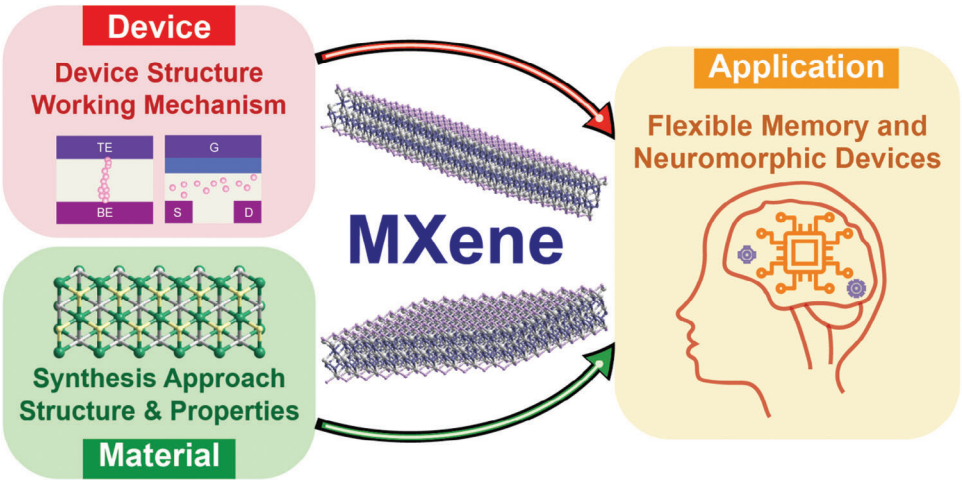

Figure 1. This review article focuses on MXenes-based flexible memory and neuromorphic devices, encompassing devices, materials, and recent advancements.

(**Figure 2a**).[44] The development and formation of conductive filaments (CFs) are often related to the type of electrodes and resistive switching (RS) materials used.[45] Electrochemical metallization (ECM) is a typical filamentary-type operation mechanism, involving the electrochemical redox processes of metal atoms in electrodes and RS layers. For ECM memristors, electrochemically active metals like Cu and Ag are commonly adopted as the TEs,[46] while inert metals like Pt and Au are used as the BEs.[47] In this process, active metal atoms undergo oxidation and are transformed into cations, which are driven toward the BE by an

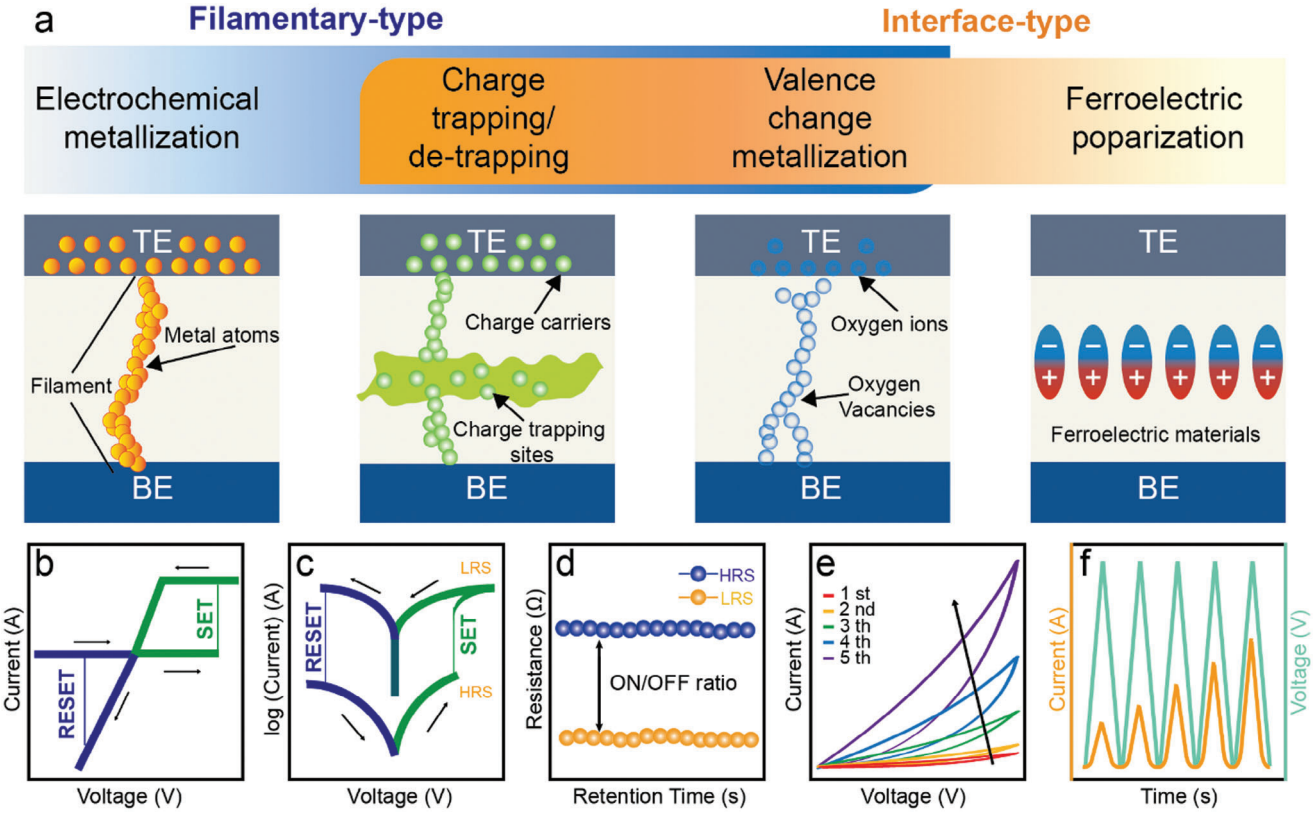

Figure 2. Structures, mechanisms, and electronic characteristics of memristors. a) Four typical operation mechanisms of memristors categorized into filamentary- and interface-type. b) Typical digital switching *I–V* curve of nonvolatile memristor illustrated on double-linear coordinates. c) Typical digital switching *I–V* curve of nonvolatile memristor replotted with current on a logarithmic scale. d) Retention characteristics of memristor. e) Analog switching *I–V* curves when scanned by five consecutive voltage cycles. f) Current and voltage data in the consecutive pulses as a function of time.

electric field. At the inert BE, these cations undergo reduction and are converted back into metal atoms. During the process, the reduced metal atom precipitates are produced to form CFs. When the CFs create connections between the TEs and BEs across the RS layers, the SET process occurs with the device's transit to the low-resistance state (LRS). In contrast, by applying reverse voltage bias, the RESET process occurs due to the decomposition of the CFs. The devices recover from the LRS to the high-resistance state (HRS). Since ECM memristors generally exhibit nonvolatile behaviors with good retention properties as well as a large ON/OFF ratio, they are ideal for data storage applications.

The mechanisms of charge trapping/de-trapping mechanism and valence change mechanism (VCM), primarily depending on the characteristics of the RS materials, can manifest as either filamentary- or interface-type. Bipolar switching behaviors attributed to the charge trapping/de-trapping process are often related to the abundant charge-trapping sites within the RS layers.[48] Taking the filamentary-type mechanism as an example, charge carriers will be transmitted from electrodes to charge-trapping sites by applying external voltage bias. When external electric field applied reaches a specific value, nearly all the charge-trapping sites are occupied by charge carriers which accumulate to eventually form a CF linking the TE and the BE, resulting in the switching from HRS to LRS. Oppositely, the charge carriers captured before will be released by applying reverse voltage bias, resulting in the decomposition of CF and the recovery from LRS to HRS. The charge-trapping phenomenon promotes slow change in resistance, facilitating the successful emulation of synaptic functions. Nanostructures of RS materials can provide additional adjustable charge-trapping sites, enhancing the device's performance. Up to now, various nanomaterials have been reported to charge trapping/de-trapping-based RS materials, including MXenes,[49] carbon nanotubes (CNTs),[50] and metal nanoparticles (NPs).[51]

VCMs are commonly found in the oxide- and perovskite-based memristors, involving the movements of oxygen or halogen vacancies.[52] The migration and redistribution of donor-type defects result in the change of valence, thereby resulting in the alteration of local conductivity of the active layers.[53] For example, in filamentary-type oxide-based memristor, oxygen ions can migrate to the anode under external voltage bias. The emergence of abundant oxygen vacancies in the active layers can form anoxic CFs, thereby decreasing the resistance to the LRS. Inversely, the reverse switching to HRS occurs when oxygen vacancies recombine under reverse voltage bias, leading to the breakdown of CFs and RESET behavior. Besides, for interface-type VCM, the RS behavior usually occurs at the interface, probably stemming from the modulation of Schottky barrier,[54] which can be influenced by varying the strength of external voltage bias or adjusting the initially formed CFs.[55]

Ferroelectric memristor represents another interface-type device based on the ferroelectric polarization properties of applied functional materials/structures including ferroelectric polymers,[56] ferroelectric tunnel junction (FTJ),[57] and metal-ferroelectric-metal.[58] Their conductance variations are driven by the switching of lattice noncentrosymmetry-induced polarization, which represents a purely electronic mechanism distinct from filament formation or rupture. With the characteristics of spontaneous, high controllable, and nonvolatile polarization,[59] ferroelectric devices not only exhibit advantages like nonvolatility, precise conductance control, high energy efficiency (<1 fJ bit^{-1}), and switching speeds (<600 ps),[60] but also overcome the limitations observed in filamentary-type devices regarding the number of conduction states and the uniformity of cycle-to-cycle/device-to-device performance.[61] Ferroelectric memristors have shown promising potential as analog, multibit memory components.[62] For example, a Hf_xZr_{1-x}-O_2-based FTJ memristor was fabricated achieving more than 16 distinguishable conductance states along with a mean cycle-to-cycle variation of less than 1.5%,[55] establishing the competitive potential of FTJs as memristive devices for multilevel storage applications.

Memristors are categorized into digital and analog types according to the mode of current change when applying external electric fields, and. the phenomenon of co-existing digital and analog RS behaviors can be observed in some memristors.[63] As depicted in Figure 2b, for digital-type memristors with gradually increasing voltage applied, the current across the RS layer abruptly changes when the applied voltage exceeds SET voltage (V_{SET}). Under reverse voltage sweeping, the current suddenly drops, which means the RESET process. A typical *I*–*V* curve is depicted in Figure 2c on a logarithmic scale, exhibiting two distinguished resistance states (LRS and HRS). Based on the resistance state retention capacity, memristors can be classified as nonvolatile and volatile. In a nonvolatile memristor, the resistance state can be retained after the external input is removed, and the duration time is called "retention time".[64] Figure 2d demonstrates the retention performances at a given read voltage. The nonvolatile behaviors are characterized by exceptional stability and imperceptible degradation of the ON/OFF ratio during a retention period, where the ON/OFF ratio is defined as the resistance between LRS and HRS. Another term, "endurance", refers to the ability to resist fatigue degradation, quantified as the maximum number of write/erase cycles performed before the memristor becomes unreliable. A higher number of testing cycles without significant degradation demonstrates better durability of the device.

On the contrary, in analog-type memristors, as depicted in Figure 2e, the measured current exhibits a gradual rather abrupt change during voltage sweeping. With an increasing number of pulses, the response current progressively rises (Figure 2f), indicating the conductance can be gradually modulated. This resistance variation process under different voltage pulse simulations resembles the alteration of synaptic weight (SW) observed in natural synapses,[65] which is advantageous for simulating artificial synapse functions and constructing neural networks capable of adaptive learning.[66]

Additionally, the current conduction mechanisms of the memristor, primarily depending on the electrodes, dielectric layer, and the properties of the interfaces formed, can be broadly divided into bulk-limited and injection-limited types.[67] Trap-limited space charge limited current (SCLC) and trap-assisted tunneling (TAT) are typical bulk-limited mechanisms observed in memristive devices, elucidating charge trapping/de-trapping phenomena as well as corresponding RS behaviors.[68] At low applied fields, the bulk contains a limited number of thermally generated mobile carriers, leading to ohmic conduction where the current density is proportional to the electric field.[69] As sufficient carriers are injected from the contact and

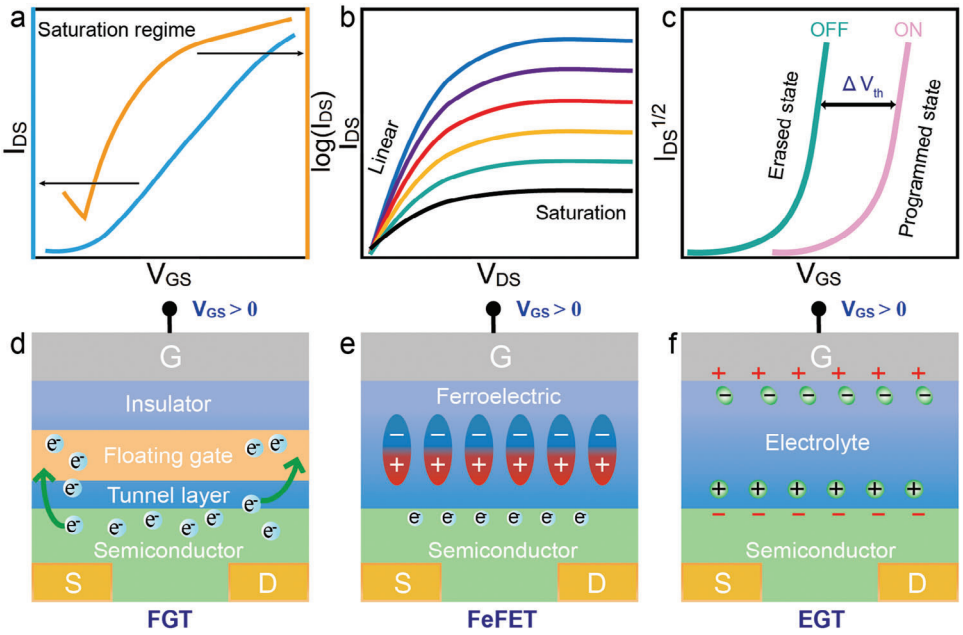

Figure 3. Structures, mechanisms, and electronic characteristics of transistors. a,b) The transfer (a) and output (b) curves of typical FETs. c) Scheme of device operation for transistor-based memory. d–f) Diagrams of three typical types of transistors under positive gate voltage bias: FGT (d), FeFET (e), and EGT (f).

accumulate within the bulk to form a space charge region, the material's conductivity diminishes, and the current is governed by the drift velocity of the accumulated carriers. This mode of conduction mechanism is referred to as SCLC.[70] TAT is a conduction process where electrons from the cathode are trapped and then tunnel through barriers, allowing carriers to tunnel through energy barriers that are too high for direct tunneling.[71] In contrast, Schottky emission is considered a type of injection-limited mechanism, where electrons are heated and then injected across a Schottky barrier into the conduction band (CB) of the insulating material, resulting in enhanced carrier transport and reduced impedance in the memristor.[72] Thus, the interplay between these mechanisms governs the overall electrical behavior and switching dynamics of the memristor. Multiple mechanisms can coexist within a single memristor, depending on the resistance state (whether it is filamentary or interface) as well as operating conditions and parameters.

2.1.2. Three-Terminal Devices

Despite the simplicity and ease of manufacturing, two-terminal devices encounter issues when integrated into crossbar arrays since inaccurate reading and programming can occur when current flows through unselected cells.[73] In contrast, three-terminal transistors independently modulate SW through the gate (G) terminals, eliminating the need for additional circuit components to select target cells.[74] This facilitates synchronous information transmission and learning processes. In addition, by exploiting functional expandability, three-terminal devices better emulate neural functions of brain and body synapses,[6] revealing potential applications in artificial neuromorphic systems. In a synaptic transistor, the G electrodes perform as presynaptic neurons while the semiconductor channels between the source (S) and drain (D) electrodes simulate postsynaptic neurons. When the external voltage is applied to the G electrode, it modulates the conductance of the channel. The variable channel conductance in transistors can be viewed as adjustable SWs in biological systems. Hence, three-terminal devices can be implemented to mimic more complex synaptic functions, which is an effective technology in the fabrication of bionic synapses for neuromorphic engineering. Additionally, three-terminal devices can provide more functional diversity such as multilevel storage,[75] nondestructive reading,[76] and array-level isolation.[77] According to the working mechanisms, three-terminal transistor-based devices can be broadly categorized into several types, including floating gate transistors (FGTs), ferroelectric field effect transistors (FeFETs), as well as electrolyte-gated transistors (EGTs).

FETs are active devices in which the channel materials' conductive capability can be modulated via the controlled electric field.[78] Specifically, charges that flow through the channel are controlled by gate-source voltage (V_{GS}).[79] As shown in **Figure 3a**, the transfer characteristic is described as channel current (I_{DS}) changed with the variation in V_{GS} at constant drain-source voltage (V_{DS}). Similarly, when V_{GS} is kept constant, the variation of I_{DS} with V_{DS} is known as the output characteristic. A typical output curve with distinguishing current saturation is shown in Figure 3b. In the saturation regime, when the V_{GS} exceeds the threshold voltage (V_{TH}), I_{DS} can be calculated based on the following equation:

$$I_{DS} = \frac{W}{2L}\mu C_i \left(V_{GS} - V_{TH}\right)^2 \quad (1)$$

where L and W denote the length and width of the channel, respectively; μ represents charge mobility; and C_i is the capacitance per unit area of the dielectric layer.

Structurally speaking, the FGTs, FeFETs, and EGTs are commonly developed based on typical FET structures. Compared to the typical FET, the FGT has an additional floating gate (FG) and tunneling layer for trapping charge carriers and blocking captured charges, respectively (Figure 3d).[80] The trapped charges can produce a built-in electric field, thereby modulating I_{DS}. Under the influence of V_{GS}, charges are captured and released from the FG layer, known as programming and erasing operations, leading to the programmed and erased states of I_{DS} (Figure 3c), which are also named "ON" and "OFF" states, respectively. The FGT is widely employed as a device structure for data storage and synaptic behavior emulation due to its ability to achieve multiple conductance states through modulation of FG materials and stimulation conditions (e.g., V_{GS}).[81] Moreover, FGTs have the advantage of high memory capacity and long-term retention. However, the use of FGTs in flexible neuromorphic computing systems faces limitations in achieving flexible compatibility and high-power consumption resulting from the requirement for a large operation voltage for charge injection.[82]

Except for two-terminal memristors, ferroelectric materials have also been employed for constructing FeFETs,[19] as shown in Figure 3e. The polarization state can be finely tuned by adjusting V_{GS}, which influences the carrier concentration through coulomb interaction with the channel layer and polarization in the ferroelectric layer.[83] Compared with FGTs, FeFETs exhibit simpler structures and are also suitable to be applied as nonvolatile memory and neuromorphic devices. Moreover, ferroelectric polymers exhibit exceptional flexibility and cost-effectiveness, making them highly promising candidates for developing flexible electronics.[84]

Both FGTs and FeFETs are commonly more likely to exhibit LTP than STP behaviors. In comparison, EGTs (Figure 3f) can exhibit both LTP and STP.[85] EGTs encompass electric-double-layer transistors (EDLTs) as well as electrochemical transistors (ECTs). In EDLTs, I_{DS} is modulated by V_{GS} via a capacitive field-effect mechanism at channel/electrolyte interface, using ions of electrolyte to induce conductance changes in the channel.[86] The creation of a sub-nanometer gap capacitor at the interface enables EDLTs to achieve significant capacitance (≈μF cm^{-2}) and operate at ultralow voltages,[87] thereby presenting a novel approach for fabricating energy-efficient artificial synapses.[88] The channel conductance of ECTs is effectively modulated by the electrochemical doping and restoration of ions in the electrolyte dielectric layer, resulting in low voltage and large capacitance. These characteristics, combined with their compatibility with aqueous environments, render ECTs, particularly organic ECTs (OECTs), highly suitable for bioelectronic applications such as neuromorphic devices.[87] Moreover, due to the ability to deposit and pattern electrolytes using solution-processing methods, EGTs offer flexible architectures and are compatible with flexible devices.[89]

2.1.3. Synaptic Plasticity

Building hardware-level neuromorphic computing systems based on artificial neural networks (ANNs) becomes a research hotspot,[90] demonstrating appealing prospects in executing AI algorithms for applications like image analysis with latency and energy efficiency unachievable by conventional computing.[91] At the biological level, BNNs are composed of ≈1011 neurons, massively interconnected by synapses for information processing. As shown in **Figure 4a**, a biological synapse is a connection between axon and dendrite,[92] facilitating signal transmission between neurons, which generates synaptic plasticity—an essential foundation for learning and memory. Similarly, ANNs enable self-learning between artificial neurons by connecting numerous processing units, as shown in Figure 4b. At the device level, the functions of axons, dendrites, somas, and synapses are emulated by various memristor- and transistor-based technologies.[93] The SWs, referring to the strength of connections between pre- and postsynapses, are depicted by the conductance values of these devices in ANNs. Consequently, ANNs are adaptive nonlinear information processing systems featuring self-organizing and real-time learning capabilities.[94]

Synaptic plasticity, indicating the variation of SW,[44a,95] is the important research content for synaptic devices.[96] In practice, to evaluate synaptic functionality, the postsynaptic current (PSC) is measured in response to stimulation. Figure 4c illustrates a typical excitatory PSC (EPSC) induced by a single pulse. Similarly, the stimulating pulse can induce an inhibitory PSC (i.e., IPSC).[97] Based on the duration of the SW changes after stimulations, synaptic plasticity is classified into STP and LTP,[98] which range from milliseconds to hours, or even days. For two consecutive pulses, the synaptic devices exhibit an increased response to the latter pulse compared to the previous one, resulting in PPF behavior (Figure 4d), which serves as a fundamental mechanism for temporal information processing between artificial neurons.[99] Inversely, the PPD refers to a gradual attenuation of subsequent synaptic responses. PPF/PPD index is the evaluation of the STP behavior in relation to the time interval (Δt) between successive pulses.[100] For instance, as depicted in Figure 4e, a gradual decrease in the PPF index is observed with increasing Δt, where a higher PPF index signifies enhanced tunability of the EPSC by voltage pulses. Through appropriate training protocols involving variations in stimulus repetition number, amplitude, frequency, and duration, STP can be transformed into LTP. Conversely, Figure 4f illustrates long-term potentiation/depression phenomena induced by successive positive/negative voltage pulses resulting in an increase/decrease in SW. These mechanisms underlie fundamental biological processes associated with memory formation and learning activities wherein SW can either strengthen or weaken over time.[9b]

Hebbain learning rule, with STDP and SRDP as paradigms,[101] is important for high-level learning and memory processes, which have been adopted in ANNs to effectively address complex scenarios with enhanced learning efficiency.[102] STDP represents the dependence of change in SW (Δw) on the spike order and Δt between pre- and postsynaptic spikes.[35b,103] As described in Figure 4g, four distinct forms of STDP behaviors arise from varying Δw.[104] By comparison, SRDP relies on the firing rate of presynapse for the weight update.[105] Commonly, high-frequency (> 20 Hz) pulses to the presynapse lead to long-term potentiation, while low-frequency (<5 Hz) pulses lead to long-term depression.[104]

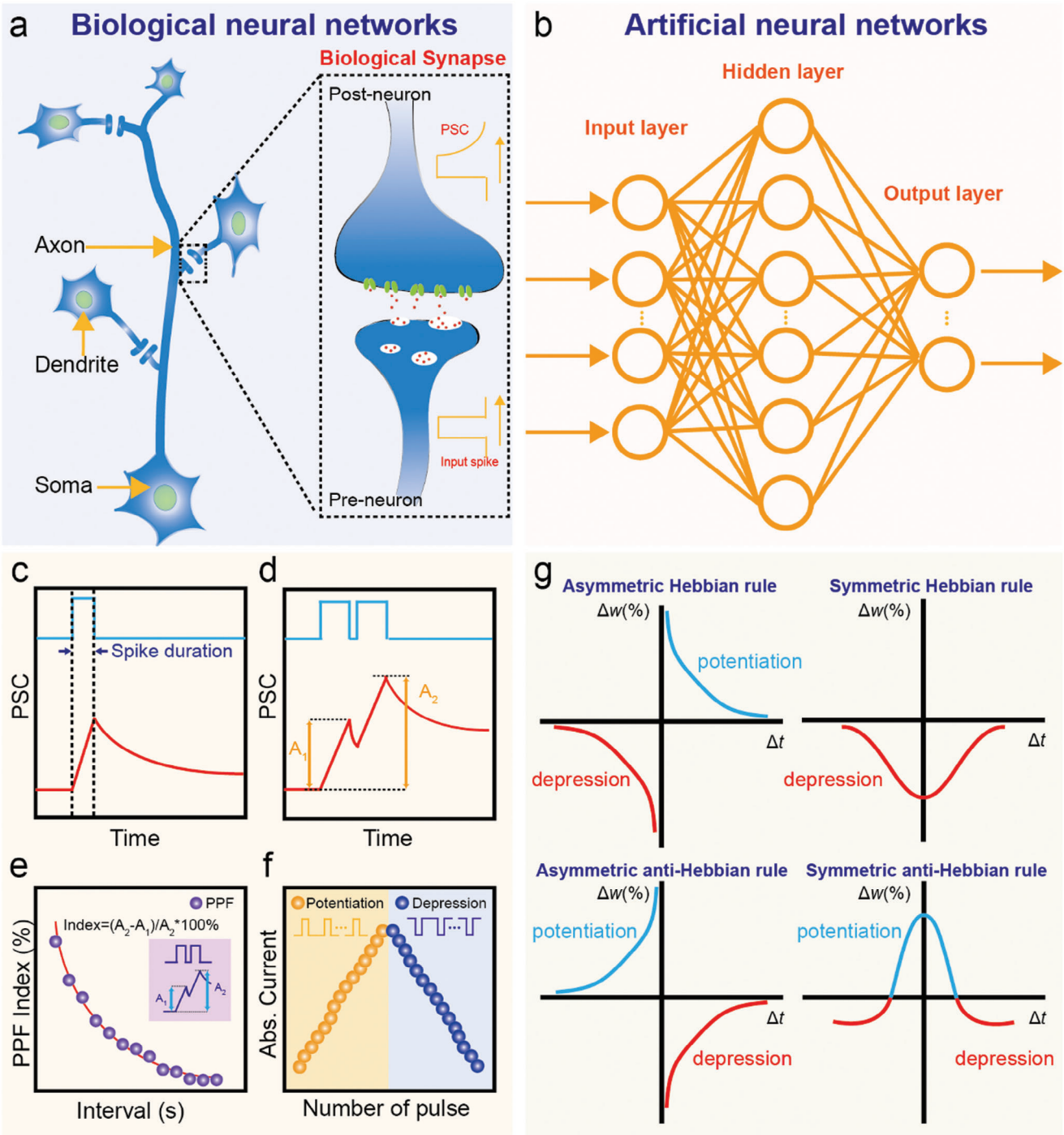

Figure 4. Schematic diagrams of BNNs and ANNs, and the simulations for typical synaptic behaviors. a) Schematic of BNNs (inset: a biological synapse composed of pre- and postsynaptic structures). b) Basic structure of basic ANNs comprising input, hidden, and output layers. c–g) The typical curves obtained by mimicking various synaptic behaviors based on neuromorphic devices: EPSC (c); PPF (d); PPF index (e); long-term potentiation/depression (f); and four types of STDP related to asymmetric/symmetric Hebbian/anti-Hebbian rule (g).

2.2. Flexible Devices

Flexible devices, characterized by their lightweight, thin, and stretchable properties, have garnered considerable interest in both research and industry.[106] To address the limitations of traditional rigid devices, particularly in terms of mechanical deformability, substantial efforts have been dedicated in recent years. For example, by applying free-standing architecture (**Figure 5**a), Jang et al. reported an ultrathin organic flexible synaptic device that demonstrated reliable synaptic functions under folded

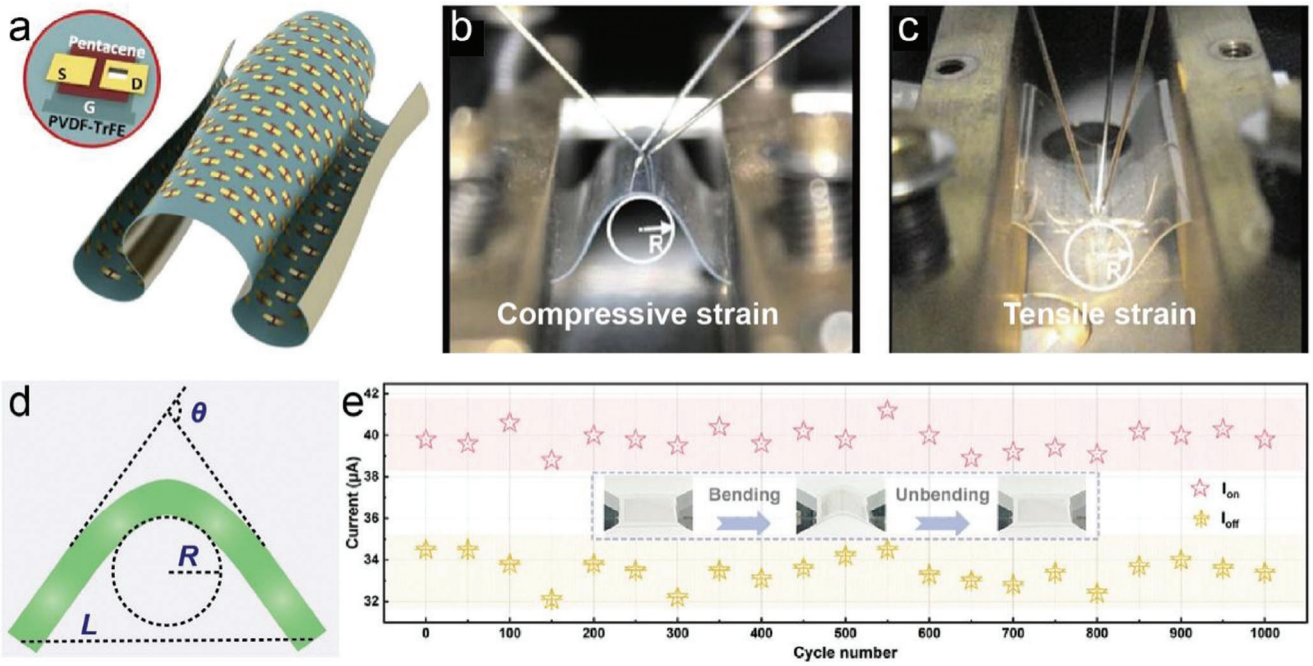

Figure 5. Illustrations and parameters of flexible devices. a) Images of flexible artificial synapse containing an illustration of the device structure. Reproduced with permission.[107] Copyright 2019, American Chemical Society. b,c) Illustrations of flexible devices bent in convex (b) and concave (c) directions. Reproduced with permission.[108] Copyright 2009, AIP Publishing. d) Three parameters describing the bending state (bending angle (θ), bending radius (R), and end-to-end distance (L)). e) Mechanical endurance of the device evaluated by testing ON/OFF current (I_{on}/I_{off}) over 1000 bending cycle tests. Reproduced with permission.[109] Copyright 2023, Wiley-VCH.

conditions for more than 6000 spikes, demonstrating its potential applications in wearable intelligent electronics.[107] The performance of these flexible devices is closely connected with the materials used and is typically evaluated based on common parameters such as bending radius and bending cycle. This section briefly discusses key characterization parameters and commonly used materials for flexible applications.

2.2.1. Key Parameters

In the context of flexible electronics, ensuring reliable data collection poses a significant challenge as it necessitates optimal performance even during processes involving bending, folding, compression, or stretching.[110] In practice, it is evaluated by testing and recording bending deformations under tensile/compressive strain in convex/concave directions, as indicated by Figure 5b,c.[107]

Generally, bending states are described by three parameters: bending angle (θ), bending radius (R), and end-to-end distance (L) (Figure 5d). Individual L can be controlled by fixing one side of the translation table and moving the other, providing a rough assessment of the bending process. In most cases, for devices in convex/concave directions, R and θ (0–180°) are applied to characterize the flexibility of the device. Smaller R indicates better flexibility as it correlates with the tensile/compressive strain of flexible devices, in addition to the device's intrinsic thickness (D) and Young's modulus of the device.[111]

Commonly, the bending cycle test under a certain R is applied to evaluate the reliability of the device's flexibility, known as durability. As shown in the durability illustration in Figure 5e, no obvious differences in current after applying multiple bending cycles are observed, thus demonstrating excellent flexibility and mechanical stability.[109] The evaluation of flexibility necessitates the consideration of stretchability as a crucial parameter. Stretchable devices must maintain their electrical performance even when subjected to mechanical elongation deformation ($\Delta L/L_0$), where L_0 and ΔL represent the initial and stretchable lengths of the device, respectively.[112]

Other parameters such as bio-compatibility, chemical stability, and optical transmittance are also important for various applications, such as medicine. Exceptional bio-compatibility ensures the seamless integration of flexible electronics with soft body tissues and facilitates their spontaneous degradation, promoting applications in artificial e-skin, biomedical implants, and environmental monitoring.[113] Concerning chemical stability, noble metals such as Pt and Au with good chemical stability in various physiological environments, play a crucial part in neural interface electrodes for flexible implantable devices like medical robotics.[114] Flexible electronics with excellent optoelectronic properties especially high optical transmittance are of the essence for potential applications like human augmentation and health monitoring.[115] With the emerging proliferation of e-skin, high transparency facilitates the reduction of the psychological discomfort of wearing flexible devices on the skin.[116]

2.2.2. Materials

Conventional materials used in memory and neuromorphic devices are typically thick and rigid, which makes them unsuitable for flexible electronics.[117] Therefore, the careful selection of materials for each component of high-performance flexible devices is crucial. In this section, the common flexible materials for each functional part of the flexible devices including substrates, electrodes, intermedia/dielectric layers, semiconductor layers, and related design/selection strategies are briefly discussed.

Substrates: The choice of substrates influences the mechanical responses of the devices.[118] In specific applications, such as soft robotics, it is imperative to investigate the vulnerability of substrate materials to physical damage, encompassing bending, twisting, and folding. Therefore, it holds great significance to carefully select flexible substrate materials with distinctive characteristics.[119] First, key requirements include excellent dimensional mechanical and chemical stability to support the device, as well as the consideration for potential strain-induced damage and cracking from thermal expansion. Second, excellent flexibility and functional consistency under different circumstances are needed for various wearable applications. Third, substrates should possess good surface uniformity so that the electrodes can be directly grown or deposited on their surface. Finally, considering the potential industrial application, issues like cost and machinability cannot be ignored.

Plastic films, metal foils, and fibrous materials belong to common flexible substrates. Among these, plastic films (e.g., organic polymer substrates) are prominent due to their low modulus, lightweight, cost-effective, chemical stability, ideal mechanical properties, relatively flat surface, and optical transparency.[120] Here, the common flexible polymer substrates, including polyethylene-2,6-naphthalate (PEN),[121] polyethylene terephthalate (PET),[122] polyimide (PI),[123] polydimethyl siloxane (PDMS),[124] and polyethersulfone (PES),[125] are discussed.

PEN and PET are low-cost plastic films with outstanding stability, excellent optical transmittance, and high flexibility in the out-of-plane direction, making them primary substrates of choice for building flexible devices. By comparison, PEN exhibits better insulation, stability, and hydrolysis resistance, but relatively high tensile and compressive stiffness limit its stretchability. PET offers advantages such as low cost and high transparency (>85%) but suffers from the issue of relatively low glass transition temperature (about 78 °C), hindering its high-temperature applications.[126] Conversely, PI can serve as a substrate for applications involving temperatures up to 300 °C due to its higher transition temperature.[127] By unique thermal polymerization and precursor coating preparation, PI flat films exhibit surface roughness around 1 nm, much less than that of PET and PEN. However, PI usually appears yellow with poor transmittance (60–70%), which limits its suitability for developing optical flexible devices. Besides, PDMS exhibits not only high flexibility and stretchability but also super-high transparency and biocompatibility, which is a promising substrate candidate for attachment to the skin or insertion into the body. Its remarkable durability against mechanical deformations promotes its wide application in the fields such as strain sensors.[128] However, the working temperature of PDMS is limited between −45 and 200 °C, which is also inappropriate for high-temperature fabrications and applications. PES exhibits significant resistance to acid or base environments and presents excellent optical transparency (> 90%).[119] However, the current overall manufacturing development is constrained by the exorbitant cost of PES.

In general, each flexible substrate materials present unique advantages, necessitating careful selections based on device preparation conditions and application requirements.

Electrodes: The mechanical characteristics of flexible devices are also significantly affected by electrodes.[129] To achieve high-performance and diversified applications, several requirements for flexible electrodes such as high flexibility, superior conductivity, desirable bio-compatibility, and suitable work function need to be underlined.[118,130] Indium tin oxide (ITO) films have been extensively employed as electrodes because of their optical transparency and electrical conductivity.[131] But with mechanical characteristics of stiff and brittle,[132] ITO films could easily rupture under small stretching strains.[133] To overcome this disadvantage, researchers have investigated an array of flexible alternative electrode materials including metals, conductive polymers, and nanomaterials.[134]

Metal electrodes like Au and Al are widely utilized in previous studies on flexible electronics owing to their excellent conductivity, mature preparation technologies, and stability.[135] Although metals are not intrinsically flexible in bulk form,[136] approaches like constructing conductive networks based on metal nanomaterials have been studied. Simultaneously, special structural design (e.g., ultrathin form,[137] three-dimensional (3D) structure,[138] oxide/metal/oxide structure)[138] can largely enhance their flexibility, promoting wide applications. However, their applications as flexible electrodes also face challenges such as diffusions of metal atoms, easy oxidation in the air, and thickness limitation due to the Ostwald ripening effect.[139]

Conductive polymer is another kind of flexible electrode with excellent flexibility and processability.[140] Among polymer electrodes, poly(3,4-ethylenedioxythiophene): polystyrene sulfonate (PEDOT: PSS) has been extensively employed because of their outstanding film uniformity, attractive bio-compatibility, and easy fabrication techniques (e.g., inject printing).[141] Since pure PEDOT: PSS faces the challenges of inherent brittleness, low conductivity, and easy degradation under ambient conditions, it's not suitable for flexible applications.[142] Incorporating ionic liquids (e.g., 1-ethyl-3-methylimidazolium tetracyanoborate) can help soften polymer chains as well as enhance electrical conductivity.[143]

Moreover, nanomaterials such as silver nanowires (Ag NWs) and CNTs possess low contact resistance, high mechanical flexibility, and easy fabrication, promoting their applications in flexible electrodes.[144] Ag NWs exhibit some distinctive characteristics including excellent light transmittance, high conductivity, and excellent mechanical deformability, which facilitates the commercialization of Ag NW inks/films, application expansion, and technological innovation.[145] However, fractures at wire–wire junctions can cause a significant increase in sheet resistance of Ag NWs under bending and stretching conditions. Recently, it's reported that electrodeposited hierarchical silver network electrodes consisting made from Ag NWs and Ag micromesh exhibit less degradation in sheet resistance during repeated bending, outperforming commercialized ITO.[146] CNTs, categorized as single- or multiwalled based on the number of

graphene sheets, generally offer superior mechanical robustness, excellent conductivity, and good thermal stability, with simple fabrication methods like drop-casting and spin-coating.[147] Nevertheless, the high Young's modulus from their strong internal C-C networks limits their use in stretchable electronics.[148]

Intermedia/Dielectric Layers: Intermedia and dielectric layers are crucial components of devices that simulate neurotransmitter conduction in synaptic cleft, as well as memory and learning functions.[73b] In memristors, intermedia layers resist deformation while simultaneously altering resistance under the influence of electric fields; in transistors, dielectric layers are applied to separate G electrodes from the semiconductor layers to prevent current flow and produce the capacitance effect.[73b] To optimize the device's flexibility, intermedia and dielectric layers must be easily deformable under mechanical strain.

Organic polymer materials exhibit inherent softness and flexibility, high compatibility with semiconductors and polymer substrates, and energy-efficient processability, which are suitable in flexible memristor- and transistor-based electronics.[149] In the realm of flexible memristors, composite materials incorporating nanofillers such as Ag NPs into elastic polymer hosts also offer practical methods for creating flexible intermedia layers.[150] For transistors, conventional oxide insulators with complicated fabrication processes and brittle nature have limited application in flexible electronics.[151] In comparison, polymer materials like poly(methyl methacrylate) (PMMA) along with polymer elastomers (e.g., polyurethane (PU) elastomers) have been reported as dielectrics in artificial synaptic devices to improve flexibility.[152] To address the issue of large leakage current caused by low dielectric constant and poor film density in certain organic polymers, performance enhancements have been achieved through the use of polymers with higher dielectric constants such as polyvinyl alcohol (PVA), or by the implementation of double-layered structures.[116]

For EGTs, dielectric layers are generally polymer-based electrolyte materials including polymer electrolytes, polyelectrolytes, and ion gel electrolytes.[153] Polymer-based electrolytes have the advantages of tunable viscosity characteristics and processing temperatures, allowing films prepared by various coating and printing techniques. Ionic-gated transistors (IGTs), in particular, have garnered widespread attention owing to their various merits (e.g., low operating voltage) and wide applications (e.g., wearable electronic devices).[154] The ion gels can be fabricated by mixing ionic liquids and cross-linked polymer networks, which offer lightweight, good physical/chemical stability, and transparency.

Semiconductor Layers: Within the realm of flexible electronics, a range of candidate semiconductor materials, including semiconducting polymers and nanomaterials,[6a] have witnessed substantial progress.[155] Semiconducting polymers provide the merits of intrinsic flexibility, reliability, and solution processability, indicating their potential flexible and wearable electronic applications.[156] Zero-dimensional (0D) materials (e.g., quantum dots (QDs),[157] NPs) can enhance the performance of both memristors and transistors because of their excellent electrical and optical properties.[158] Meanwhile, one-dimensional (1D) materials (e.g., nanotubes (NTs) and nanowires (NWs)) have also been widely studied for flexible devices in recent years with the advantages of high conductivity, excellent mechanical deformability, and high transparency.[159]

In comparison to 0D and 1D materials, 2D materials—characterized by having one or a few atomic layers—have intrigued many researchers owing to their extraordinary properties in the fields of thermal, optics, and electricity.[160] These unique characteristics bestow upon devices distinct advantages such as high-density integration and low power consumption[136a,161] Composed of strong in-plane chemical bonds and weak van der Waals interactions out-of-plane, planar structures impart 2D materials excellent compatibility and convenience with wafer semiconductor technology.[162] Notably, materials such as transition metal dichalcogenides (TMDs) are seen as candidates to replace conventional silicon-based semiconductors for the development of memory and neuromorphic devices.[163] Especially, it's reported that 2D materials can generally endure strain above 10%,[164] which is larger than that of conventional bulk materials.[165] For example, due to good flexibility as well as adhesion on flexible substrates, graphene is suitable for developing flexible devices like stress and strain sensing.[166] As a derivative of graphene, graphene oxide (GO) has unique surface properties due to abundant oxygen-containing functional groups, which is conducive to constructing high-performance graphene-based flexible devices' performances.[167] TMDs, with a single-layer thickness of 0.7–1 nm, exhibit high flexibility as well as light transmittance.[168] In brief, 2D materials have emerged as promising materials for next-generation flexible devices.[161d,169]

3. MXenes

MXenes, another 2D material with atomic thickness, possess a couple of advantages such as planar nanosheet structure, outstanding electrical conductivity, and excellent flexibility, making them suitable for applications as flexible semiconductor layers and electrodes. The diverse surface terminating functional groups present on MXenes enable various functionalities, such as charge trapping and catalyzing. The compatibility with other 2D materials further facilitates the development of multifunctional devices with enhanced performance. In this section, materials structures, synthesis approaches, surface modification and functionalization, and distinct properties of MXenes are discussed.

3.1. Structures

The general formula for MXene is $M_{n+1}X_nT_x$ (n = 1, 2, 3, or 4), where M represents one or two early transition metals, such as Ti, Cr, and W; X denotes C and/or N; and T_x signifies surface functional groups (typically –O, –F, –Cl, and –OH).[170] As shown in **Figure 6a**, the parent compounds of MXenes, known as MAX phases (general formula $M_{n+1}AX_n$ (n = 1, 2, 3, or 4)), with A primarily consists of group IIIA or IVA elements (Al, Si, and other elements).[171] X atoms occupy octahedral sites between the M-layers, with the A-layer interspersed with the $M_{n+1}X_n$ layers. The M-A bond is purely metallic but the M-X bond exhibits both covalent and metallic bonding characteristics. Consequently, MXenes are obtained by etching away the A-layer from the MAX phases.[172] MAX phases typically exhibit layered hexagonal phases with symmetry and belong to

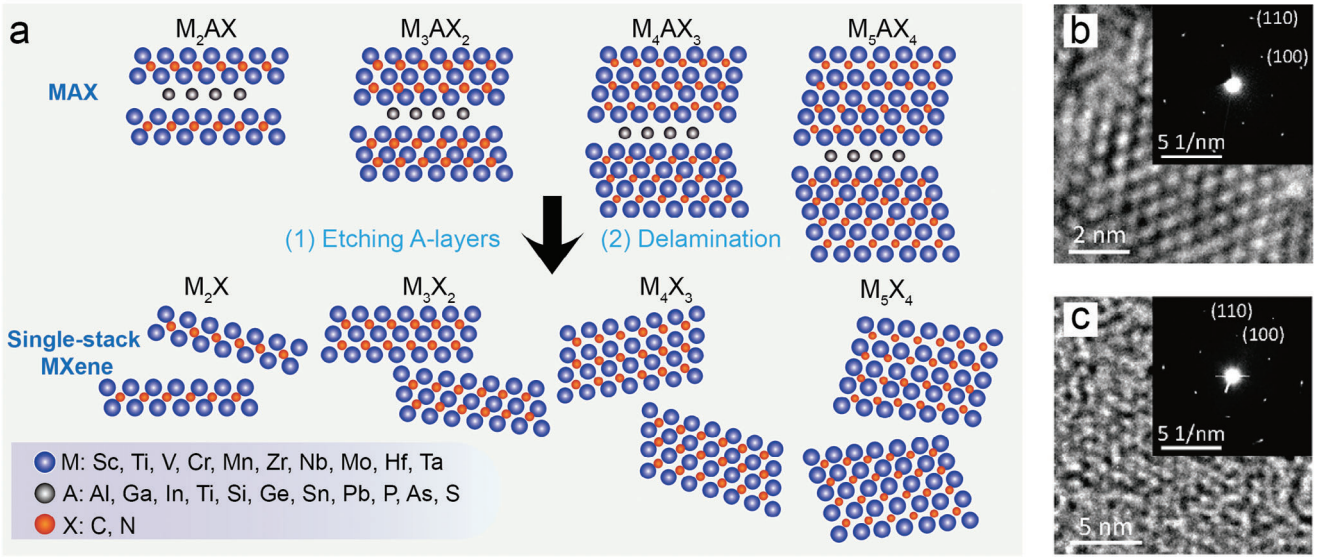

Figure 6. Synthesis schematic and characterization of MXenes. a) Synthesis of four kinds of typical MXenes (M_2X, M_3X_2, M_4X_3, and M_5X_4) from MAX phases through etching and delamination processes. b,c) HRTEM images of Nb_2AlC MAX phase (b) and Nb_2C MXene flake (c) (inset: corresponding SAED patterns). Reproduced with permission.[175] Copyright 2017, American Chemical Society.

space group P63/mmc.[173] It has been demonstrated by high-resolution transmission electron microscopy (HRTEM) as well as selected area electron diffraction (SAED) (Figure 5b). After A-layers are selectively moved, the corresponding 2D layered MXenes are gained with both M and X atoms arranged similarly to MAX phases (Figure 5c).[174]

3.2. Synthesis Approaches

On account of variations in starting materials, surface modification techniques, and other factors, synthesis strategies for MXenes are crucial in determining their lateral dimensions, chemical composition, surface terminations, and distinct properties. Generally, synthesis approaches are categorized into "top-down" and "bottom-up" types.[176] "Top-down" approaches concentrate on exfoliating crystals into MXene flake, while "bottom-up" approaches emphasize the direct growth of MXenes from atoms or molecules.[177] This section discusses the mechanisms, advantages, and disadvantages of various synthesis approaches.

3.2.1. Top-Down Approaches

Currently, "top-down" is the predominant type employed in laboratories for synthesizing MXenes,[178] involving selective etching of element A from MAX phases to yield one or several-layered flakes.[179] Common techniques include wet chemical etching or molten salt etching, further categorized into fluoric acid (HF) etching, fluoride-based salt etching, alkali-based etching, electrochemical etching, as well as Lewis acid molten salt etching.

HF etching, for instance, is widely used for preparing single- or few-layer MXene nanosheets[180] HF at a concentration of 50 wt.% was first utilized to etching Ti_3AlC_2 MXene in 2011, as depicted in **Figure** 7a.[181] Multiple chemical reactions occur during the etching process:

$$Ti_3AlC_2\,(s) + 3HF\,(aq) = AlF_3\,(aq) + Ti_3C_2\,(s) + \frac{3}{2}H_2\,(g) \quad (2)$$

$$Ti_3C_2\,(s) + 2H_2O\,(aq) = Ti_3\,C_2(OH)_2\,(s) + H_2\,(g) \quad (3)$$

$$Ti_3C_2\,(s) + 3HF\,(aq) = Ti_3\,C_2F_2\,(s) + H_2\,(g) \quad (4)$$

Equation 2 represents the primary reaction between solid Ti_3AlC_2 and HF solution, which selectively removes Al atoms. The scanning electron microscopy (SEM) images (Figure 7b,c) illustrate the transformation of Ti_2AlC_3 morphology from compact particles to loosely arranged accordion-like lamellae after the etching process.[182] Equations 3 and 4 indicate that surface terminals, such as –OH and –F, can form on the layered Ti_3C_2. The Ti atoms exposed on both sides of the Ti_3C_2 layer easily link with T_x to lower the total surface energy.[182,188] Ultrasonic treatment then disperses the accordion-like $Ti_3C_2T_x$ into single or few layer(s). Over time, numerous MXenes have been synthesized utilizing HF under etching times, HF concentrations, and reaction temperatures, resulting in various morphology and surface-terminating functional groups of MXenes.[189] Although HF is effective for the etching process, it presents safety concerns due to its smoky nature, high irritability, and corrosiveness. As an alternative to HF, fluoride-based salt etching agents such as the LiF/HCl mixture have been considered highly suitable. Consequently, fluoride-based salt etching agents like LiF/HCl are considered suitable alternatives, as they are milder and generate HF in situ through reactions (Equation 5).

$$LiF + HCI = HF + LiCl \quad (5)$$

LiF/HCl etching agent can produce high-quality MXene with good hydrophilicity, excellent electrical conductivity, and abundant surface terminals. Additionally, preintercalation with Li^+

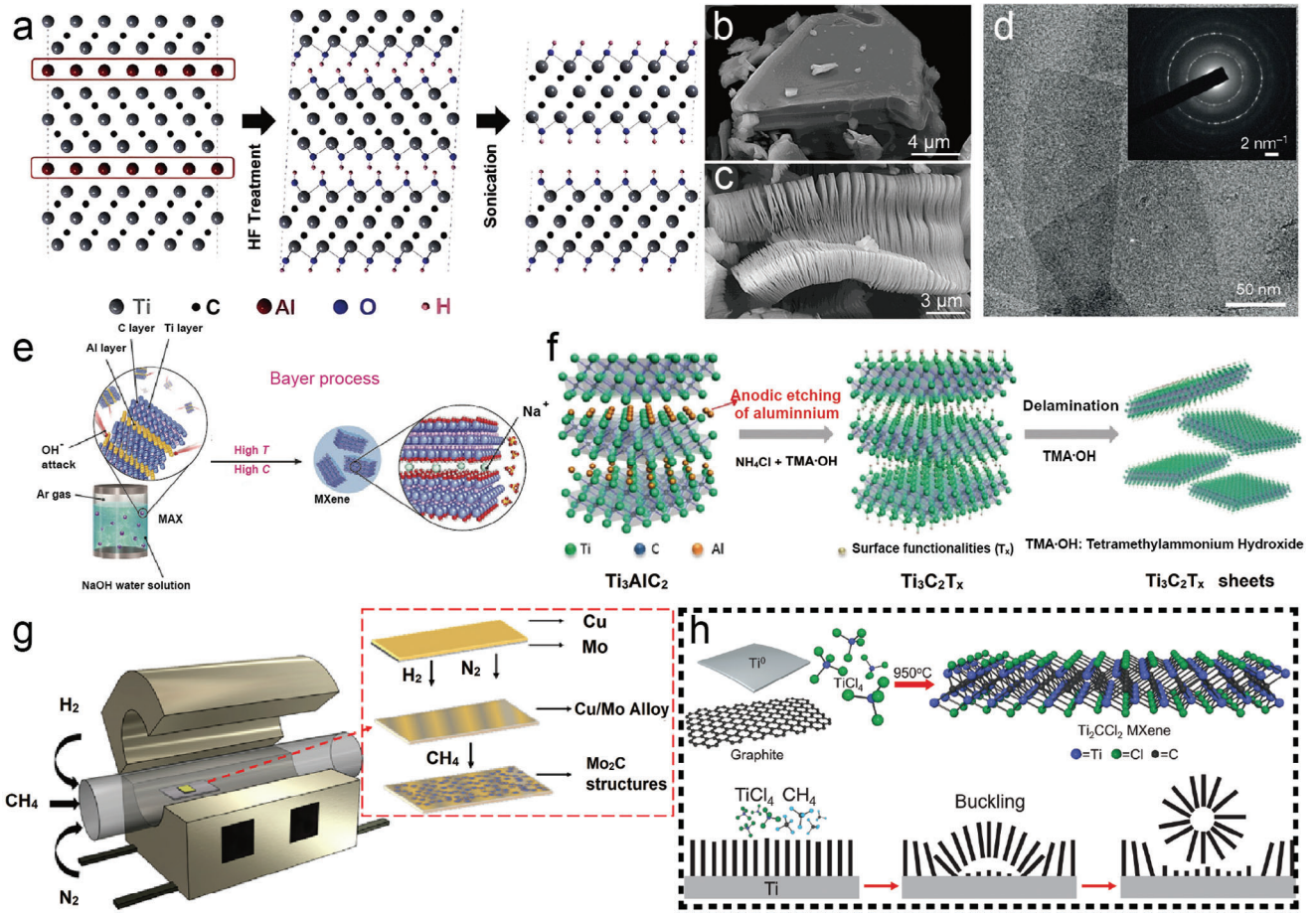

Figure 7. Different synthesis approaches of MXenes. a) Schematic of the exfoliation process of Ti_3AlC_2. Reproduced with permission.[181] Copyright 2011, Wiley-VCH. b,c) SEM images of Ti_3AlC_2 before (b) and after etching with HF (c). Reproduced with permission.[182] Copyright 2012, American Chemical Society. d) Transmission electron microscopy (TEM) image of $Ti_3C_2T_x$ obtained by employing LiF/HCl as etching agent (inset: overall SAED pattern). Reproduced with permission.[183] Copyright 2014, Springer Nature. e) Schematic of preparing $Ti_3C_2T_x$ etched by NaOH. Reproduced with permission.[184] Copyright 2018, Wiley-VCH. f) Schematic diagram of electrochemical etching of $Ti_3C_2T_x$ followed by a layering process. Reproduced with permission.[185] Copyright 2018, Wiley-VCH. g) Schematic of preparing Mo_2C by using the CVD technique (inset: the growth process of Mo_2C films). Reproduced with permission.[186] Copyright 2022, AIP Publishing. h) Schematic diagram of Ti_2CCl_2 produced by the CVD method. Reproduced with permission.[187] Copyright 2023, Amer Assoc Advancement Science.

ions can weaken interlayer interactions, promoting larger interlayer spacing. This results in MXenes with large lateral sizes (about 0.5–1.5 μm level), ultrathin thickness (1–2 layers), and few defects (as depicted in Figure 7d). After the etching and washing, the resulting MXenes have clay-like plasticity, allowing them to be rolled into thin films with thicknesses on the order of tens of microns. Except for LiF/HCl, other fluoride salts like NaF,[190] NH_4F, and KF, as well as acids like H_2SO_4 can be applied as etching agents.[191]

To circumvent hazardous HF and fluoride salts, milder, greener, and safer alkali-based etching was further discovered and developed. Benefiting from the strong bonding ability with the A atoms, alkali thereby can achieve selective etching of the MAX phases. For example, Ti_3AlC_2 can react with NaOH under high temperatures (270 °C) to fabricate supercapacitors with high-purity (92 wt.%) $Ti_3C_2T_x$ electrodes (Figure 7e).[184] MXenes can also be synthesized through electrochemical etching, which utilizes an electrolyte solution, anode, and cathode. Yang et al. reported an anodic corrosion of Ti_3AlC_2, peeled by an electrolyte (pH > 9) of 1.0 M ammonium chloride (NH_4Cl) and 0.2 M tetramethylammonium hydroxide (TMAOH), enabling destroying Ti-Al bond because of the strong binding affinity of Cl- to Al (Figure 7f).[185] The Lewis acid molten salt etching method is also environmentally friendly without hazardous chemicals.[192] During the etching process, the cations of the molten salt can capture the A-layer, thereby exfoliating MAX phases. However, the synthesis process involves annealing Lewis acid salt to 550–800 °C, which is heat- and energy-consuming.[192,193]

3.2.2. Bottom-Up Approaches

The MXene nanosheets obtained from "top-down" strategies often exhibit diminutive dimensions and extensive defects. To overcome this issue, "bottom-up" synthetic approaches including chemical vapor deposition (CVD) and template methods, have

been developed.[194] "Bottom-up" approaches produce MXenes from the atomic level, resulting in films with high-quality, large-area, and ultra-thin thickness.

The synthesis of MXenes with precise thickness and composition by the CVD system has been successfully demonstrated,[195] undergoing a gas phase reaction under a high temperature.[195a] Öper, et al. successfully synthesized large-area Mo_2C flakes with controlled thickness on a Cu/Mo substrate using a CVD system and CH_4 gas as the carbon source. The thickness of Mo_2C flakes was modulated by adjusting the N_2/H_2 gas ratio and CH_4 flow rate (Figure 7g).[186] Moreover, Wang et al. synthesized Ti_2CCl_2 MXenes, which are widely employed, through CVD by reacting $TiCl_4$ and CH_4 on a Ti metal surface. This led to the perpendicular growth of Ti_2CCl_2 sheets on the surface (Figure 7h).[187] However, the stringent preparation conditions employed in CVD, including elevated temperatures and pressures, prolonged reaction time, as well as expensive equipment and materials, impose limitations on the scalability of this synthetic approach.[196]

In conclusion, no universally applicable synthetic approach for MXenes exists yet. For instance, HF etching is commonly employed to prepare small planar size and defective MXenes, while the combination of acids and salts is utilized to synthesize large plane and less defective MXenes; however, both methods involve the use of hazardous HF and fluoride salts, raising safety concerns. While various methods offer distinct advantages and limitations, careful selection based on specific applications is essential to obtain desired MXenes with optimal properties and performances.[197]

3.3. Surface Modification and Functionalization

Despite the remarkable physicochemical properties exhibited by MXene materials, they still fall short of meeting the specific requirements for certain applications. For instance, in the biomedical field, MXenes encounter challenges related to their toxicity and slow degradation.[198] To solve these issues and achieve enhanced properties, surface modification and functionalization including the termination with functional groups, polymer modification and composites, and small-molecule organic compound functionalization, are necessary.[199] Typically, as-prepared MXenes are terminated with functional groups, a process that can be controlled during etching through the selection of etching agents and methods. Polymer-based surface chemistry strategy is one of the popular and low-cost surface modification strategies of MXenes, involving the immobilization of selected polymers on the MXene surfaces.[199] An example is poly[(9,9-dihexyl-9H-fluorene)-alt-(1,4-diethynylbenzene)] (PDFD)-MXene for nonvolatile memory devices with excellent environmental stability and solution processability (**Figure 8a**).[200] Due to the complete encapsulation of MXene in the polymer matrix, PDFD-MXene demonstrates significantly enhanced stability, leading to consistent device performance even after prolonged exposure to moist air (> 60 days, humidity of 50%, temperature of 30 °C). This exemplifies the strong evidence supporting the feasibility of covalent functionalization between MXenes and conjugated polymers.

Furthermore, the interaction between terminating functional groups on MXenes and small-molecule organic compounds enables desirable properties tailored for specific requirements.[202] For instance, to enhance the surface smoothness and functionalize MXenes, a spiropyran MXene (MXene-SP) exhibiting better material/metal contact and hole/electron transport was fabricated from 4-bromophenyl-functionalized MXene (MXene-BP) (Figure 8b).[201] The resulting ITO/MXene-SP/ITO device exhibits nonvolatile and optoelectronic dual-response RS characteristics, attributed to high yield (>90%) reversible structural isomerization capability of MXene-SP and MXene-MC (MC: ring-opened merocyanine) under different light illuminations.

3.4. Properties

The diverse composition, tunable surface, and bulk chemistry of MXenes offer valuable and distinctive properties,[203] rendering them promising candidates for fabricating advanced flexible materials for memory and neuromorphic devices.[204] The following sections present an overview of MXene properties encompassing electrical, mechanical, stability, optical, and ferroelectric characteristics.

3.4.1. Electrical Property

The electrical characteristics of MXenes are influenced by material structure, bonding nature, surface terminations, and defects.[205] Especially, due to the variations in the composition and surface functionalization, MXenes can be viewed as metallic, semiconducting, and topologically insulating.[206] For example, $Ti_3C_2T_x$ MXene has excellent conductivity (>2.40×10^4 S cm^{-1}), primarily attributed to the surface functional groups on the nanosheet surfaces and electrons of Ti atoms, positioning it as a competitive candidate for electronic applications.[25,207] As indicated by density functional theory (DFT) calculations, pristine MXenes without terminal groups generally behave as metals, as evidenced by the overlapping of CBs and valence bands (VBs) at the Fermi level.[208] The presence of abundant surface terminations may lower the Fermi level below d orbital of M atoms, leading to the generation of band gap and transformation into semiconductors. However, most $M_{n+1}X_nT_x$ MXene (e.g., $Ti_3C_2T_x$) exhibit metal properties owing to the large n value, regardless of whether there is a surface termination.[209] For monolayer MXenes, electronic structures are possibly tuned by adjusting surface functional groups and corresponding geometric conformation,[210] while intercalating agents in multilayer MXenes can increase resistance by expanding interlayer spacing.[211] In addition, MXene possesses other merits such as high mobility (1 cm^2 V^{-1} S^{-1}), high charge carrier density (3.8×10^{22} cm^{-3}), and tunable work function via controlled surface chemistry.[212] By leveraging the high conductivity and nanoscale carrier transport channel length of MXene, synaptic transistors with MXene electrodes can realize linear conductance tuning.

3.4.2. Mechanical Property

By theoretical calculations (DFT and molecular dynamics (MD)), it's predicted that in-plane Young's modulus of Ti_2C, Ti_3C_2, and

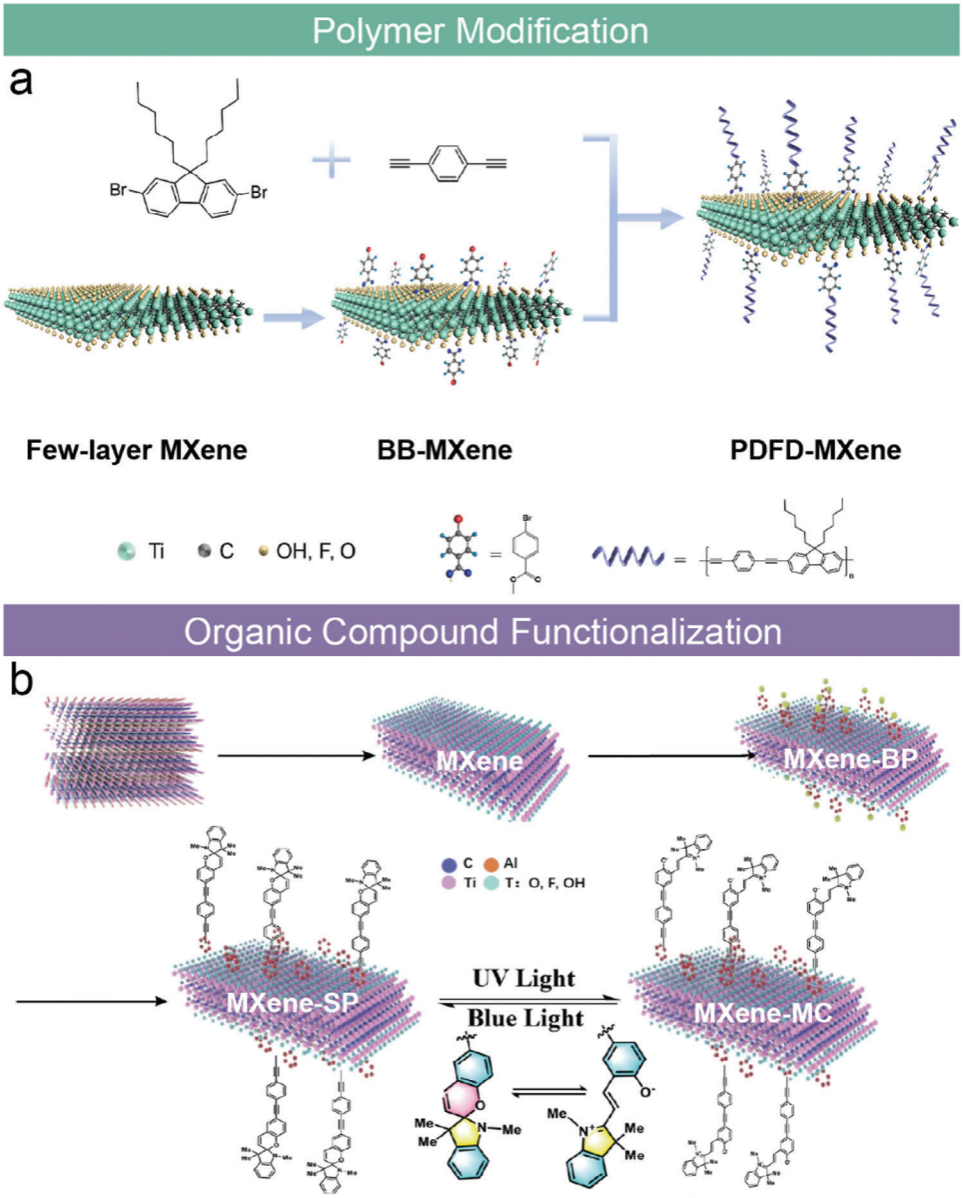

Figure 8. Surface modification and functionalization of MXenes. a) Synthesis scheme of PDFD-MXene. BB-MXene is synthesized by reacting $Ti_3C_2T_x$ with 4-bromobenzoyl chloride, with PDFD polymer chains grown directly on the surface of BB-MXene. Reproduced with permission.[200] Copyright 2023, American Chemical Society. b) Synthesis scheme of MXene-BP, MXene-SP, and MXene-MC. MXene-BP is prepared by the reaction between MXene and p-bromophenyl diazonium salt; MXene-SP is synthesized via the Sonogashira coupling reaction of 6-bromo-1,3′,3′-trimethylspiro [chromene-2,2′-indoline] and MXene-BP. Reproduced with permission.[201] Copyright 2023, Wiley-VCH.

Ti_4C_3 exceeds 500 GPa.[213] The experimental results indicate that single-layer $Ti_3C_2T_x$ has Young's modulus of 330 ± 30 GPa, which is higher than that of other 2D materials having the same thickness (e.g., reduced graphene oxide (rGO), GO). At break, the tensile strength of single-layer $Ti_3C_2T_x$ is 17.3 ± 1.6 GPa.[213b,214] As evidenced by theoretical calculations and experimental research, various parameters, including structural characteristics, film thickness, flake size, compositions, and surface terminations, contribute to the diverse mechanical properties of 2D MXenes.[36a,215] Young's modulus of M_2X, M_3X_2, and M_4X_3 exhibit a decreasing trend as the film thickness increases.[216] Considering different transition elements, Nb-based single-layer Nb_4C_3T MXene exhibits higher Young's modulus (386 ± 14 GPa) than Ti-based single-layer $Ti_3C_2T_x$ MXene.[26] Additionally, composites like PVA/MXene benefit from interfacial interactions, resulting in improved tensile strength than pure MXene.[217]

3.4.3. Stability

Stability is essential for their practical applications of MXenes, as these materials may undergo a series of chemical and

thermal treatments during device fabrication and in the working environment. Under inert gas atmospheres or vacuum, since the lattice energy is negative, MXenes have relatively high thermal stability.[218] But notably, MXenes are very susceptible to oxygen and water environments and gradually transform to TiO_2.[219] This transformation may result in sacrificing the merits like high conductivity and good solution processability of MXenes.[220] Other parameters like temperature can also affect the oxidative stability of MXenes.[221] The reduced kinetic rate at low temperatures decelerates oxidation, resulting in excellent antioxidant protection of frozen $Ti_3C_2T_x$ MXene films while maintaining their electrical conductivity.[222] However, when exposed to an oxygen environment at elevated temperatures (e.g., 450 °C), single-layer $Ti_3C_2T_x$ can rapidly undergo a fast transformation into TiO_2.[223]

3.4.4. Optical Property

MXenes exhibit significant electron transport properties and impressive optical properties from UV to near-infrared ranges, making them suitable for optical applications like optoelectronic memristors.[224] The optical properties of MXenes include excellent transparency, photo-thermal effect,[225] and remarkable plasmonic effect.[226] 5 nm thick $Ti_3C_2T_x$ films can achieve a transmittance of up to 91.2%, with light absorption capabilities within the range of 300–500 nm, which holds significant importance for applications involving transparent conductive electrodes and other optoelectronic devices.[227] Surface functional groups and chemical compositions also significantly manipulate their optical characteristics.[228] By employing DFT calculations, it's concluded that in the UV region, all surface terminations contribute to higher absorption and reflectivity of $Ti_3C_2T_x$ MXenes; in the visible range, F- or OH-terminated $Ti_3C_2T_x$ exhibits lower absorption and reflectivity compared to that of pristine MXene.[229] Furthermore, elemental substitution on M and X sites, such as partially substituting C with N in Ti_3AlC_2 MAX phases, results in the formation of Ti_3CNT_x MXenes, which exhibit a blue shift in the main absorption peak relative to $Ti_3C_2T_x$.[228b] Surface modifications, including the doping of magnetic transition metals (e.g., Fe, CO, and Ni), can increase the optical absorption coefficient of Ti_3C_2 across the UV, visible, and near-infrared regions, likely related to alterations in the electronic structure resulting from the addition of magnetic atoms.[230] Certain MXene materials possess electrochromic attributes where their optical absorption shifts in response to an applied electrical field, making them ideal for applications in smart windows, screens, and other gadgets that demand color changes adjustable transparency, or the ability to change colors.[231] Additionally, given the irreversible oxidation of MXenes, previous studies have shown that partially oxidized $Ti_3C_2T_x$ can produce photocurrent under visible optical pulse stimulation,[232] facilitating the simulation of visual image processing in brain-inspired devices.

3.4.5. Ferroelectric Property

Among the structural phases of MXene, the mixed configuration without inversion symmetry has been identified,[233] resulting in an internal dipole moment. Sc_2CO_2 MXene was first predicted to be ferroelectric, with both in- and out-of-plane polarization.[234] Since then, the prediction of ferroelectric MXene (e.g., Nb_2CS_2, Y_2CO_2, $Zr_2C(OH)_2$, and Nb_2NF_2) as well as multiferroic $Hf_2VC_2F_2$ are also been verified.[233,235] In the experiment, pure $Ti_3C_2T_x$ MXenes are known as electrically conductive materials. However, owing to the presence of TiO_2 after heat treatment, the crystal structure of MXenes is distorted, which induces the coexistence of in-plane and out-of-plane electric polarization under an external field and they start to exhibit ferroelectric behavior.[236] Tahir et al. reported the existence of ferroelectric and multiferroic in free-standing $Ti_3C_2T_x$ MXene film at room temperature upon heating.[237] Moreover, in double transition metal carbide $Mo_2TiC_2T_x$, the co-existence of ferroelectric and magnetic is verified, which may provide a platform for future data storage applications.[238]

4. Applications of MXenes in Flexible Memory and Neuromorphic Devices

Due to their superior properties, MXene materials, mostly $Ti_3C_2T_x$, have been widely employed in memory and neuromorphic devices.[24,100,239] Numerous efforts focus on the applications of data storage devices, artificial synapses, and neuromorphic systems.[24] MXenes, with their excellent metallicity, open up possibilities for fabricating more stable nonvolatile data storage devices with long data retention times, high-speed switching, and low power consumption.[240] In artificial synapses and neuromorphic computing, MXenes offer excellent electron transport dynamics, high mobility, and short ion transport distances, thereby facilitating the creation of synaptic devices with notable synaptic plasticity as well as learning capabilities.[241] Additionally, as portable and wearable electronic technologies advance, MXenes with great flexibility have the potential to develop high-performance flexible memory and neuromorphic devices.[45] We will introduce some typical two- and three-terminal flexible MXene-based devices in this section.

4.1. MXenes for flexible memory

MXenes, known for their exceptional electrical conductivity, are not directly suitable for use as RS layers. To overcome this limitation and enhance device performance, extensive research has focused on doping, surface modification and functionalization, and other strategies.[40] This section delivers a discussion of the utilization of MXenes in flexible memory (**Table 1**).

Recent studies have notably explored MXene-polymer hybrid materials as RS layers in memristors.[29d,250] In 2019, Ding et al. first demonstrated an RRAM using MXene (Ti_3C_2)-polyvinylpyrrolidone (PVPy) composite films as active RS materials on a flexible PEN substrate.[242] The remarkable wetting properties and water solubility of PVPy facilitate the fabrication of Ti_3C_2@PVPy composites. The RS behaviors can be explained by charge-trapping-assisted hopping conduction model (**Figure 9a**). Initially, Ti_3C_2@PVPy composite behaves as an insulator. Upon the application of positive bias, charge carriers are injected into Ti_3C_2 nanosheets. As the voltage increases, trapped carriers accumulate, resulting in the formation of CFs.

Table 1. MXenes for flexible memory.

Structure	Substrate	ON/OFF ratio	Endurance	Retention time (s)	Bending radius (mm)	Bending cycle	Application	Refs.
Al/Ti_3C_2@PVPy/ITO	PEN	10^4	1000	5×10^4	13	1000	Multistate information storage	[242]
Ag/$Ti_3C_2T_x$-PVA/ITO	PET	<10	50	7.5×10^3	–	100	Nonvolatile memory	[243]
Al/$Ti_3C_2T_x$-OP/ITO	PET	$10^{4.1}$ $10^{2.7}$	–	4000	21	5000	Multilevel resistive memory	[244]
$Ti_3C_2T_x$/GO/$Ti_3C_2T_x$	–	<10	2400	10^4	–	–	Data storage	[245]
$Mo_2TiC_2T_x$/GO/ $Mo_2TiC_2T_x$	–	100	5000	10^5	–	–	Data storage	[246]
$Ti_3C_2T_x$/Ag/NPs@$Ti_3C_2T_x$/Ag/$Ti_3C_2T_x$/ZnO/ PM6:Y6:PC_{71}BM/ MoO_3/Ag	PEN	10^3	4×10^3	10^4	6	2000	Memristive solar cell	[247]
$Mo_2TiC_2T_x$/FE-$Ti_3C_2T_x$/$Mo_2TiC_2T_x$	–	10^3	200	10^4	–	–	Data storage	[248]
$Mo_2TiC_2T_x$/FE-$Ti_3C_2T_x$@nFE-$Ti_3C_2T_x$/$Mo_2TiC_2T_x$	–	10^3	1000	4000	–	–	Data storage	[240a]
$Ti_3C_2T_x$/Fe-$Ti_3C_2T_x$@BFO/$Ti_3C_2T_x$	–	10^2	1000	10^4	–	–	Multifunctional memory	[249]

Conversely, applying reverse voltage releases the trapped carriers, resulting in CF rupture and triggering the RESET process. Under voltage pulses, the device exhibited typical bipolar RS behavior, with excellent reliability (>1000 cycles). Figure 9b illustrates the stability of current values during 10 voltage pulse repetitions across various compliance currents (I_{CC}), indicating distinct and stable resistive states for multilevel data storage. Furthermore, these states can be retained for at least 5000 s (Figure 9c,d), showcasing excellent retention capacity suitable for high-density storage. Notably, the flexible device could maintain reliability under mechanical stress with the $\theta = 90°$ and $R = 13$ mm (Figure 9e), affirming Ti_3C_2's potential for high-performance flexible multilevel data storage devices in the future. In 2023, Ling et al. constructed a robust MXene-based memristor with the Ag/$Ti_3C_2T_x$-PVA/ITO/PET structure, demonstrating outstanding flexibility.[243] Atomic force microscope (AFM) image of $Ti_3C_2T_x$-PVA hybrid nanofilm (Figure 9f) reveals a uniform dispersion of $Ti_3C_2T_x$ in PVA layer, originating from its hydrophilicity. The device retained stable bipolar RS characteristics after 100 mechanical bending tests (Figure 9g,h), thereby demonstrating exceptional mechanical stability and reproducibility, making it ideal for intelligent wearable electronics.

Surface modification, a crucial step for optimizing the properties of nanomaterials,[251] often involves the use of organic compounds as modifiers to affect the structure and properties of MXenes. For instance, by introducing octyl phosphonic acid (OP) to the surface of $Ti_3C_2T_x$, Sun et al. achieved enhanced electrical as well as optical properties.[244] The successful modification of $Ti_3C_2T_x$-OP is confirmed by X-ray photoelectron spectroscopy (XPS) (Figure 9i). By utilizing the modified $Ti_3C_2T_x$-OP alongside Al and PET as the active layer, electrode, and substrate, respectively, the authors fabricated a flexible multilevel resistive memory device with impressive flexibility, long retention time, and a high ON/OFF ratio (Figure 9j). The RS mechanism is thought to involve a filamentary-type charge trapping/de-trapping process influenced by Al ion diffusion. When the bias voltage reaches the first threshold voltage (V_{TH1}), the CFs are developed since charge traps are quickly filled. As the voltage rises to the second threshold voltage (V_{TH2}), TEs and BEs are fully connected by these CFs, resulting in Ohmic conduction (Figure 9k). Remarkably, after 5000 bending cycles with a 2.1 cm radius, this device maintained stable ternary RS characteristics, showing no degradation even after 4000 s. This demonstrates that OP effectively modifies MXene, providing a new avenue for developing high-performance flexible memory.

Benefiting from excellent mechanical strength and electrical conductivity, MXenes also serve as effective electrodes for flexible device development.[252] In 2021, Fatima et al. utilized free-standing $Ti_3C_2T_x$ as electrodes to create a flexible memristor with an MXene/GO/MXene structure.[245] The uniform MXene paper, produced via the fluoride-based salt etching method (LiF/HCl), exhibited conductive behavior similar to rGO electrodes. The resulting device demonstrated excellent retention characteristics (10^4 s) and high durability (>2400 cycles). In 2022, they replaced $Ti_3C_2T_x$ with $Mo_2TiC_2T_x$ to construct a flexible $Mo_2TiC_2T_x$/GO/$Mo_2TiC_2T_x$ memristor,[246] achieving impressive durability of 5000 cycles and retention time extended to 10^5 s, laying a foundation for practical flexible data storage. However, the flexibility and mechanical durability tests of these free-standing $Ti_3C_2T_x$ and $Mo_2TiC_2T_x$ films are missing and need further examination. Except for free-standing MXene film, MXenes hybrid systems with good flexibility and excellent conductivity also have attracted significant interest. Nirmal et al. reported multilayer hybrid MXene/Ag/MXene structures as flexible, transparent, and conductive electrodes in a flexible organic solar cell with memory functionalities.[247] The device maintained flexibility over 2000 bending cycles and operated through 4000 switching cycles without discernible degradation, underscoring its reliability as a flexible nonvolatile memory device.

The development of MXene-based ferroelectric memristors remains in its infancy compared to other 2D materials.[253] Self-standing MXene films, benefiting from ferroelectricity after heat treatment, can be utilized to develop flexible ferroelectric memristors for data storage. In 2023, Fatima et al. used $Ti_3C_2T_x$ and

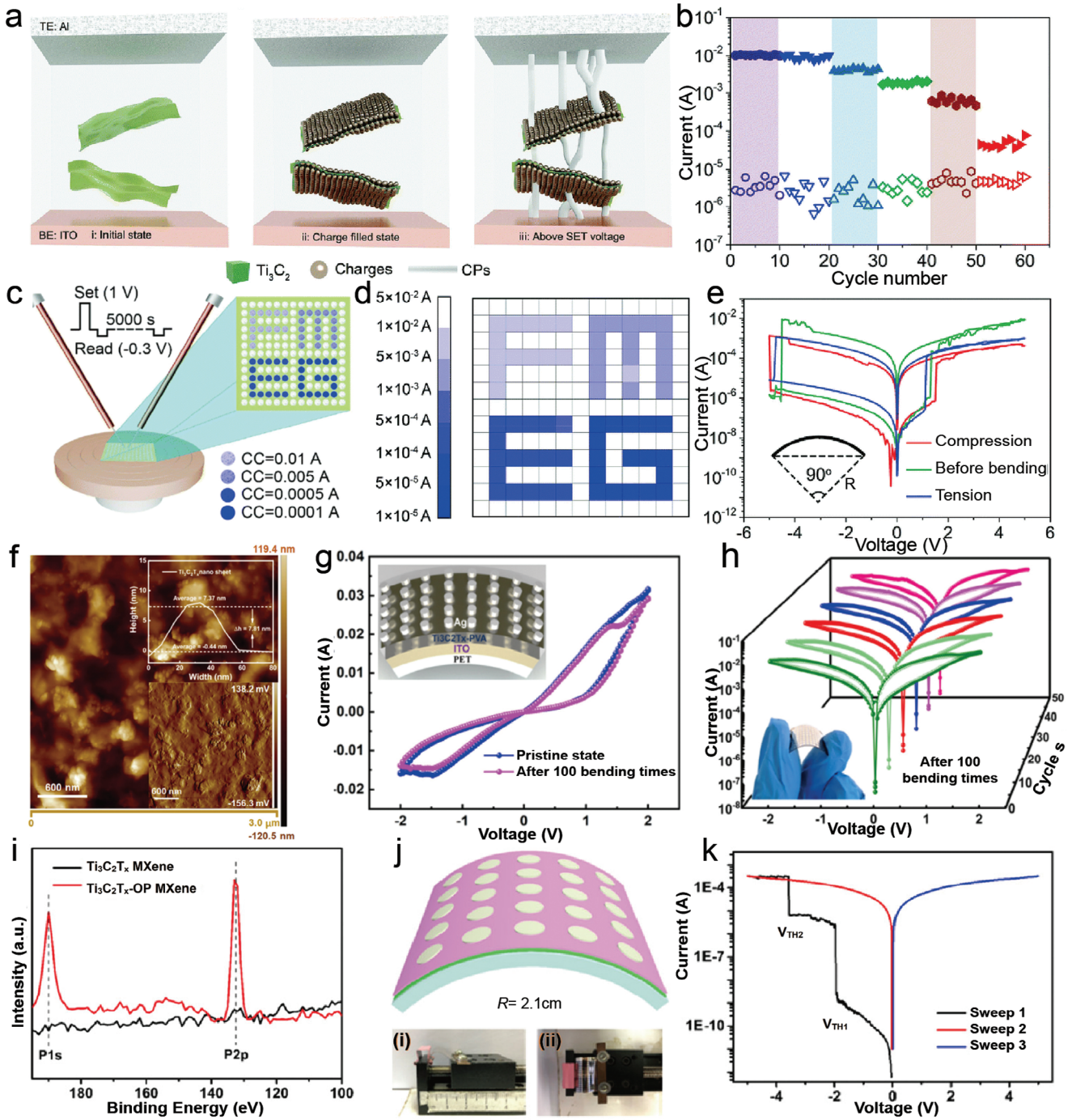

Figure 9. MXene-based flexible memristors for data storage. a) Schematic illustrations of RS mechanism involving charge-trapping-assisted hopping. b) Reversible RS behaviors under 60 cycles, with decreasing I_{CC} from left to right. c) Illustration for testing the device retention capacity under four different I_{CC} values. The devices under different I_{CC} values for forming four English letters. "F": 0.01 A; "M": 0.005 A; "E": 0.0005 A; "G": 0.0001 A. d) LRS current values recorded after 5000 s of the SET process (read: –0.3 V). e) *I–V* curves of flexible memory under compression and tension compared to the unbent state. Reproduced with permission.[242] Copyright 2019, Royal Society of Chemistry. f) AFM image of uniform $Ti_3C_2T_x$-PVA hybrid film (inset: AFM cross-sectional profile of a single $Ti_3C_2T_x$ nanosheet). g) *I–V* curves over 100 bend cycles with the structure diagram of the flexible memristor. h) *I–V* curves from 50 consecutive tests after 100 bending times. Reproduced with permission.[243] Copyright 2023, Elsevier. i) Comparison of XPS of MXene before and after OP modification. j) Schematic of flexible $Ti_3C_2T_x$-OP MXene memory device with main view (i) and top view (ii). k) Steady ternary characteristic of the device recorded after 5000 bending cycles. Reproduced with permission.[244] Copyright 2020, American Chemical Society.

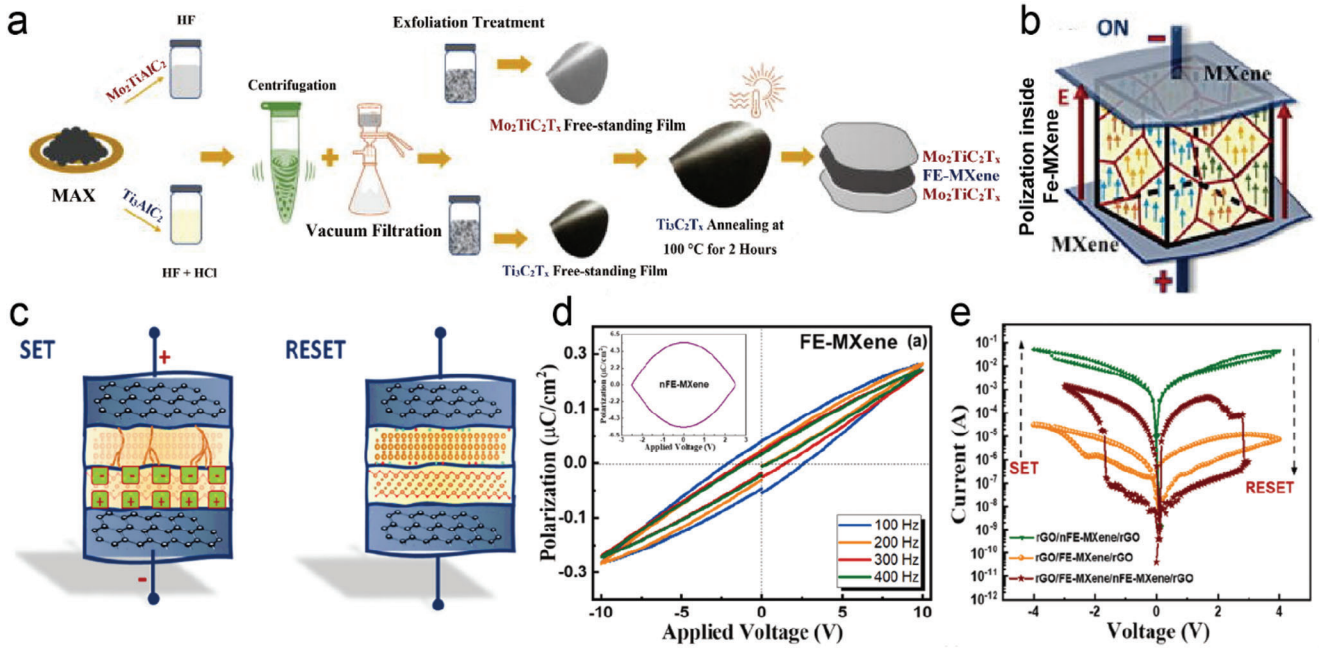

Figure 10. MXene-based flexible ferroelectric memristors for data storage. a) Synthesis diagram of $Ti_3C_2T_x$ and $Mo_2TiC_2T_x$ MXene films. The $Ti_3C_2T_x$ MXene film is subjected to heat treatment in an ambient environment to induce ferroelectricity. b) RS behavior of the device at "ON" state with polarization inside FE-MXene. Reproduced with permission.[248] Copyright 2023, AIP Publishing. c) Operation mechanism of rGO/FE-MXene/nFE-MXene/rGO-based memristor. d) The hysteretic polarization curves of FE-MXene film under four frequencies (inset: curves of nFE-MXene). e) The first *I*–*V* cycle of three memristors. Reproduced with permission.[240a] Copyright 2023, Elsevier.

$Mo_2TiC_2T_x$ to create a flexible nonvolatile ferroelectric memristor with all MXene-based middle layers and electrodes.[248] The $Ti_3C_2T_x$ film was pretreated at high temperatures to induce ferroelectricity and then connected to $Mo_2TiC_2T_x$ electrodes using a PVPy binder (**Figure 10a**). As shown in Figure 10b, the dipoles within the ferroelectric $Ti_3C_2T_x$ (FE-$Ti_3C_2T_x$) align with the external electric field, enabling switching between LRS and HRS. This all-MXene device exhibits nonvolatile bipolar switching behavior with improved endurance (200 cycles) and retention time (10^4 s) under a voltage window of ±4 V. By incorporating nonferroelectric (nFE) $Ti_3C_2T_x$ with FE-$Ti_3C_2T_x$ as an active layer, the researchers fabricated a flexible ferroelectric memristor demonstrating nonvolatile bipolar switching characteristics.[240a] As depicted in Figure 10c, the application of an external bias aligns ferroelectric domains, leading to nonzero electric polarization in FE-MXene layer and facilitating CF formation in the nFE-MXene layer. The hysteresis loops illustrating polarization behavior for both nFE-MXene and FE-MXene are presented in Figure 10d (inset), demonstrating ferroelectricity linked to TiO_2 formation upon heating. Compared to devices utilizing individual nFE-MXene or FE-MXene, the rGO/FE-MXene/nFE-MXene/rGO memristors exhibited significantly enhanced switching characteristics with an improved ON/OFF ratio (10^3) (Figure 10e), requiring low operating voltage requirements (±3 V) and demonstrating exceptional endurance capabilities (1000 cycles). These high-performance FE-MXene devices present substantial potential for ferroelectric memristive storage.

For MXene hybrid composites, incorporating Ti_3C_2 into perovskite ferroelectrics, such as lead zirconate titanate (PZT) and Bismuth Ferrite (BFO), has enhanced RS properties,[254] with further improvements of ferroelectric response observed after heat treatment.[240b] Nonvolatile MXene-PZT ferroelectric memristive devices have demonstrated their capability for logic calculations and neuromorphic systems,[253] providing potential solutions to communication bottlenecks and enhancing computing efficiency for data-intensive tasks. Similarly, Sattar et al. utilized Fe-$Ti_3C_2T_x$-assisted BFO as the intermediate layer to fabricate a flexible ferroelectric memristor with $Ti_3C_2T_x$ free-standing electrodes.[249] This device exhibited co-existing negative differential resistance and resistive switching, maintaining reproducibility up to 10^3 cycles, alongside an enhanced memory window after doping MXene into BFO, indicating its potential for multifunctional and multilevel data storage.

While the development of MXene-based flexible memristors remains nascent, their unique characteristics render them suitable for high-quality data storage, particularly in multilevel applications. However, as previously mentioned, the lack of durability tests on free-standing MXene films necessitates further evaluation and enhancement of their flexibility for practical applications.[240a,245,246,248,249] Additionally, it is essential to explore other MXenes beyond $Ti_3C_2T_x$ for flexible memory applications.

4.2. MXenes for Flexible Neuromorphic Devices

For flexible neuromorphic computing applications, MXenes have been utilized in both two- and three-terminal devices. In this section, we will discuss the applications of the MXenes in flexible neuromorphic devices (**Table 2**).

Table 2. MXenes for flexible neuromorphic devices.

Device	Structure	Substrate	Synaptic functions	Bending radius (mm)	Bending cycle	Application	Refs.
Memristor	Ag/TiO_x/$Ti_3C_2T_x$/Au	PI	EPSC, PPF, STP, LTP, and SRDP	1.0	10 000	Handwritten digit recognition	[255]
Memristor	Ag/p-$Ti_3C_2T_x$/ITO	PET	EPSC, PPF, LTP, and STDP	–	1000	Handwritten digit recognition	[239c]
Memristor	Au/$Ti_3C_2T_x$/gel electrolyte/$Ti_3C_2T_x$/Au	PET	EPSC, PPF, and LTP	–	–	Adaptive handwritten number classification	[256]
Memristor	Ag/ICE layer/$Ti_3C_2T_x$/C	PET	STM, LTM, and EPSC	–	1000	Material and motion recognition	[257]
Memristor	ITO/Ti_3C_2-ZnO/Al	PDMS	LTP	3.5	400	Multimodal in-sensor computing	[258]
Memristor	Ag/TiO_x/$Ti_3C_2T_x$/Au	PI	EPSC, PPF, and LTP	1.0	–	Human respiratory states classification	[259]
Transistor	Graphene(S-D)/$Ti_3C_2T_x$/TiO_2/ion-gel/graphene	PEN	EPSC, PPF, IPSC, PPD, and LTP	4.62	1000	Memory	[260]
Transistor	m-CNTs(S-D)/ s-CNTs/Al_2O_3/Ti_3C_2F/HPI insulator/m-CNTs	PI	EPSC, PPF, IPSC, and PPD	6	1000	Handwritten digit recognition	[261]
Transistor	$Ti_3C_2T_x$(S-D)/S-$Ti_3C_2T_x$/$Ti_3C_2T_x$	PET	–	–	1000	Image recognition	[109]

The strategies including metal oxide doping, partial oxidation, and controlled etching can be employed in two-terminal devices to improve the device properties. The integration of MXenes with metal oxides effectively mitigates the random formation of CFs, leading to devices that exhibit a high ON/OFF ratio and low power consumption.[262] Irreversible oxidation often occurs at the defects or edges of MXene films, converting the MXene into TiO_2.[263] Although oxidation limits the lifetime of MXenes, it also enables the synthesis of MXene-TiO_2 composites. Previous studies have demonstrated that devices based on MXene-TiO_2 composites exhibit excellent nonvolatile memory characteristics and emulate synaptic functions.[212b] In 2023, Huang et al. developed a flexible artificial synapse crossbar array with Ag/TiO_x/$Ti_3C_2T_x$/Au structure (**Figure 11a**).[255] The TiO_x/$Ti_3C_2T_x$ film was fabricated through a straightforward annealing process, exhibiting exceptional optical transparency (≈ 90%) as well as excellent oxidation resistance (>30 days). The proposed device demonstrated remarkable flexibility with R = 1.0 mm, mechanical endurance of 10^4 bending cycles (Figure 11b), and low device-to-device variability (12.91% for SET process and 11.83% for RESET processes). Additionally, leveraging continuous conductance modulation, the synapse was utilized to construct an ANN that achieved high handwritten digit recognition precision (>96.44%) from the National Institute of Standards and Technology (MNIST) dataset (Figure 11c).

Gosai et al. demonstrated an Ag/partially-etched MXene (p-$Ti_3C_2T_x$)/ITO/PET flexible device by controlling the etching of Al ions in $Ti_3C_2T_x$ MXene.[239c] The RS mechanism, as depicted in Figure 11d, involves the infiltration of Al ions and the migration of oxygen vacancies. In comparison to the fully-etched MXene (f-$Ti_3C_2T_x$)-based device, the incorporation of a minor fraction of Al ions (8%) significantly reduces the operating voltage from 7 to 1 V, due to decreased series resistance and enhanced ion migration efficiency. Additionally, the p-$Ti_3C_2T_x$-based device exhibited remarkable nonvolatile data storage characteristics, including multilevel retention (25 states), ON/OFF ratio of ≈10^3, retention time of up to about 10^6 s, endurance of around 10^4 cycles, and low power consumption of 0.24 nJ. As illustrated in Figure 11e, the device demonstrated high mechanical stability (up to a bending angle of ≈73°) with consistent switching behavior under diverse temperature and humidity conditions without encapsulation. This observation highlights the exceptional mechanical flexibility and reliability of the device. Furthermore, by leveraging the synaptic performance (PPF, LTP, and STDP) of the flexible p-$Ti_3C_2T_x$-based artificial synapses to construct ANN, an impressive accuracy rate of ≈95% was achieved in recognizing MNIST dataset using only 29 training epochs under both flat and bending configurations, underscoring the potential application of MXene-based devices in advancing future flexible data storage and neuromorphic computing.

A high-accuracy neuromorphic system with adaptive SW adjustment plays a significant role in high-performance computing but remains challenging. Inspired by energy storage devices, Zhao et al. proposed high-accuracy flexible artificial synapses based on $Ti_3C_2T_x$ MXene.[256] The circuit and structure design of the proposed device is illustrated in Figure 11f. By fine-tuning resistance, the coupling gel electrolyte and MXene enable precise control over ion accumulation and dissipation, effectively modulating SW. The potentiation and depression

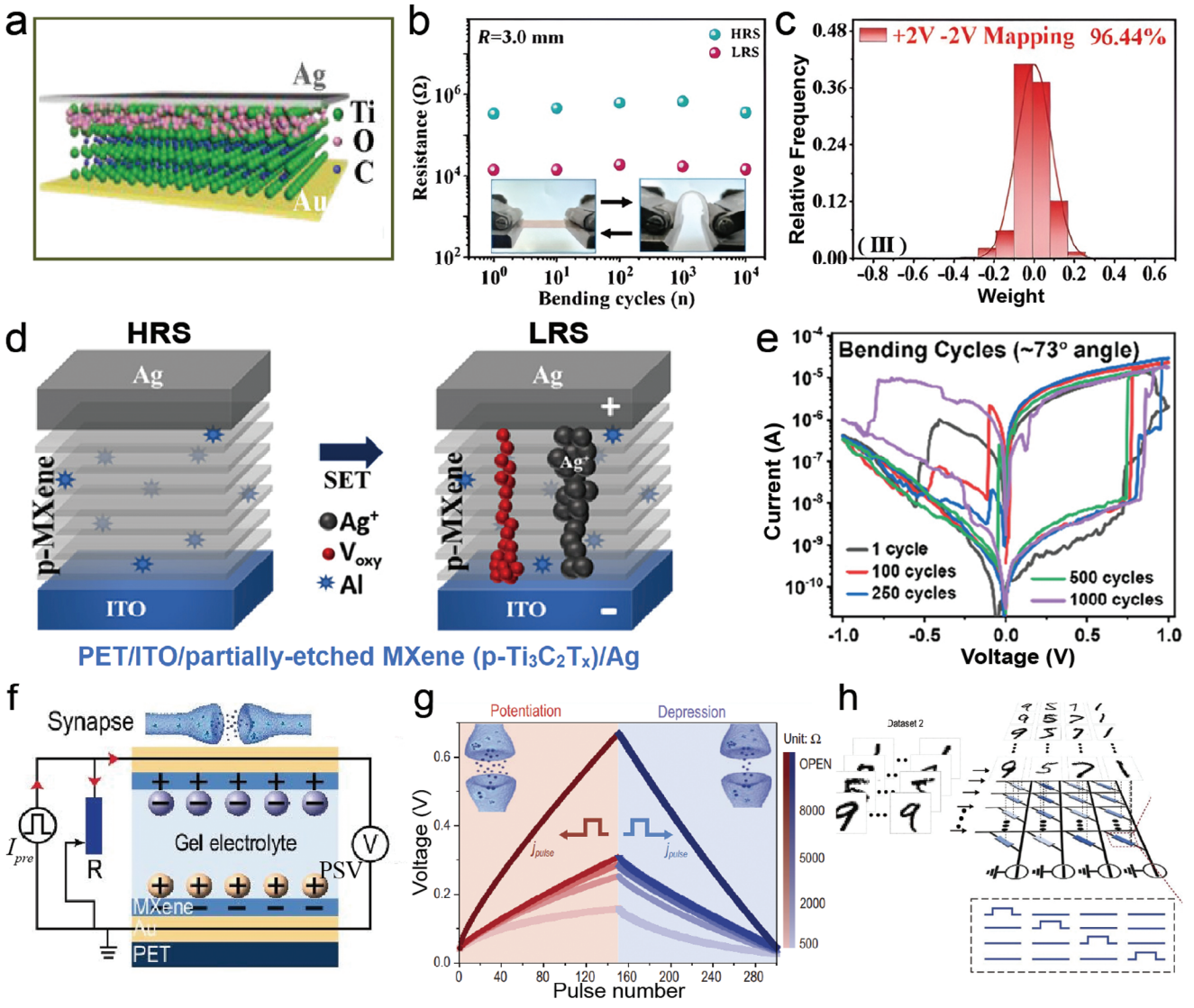

Figure 11. Two-terminal MXene-based flexible neuromorphic devices for recognition by ANN. a) Schematic illustration of $TiO_x/Ti_3C_2T_x$-based artificial synapse with atom distribution of Ti, O, and C. b) Device endurance evaluated through resistance testing of HRS and LRS after 10, 10^2, 10^3, and 10^4 bending cycles. c) The weight distribution and recognition accuracy of the device under ±2.0 V spike. Reproduced with permission.[255] Copyright 2023, Wiley-VCH. d) Schematic of the switching mechanism from HRS to LRS. e) *I–V* characteristics at 73° angle after several bending cycles (1, 100, 250, 500, and 1000 cycles). Reproduced with permission.[239c] Copyright 2024, American Chemical Society. f) Operating principle circuit and ionic distribution diagram of the MXene-based device. g) Monitored PSC under several successive voltage pulses. The blue and red lines indicate repression and potentiation processes, respectively. h) Schematic illustration of the constructed ANN for handwritten digit classification. Reproduced with permission.[256] Copyright 2022, Oxford University Press.

behaviors exhibit remarkable linearity across various resistance states (Figure 11g), facilitating the construction of neuromorphic computing systems. By incorporating an MXene-supercapacitor for weight storage and an adjustable resistance for synaptic performance modulation, the synaptic device enables adaptive approaches to construct ANN with intricate synaptic capabilities and operational modes. Through training and machine learning algorithms, adaptive handwritten number classification achieves a recognition accuracy of 95% based on ANN (Figure 11h). Despite the lack of mechanical property tests, this device presents a pioneering approach for leveraging flexible, self-adaptive, and highly precise neuromorphic computational networks.

The afferent nervous system (ANS) plays a significant role in organisms perceiving external stimuli, where synapses and hub points in nerve fibers relay neural signals from receptors to central nerves.[264] With rich functional groups on its surface, MXenes are suitable for ionic conduction in developing ANS. In 2021, Wang et al. constructed a flexible biomimetic ANS device, integrating $Ti_3C_2T_x$ artificial synapse with an ion conductive elastomer (ICE), as shown in **Figure 12a**.[257a] The internal porous network structure of ionic elastomer, shown in Figure 12b, exhibits a significant tactile response. The MXene-$Ti_3C_2T_x$ film reduces ion migration dispersity of the ICE layer, thereby increasing the signal-to-noise ratio and generating more

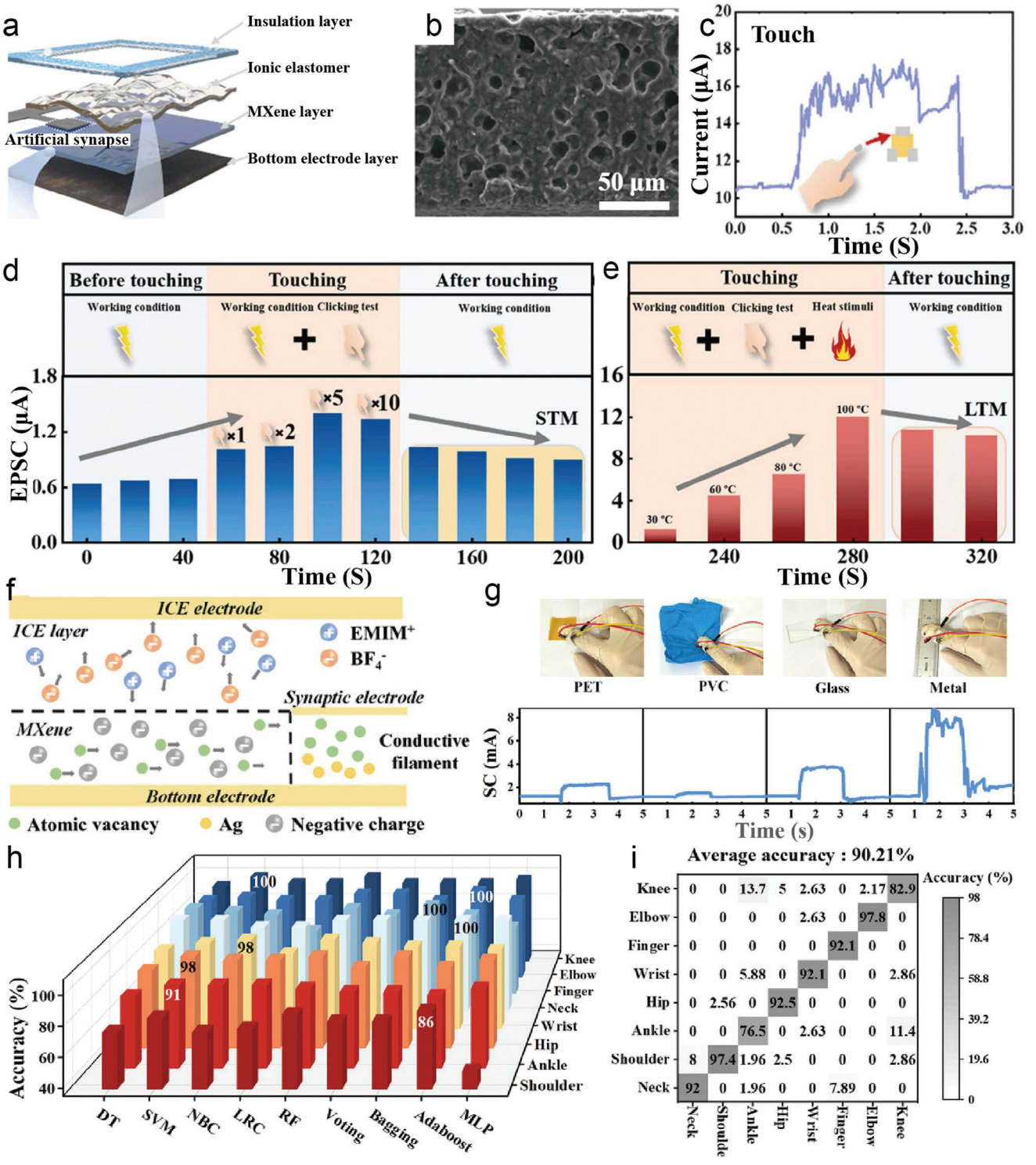

Figure 12. Two-terminal MXene-based flexible artificial ANS. a) Schematic of biomimetic ANS based on MXene layer. b) Cross-section SEM image of ionic elastomer with internal 3D porous network. c) Response current of the ICE layer for touch actions. d,e) EPSC in the first training stage (d) and the second personal experience stage (e), emulated by clicking test and heat stimuli. Reproduced with permission.[257a] Copyright 2023, Elsevier. f) Schematic illustration of the working mechanism of the proposed ANS device. g) Illustration of current response signals when contacting different materials like PET, polyvinyl chloride (PVC), glass, and metal. h) Accuracies at eight joints of nine machine learning methods. The highest accuracies of each joint for recognizing motion degrees are marked. i) The confusion matrix of different positions of moving joints (motion recognition), indicating an average accuracy of 90.21%. Reproduced with permission.[257b] Copyright 2023, Wiley-VCH.

stable PSC. The MXene-based flexible ANS device exhibited good reliability after 1000 bending cycles and could generate a stable electronic response to real body motions, such as touch (Figure 12c), making them a strong candidate for constructing ANS. Furthermore, the device emulated "operant conditioned reflex behavior" through classical "trial and error learning," which is stimulated by actual clicking action and heat exposure. In the first training stage (Figure 12d), EPSCs enhanced from 1.0 to 1.4 μA in a length-by-length manner, triggered by 10 repetitive clicks; once clicking action ceased, EPSCs returned to around 1.0 μA, reflecting short-term memory (STM). In the second stage named personal experience (Figure 12e), the introduction of heat stimuli increased EPSCs from 1 to 12 μA, which remained stable at ≈12 μA with continuous contact with a hot object, simulating transition to long-term memory (LTM). This experiment connects artificial synapses to real-world external stimuli, offering possibilities for AI robots and tactile neuromorphic chips. Additionally, this device enabled gesture and motion recognition using the same flexible ANS.[257b] This device operates based on the mechanism of migration-modulated MXene synapse CF model (Figure 12f). The distributions of positive and negative ions in the ICE can be dynamically modified by external stimuli, leading to the expulsion or attraction of charged vacancies within the MXene layer, resulting in the formation of CFs. Utilizing the multimodal sensitivity of the synapse to pressure, temperature, and deformation, the ANS device could distinguish between various materials (e.g., PET, PVC, glass, metal) (Figure 12g), achieving an average recognition accuracy of 80%. The integration of multimode sensitivity and nine machine learning algorithms was further expanded to eight limb joints for motion recognition (Figure 12h), attaining an average accuracy of 90.21%, with the optimal machine learning algorithm (AdaBoost) (Figure 12i). Thus, this synapse-based ANS, with its low power consumption, may serve as a viable alternative to conventional ANS strategy.

MXenes, with excellent conductivity, large specific surface area, and partial auto-oxidation properties, are promising sensing materials for flexible stimuli-responsive sensors.[265] For instance, leveraging the large specific surface area and partial auto-oxidation properties, Zeng et al. prepared oxidized MXene (O-MXene) by heating diluted pure MXene at 60 °C for 24 hours.[266] This process endowed the material with photoresponse to 365 nm light. Subsequently, a $Ti_3C_2T_x$ MXene-based optoelectronic memristor was demonstrated, capable of efficiently emulating synaptic functions through the coordination of light and electrical stimulation. This highlights the application potential of MXene for developing multifunctional and high-performance optoelectronic neuromorphic systems. For flexible applications, Wang et al. developed a flexible multimode ITO/Ti_3C_2-ZnO/Al/PDMS sensory memristor in 2021 (**Figure 13a**), capable of sensing both visual data and relative humidity, while also performing preprocessing functions that realize environmental adaptability simulation of the neuromorphic visual system.[258] Compared to the pure ZnO-based memristor, the Ti_3C_2-ZnO memristor, optimized for Zn/Ti atomic ratio, exhibited a larger ON/OFF ratio (10^4) and a lower V_{SET} (–0.4 V), thereby enhancing resistive state identification and providing stable information storage properties. XPS analysis of the MXene-ZnO revealed distinct differences in the TiO_2 2p signal between the HRS and LRS (Figure 13b), suggesting oxygen ion migration and subsequent formation of CFs after the SET operation, as illustrated in Figure 13c. The stability of current readings was confirmed over 400 bending cycles, indicating potential for flexible applications. MXene-ZnO devices were employed in neuromorphic visual systems with humidity-adaptability to sense as well as preprocess raw data, showcasing emulation of retinal functionality. Preprocessed information was transmitted to the ANN (784 × 25 × 10) for training in recognition tasks, as depicted in Figure 13d. Capitalizing on the high accuracy of the image preprocessing system with the MXene-ZnO memristor (Figure 13e), the researchers demonstrated an artificial retina sensing system for preprocessing information and implementing a weight updating process. Consequently, MXene composites exhibit potential applications in developing flexible and intelligent neuromorphic visual systems at the device level.

Recently, leveraging the exceptional mechanical properties of MXenes, Huang et al. developed an all-MXene near-sensing memory computing system by directly integrating a flexible MXene-based pressure sensor array (3 × 3) with a flexible MXene-based memristor array (9 × 3) to capture tactile signals and simulate perceived behaviors.[259] As shown in Figure 13f, tactile signals are transmitted from the sensor unit (MXene-based pressure sensor) to the artificial neural synapse unit (MXene-based memristor). The memristor array, featuring an Ag/TiO_x/$Ti_3C_2T_x$/Au crossbar structure on a PI substrate, exhibited good memory retention (>100 cycles) and endurance (>10^3 s) under bending conditions (R = 1.0 mm). The tactile perception processing system is illustrated in Figure 13g,h, which inputs data collected by MXene-based pressure sensors into an ANN constructed with MXene-based memristors. This ANN comprises six input neurons, nine hidden neurons, and four output neurons corresponding to four human respiratory states (apnea, bradypnea, eupnea, tachypnea), achieving a classification accuracy of 93.21%. This advancement represents a significant contribution toward next-generation robotics skins and wearable electronic devices.

In the context of three-terminal flexible synaptic devices, 2D MXenes can function as both FG and channel materials benefiting from their layered structure, exceptional conductivity, and adjustable surface chemistry.[267] Oxidation-induced TiO_2 layer that serves directly as a high-k tunneling layer, combined with a tunable work function of $Ti_3C_2T_x$ MXenes, enables MXenes to function as effective FGs.[268] For example, Kim et al. presented an electrolyte-gated graphene FET with a flexible PEN substrate with shell-like $Ti_3C_2T_x$/TiO_2 nanoflakes serving as the FG (**Figure 14a**).[260] The surface oxidations are controlled (50 °C, 120 min) so that metallic $Ti_3C_2T_x$ is surrounded by ≈6 nm of TiO_2 shell. The device exhibited ambipolar transfer characteristics with an apparent hysteresis loop, attributed to sluggish ionic motion caused by both the ion-gel and charge trapping/de-trapping processes in the $Ti_3C_2T_x$/TiO_2 nanoflakes. Due to the sluggish movement of ions caused by ion gels and charge capture/de-trapping processes in $Ti_3C_2T_x$/TiO_2 nanosheets, the device showed bipolar transfer characteristics with apparent hysteresis loops. As depicted in Figure 14b, this device underwent mechanical bending cycles under repeated flat and bending conditions (R = 4.62 mm). After 1000 bending cycles, it demonstrated exceptional retention characteristics and LTP behaviors akin to those observed in the initial state, indicating promising applications for constructing flexible neuromorphic computing

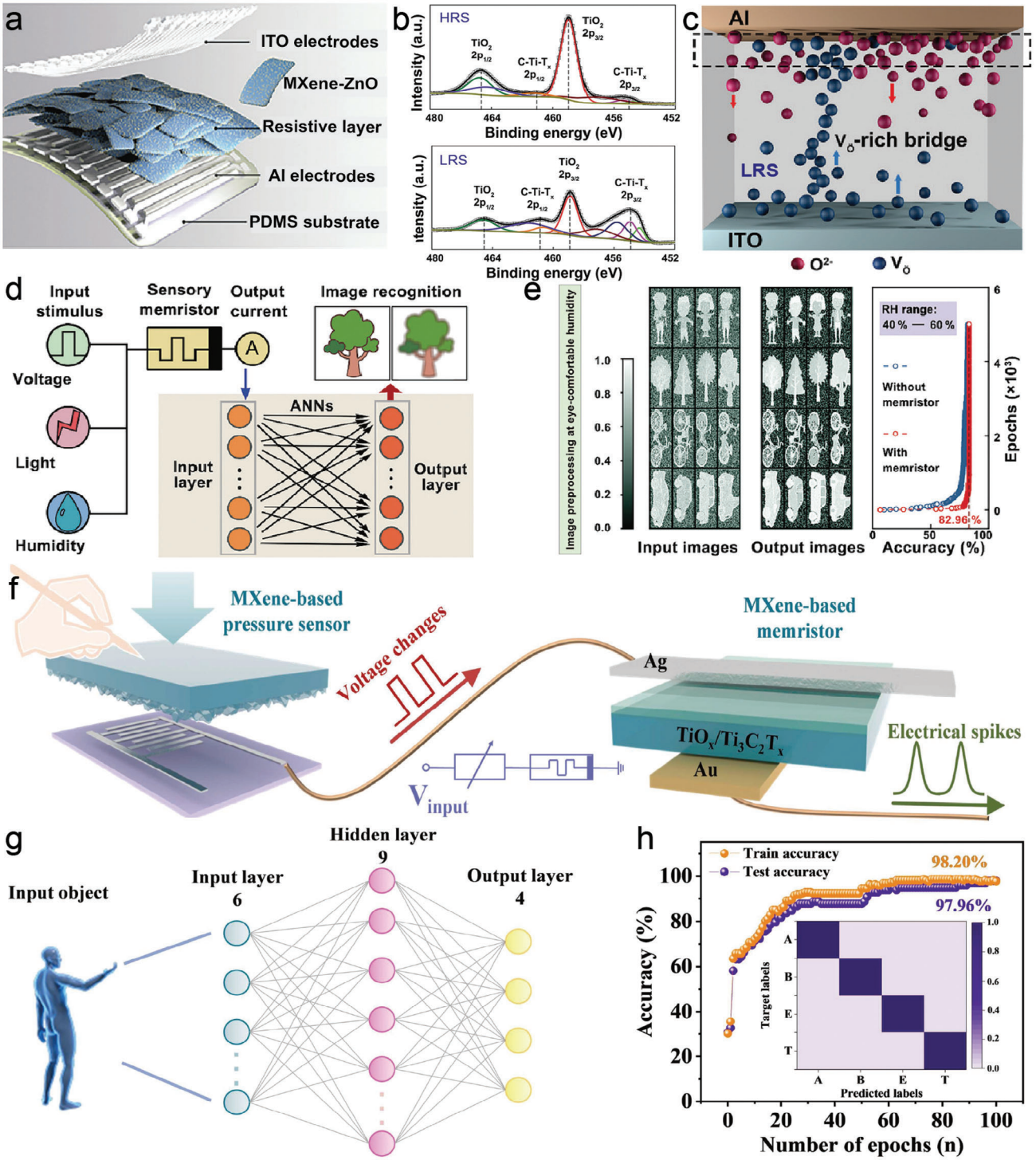

Figure 13. Two-terminal MXene-based flexible devices for in- and near-sensor computing. a) Structure diagram of the memristor with MXene-ZnO as a resistive layer. b) Ti 2p XPS of MXene-ZnO with fitted peaks of the HRS (top) and LRS (bottom). c) Distribution diagram of oxygen ion and vacancy in the LRS of the memristor, and the dash line shallows the depth of the resistive layer) (O^{2-}: oxygen ion; and $V_{ö}$: oxygen vacancy). d) Schematic diagram of the processing system employing the memristor to sense information and suppress/filter noises. e) Image preprocessing by enhancement and denoising under eye-comfortable humidity conditions. Left panel: the contrast between input and output image, with the latter derived from curve fitting based on different light intensities of electric current. Right panel: comparison of the image recognition rates of the preprocessed and unpreprocessed artificial retina sensing system. Reproduced with permission.[258] Copyright 2021, Wiley-VCH. f) Connection circuit illustration of all-MXene sensory neuron. g) Schematic diagram of the ANN with six input, nine hidden, and four output layer neurons for classifying human respiratory state. h) Recognition accuracy of train and test processes, with an inset showing the confusion matrix of four human respiratory states. Reproduced with permission.[259] Copyright 2024, Elsevier.

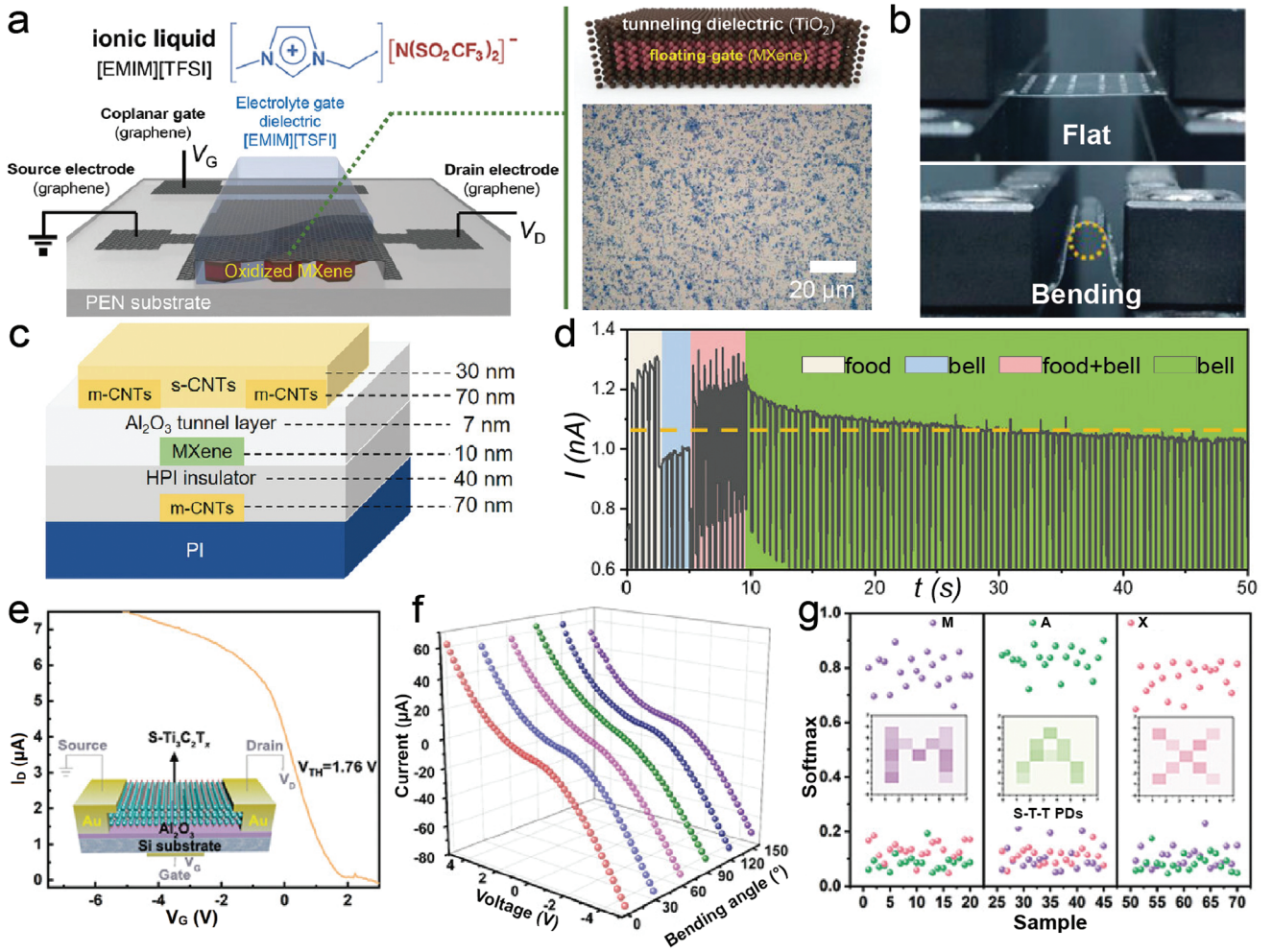

Figure 14. Three-terminal MXene-based flexible neuromorphic devices. a) Left panel: Structure diagram of the synaptic transistor featuring $Ti_3C_2T_x/TiO_2$ nanoflakes as an FG. Right panel: structure illustration and optical microscope image of $Ti_3C_2T_x/TiO_2$ nanoflakes. b) Photographic image of the device at a flat and bending state. Reproduced with permission.[260] Copyright 2022, Wiley-VCH. c) Structure diagram of the Ti_3C_2F-based FGT. d) Pavlovian associative learning behavior emulated by the FGT under the bending state (R = 6 mm). Reproduced with permission.[261] Copyright 2024, Wiley-VCH. e) Transfer curve of the S-$Ti_3C_2T_x$ transistor (inset: structure diagram of the device). f) I_{DS} response of the S-$Ti_3C_2T_x$ transistor to V_{DS} under different bending angles. g) Probability diagram of the letter ("M," "A," and "X") recognition rate based on the S-$Ti_3C_2T_x$/$Ti_3C_2T_x$-based artificial vision sensory-neuromorphic system. The output classification of softmax function was displayed in the form of probability (0–1) of the sample collected. Reproduced with permission.[109] Copyright 2023, Wiley-VCH.

systems. Additionally, Ti_3C_2F can also serve as FG for fabricating synaptic transistors (Figure 14c).[261] This device maintained its performance (e.g., transfer characteristic) without significant degradation after 1000 bending cycles, showcasing commendable mechanical flexibility and durability. Furthermore, under bending conditions (R = 6 mm), this MXene-based synaptic transistor can effectively emulate a Pavlovian experiment (Figure 14d). The device was also applied for handwritten digit recognition, achieving a high recognition accuracy of 92.0%.

Because of their narrow band gap (0–0.1 eV),[181] common $Ti_3C_2T_x$ MXenes with –F, –OH, and –O terminations are unsuitable to be directly used as photosensitive material. To open the band gap and enhance the optical applications of MXene in flexible vision sensory-neuromorphic system, Hu et al. prepared semiconducting MXene (S-$Ti_3C_2T_x$) by linking phenyl sulfonic acid groups (-phSO_3H) with metallic $Ti_3C_2T_x$.[109] Utilizing S-$Ti_3C_2T_x$ as the channel material, the resulting transistors demonstrated a gate voltage regulation effect, as demonstrated in Figure 14e, with a V_{th} of 1.76 V, indicating the opening of band gap. Additionally, by employing S-$Ti_3C_2T_x$ as the photosensitive material and unmodified $Ti_3C_2T_x$ as electrodes, a "full MXene" device was fabricated, exhibiting excellent flexibility and mechanical stability (Figure 14f). Based on this "full MXene" imagine sensor array, a flexible artificial vision sensory-neuromorphic system was constructed to perform image recognition, like human eyes. (Figure 14g).

MXene-based flexible neuromorphic systems exhibit significant advantages, including low power consumption, exceptional mechanical flexibility, and high pattern recognition accuracy. However, limitations in device integration fabrication contribute to pose challenges for their further development. Current research on MXene-based transistor-type devices remains nascent,

highlighting the need for exploration into the potential of MXenes as semiconductor, FG, and electrode materials in various applications. Addressing these challenges will expand potential applications of MXene-based devices, particularly in fields like smart wearable devices, robotics, and high-performance computing.

5. Challenges and Outlook

In summary, this review comprises 1) the basic principles of flexible memory and neuromorphic devices, involving operation mechanisms, synaptic plasticity, common parameters, and common flexible materials, 2) the brief presentation of the structure, synthesis approaches, and distinct properties of MXenes, and 3) the most recent research works concerning MXene-based flexible memory and neuromorphic devices. Undoubtedly, 2D MXenes exhibit distinctive advantages and diverse functionalities that should not be underestimated. Therefore, they provide various novel inspirations for flexible memory and neuromorphic devices. Through a comprehensive understanding of MXenes, it is possible not only to identify domains with significant development potential but also to establish a theoretical foundation for optimizing their structure and functionality. Despite notable advancements, current research on MXenes remains nascent with numerous challenges that necessitate resolution.

First, the synthesis of MXenes and their structure–performance relationship necessitates further exploration. Chemical etching is a prevailing approach for MXene synthesis but necessitates enhancement due to its employment of corrosive solvents or low yield of MXene flakes. Therefore, the future of the synthesis needs to be green, easy, low-cost, high-yield, and high-quality. Additionally, most reported devices are based on $Ti_3C_2T_x$ MXene, so further efforts are needed to develop novel MXenes with improved properties. Furthermore, understanding the impact of different material structures on MXene properties and investigating the ramifications of various synthesis methods are crucial. For instance, the stability of flexible devices is crucial; however, the surface-active functional groups make them susceptible to oxidation in humid environments. Hence, the enhancement of MXene oxidation resistance during nanostructure integration should be explored. For instance, employing dry nitrogen to evacuate dissolved oxygen and maintaining MXenes at reduced temperatures serves as a potent strategy to decelerate their oxidation process. Additionally, the lack of comprehensive insight into the impact of surface termination on MXene functional properties calls for a systematic study. The investigation of appropriate surface engineering techniques considering the type, concentration, and distribution of surface functional groups, plays a vital role in enhancing stability as well as other physicochemical properties of MXenes. With unique structures and hydrophilicity, MXene nanosheets provide solid foundations for integrating other 2D materials or polymers to fabricate composite materials, indicating the potential of composite-based flexible devices with broader applications and enhanced properties like lower power consumption. Additionally, the exceptional optical properties of MXene QDs (MQDs) have garnered significant attention in optoelectronic applications, especially as water-soluble polymer dispersants and charge-trapping centers within active layers.[269] Hybrid MQDs-polymer hybrid architectures could enable the development of flexible optoelectronic devices for neuromorphic computing.[270]

Second, in terms of device performance, innovative designs of flexible devices are crucial. While flexible devices have made significant progress, challenges remain in terms of efficiency, durability, sensitivity, and complexity. Maintaining a balance between mechanical attributes like strength, toughness, and flexibility, alongside electrochemical characteristics remains a test in the fabrication of flexible electronics. Although performances have improved, current devices are not yet capable of competing with their rigid counterparts in terms of features and performance. As many prior studies have indicated that the mechanism/principle of devices are influenced by all their constituent parts, gaining a comprehensive insight into how the influence mechanisms of MXene- or MXene-composite-based devices affect performance is crucial for advancing the field further. Beyond the development of novel materials, there is a need for novel device designs and advances in existing flexible electronics. Additionally, the lack of comparable parameters and non-standard testing protocols from different studies creates significant challenges. Therefore, universal evaluating standards and testing protocols to quantify flexible devices are urgently needed to accelerate the development of flexible electronic technologies. In most proof-of-concept studies, memristors typically adopt a common BE-based RS structure.[271] Future lateral and vertical MXene-based flexible devices are expected to operate at higher integration density, significantly reduced footprint, faster switching speeds, and lower power consumption.[91] Scaling down the feature size of MXene-based devices enables the construction of high-density, large-scale crossbar arrays, which is crucial for complex neural networks utilized in real-world applications.[272] Last but not least, the quest for energy efficiency in ANN systems that can match their biological equivalents, consuming as little as femtojoules per operation, remains a significant challenge. In many reported literature, energy/power consumption is frequently overlooked, calling for a more thorough evaluation in subsequent investigations.

Third, in terms of the application, MXene-based flexible devices offer diverse prospects for practical uses. MXenes face challenges such as patterning, which complicates device integration and fabrication. As a result, current MXene-based devices still exhibit significant gaps that hinder practical commercial applications. Most studies focus solely on utilizing devices with different MXene materials and device structures to simulate common synaptic behaviors, lacking the capabilities to fully replicate the complex functions of the human brain. The issue arises because these flexible systems fail to have the required level of functionality and performance needed to facilitate complex biological behaviors, warranting further investigation. Additionally, a promising research direction involves constructing flexible optoelectronic neuromorphic devices by leveraging previous findings that demonstrate enhanced optical response intensity through partially oxidized MXene FGs.[268] The exceptional bio-compatibility of MXenes also holds great potential for future applications. The single-function or dual-function nature of devices generally fails to suffice for replicating the intricate behaviors found in BNNs. Hence, there is an urgent need to facilitate devices' collaborative interaction to build adaptable artificial neural systems. The

fabrication of memristor/transistor arrays has become a focal point, representing a critical milestone toward the achievement of future neuromorphic computing systems. Exploring highly integrated MXene-based neuromorphic computing-assisted flexible tactile sensors also offers unconventional possibilities for advanced soft robotics and intelligent interactive equipment, such as human-machine interfaces,[273] AI interaction.[241] For AI-enabled tactile sensing applications, MXene-based neuromorphic computing systems have already demonstrated the recognition of complex handwritten input signals by ANN. Therefore, it's a promising approach to actualizing realistic sensory interaction systems for telemedicine, education, entertainment, etc.[241] Integrating sensors with MXene-based neuromorphic devices to fabricate sensory perception systems based on spiking neural networks (SNN) is also a fascinating direction of research.

In conclusion, the development of MXene-based flexible memory and neuromorphic devices is progressing rapidly. Future progress in this domain is anticipated to emerge from the convergence of materials science, device fabrication, and system architecture. The continuous advancement of technology and the growing demand for flexible devices are expected to expedite their transition from laboratory research to large-scale manufacturing. Flexible MXene-based devices are poised to play pivotal roles in data storage, synaptic function emulation, and neuromorphic computing. With ongoing breakthroughs in key technologies such as patterning, MXene-based flexible memory and neuromorphic devices will significantly contribute to advancing next-generation information technology and facilitating device-level implementations in AI applications.

Acknowledgements

The authors acknowledge grants from the National Natural Science Foundation of China (Grant No. 62304137, 62122055, and 62074104), the Guangdong Basic and Applied Basic Research Foundation (Grant Nos. 2023A1515012479, 2024A1515011737, 2024A1515010006, and 2024B1515040002), the Science and Technology Innovation Commission of Shenzhen (Grant No. JCYJ20220818100206013), the RSC Researcher Collaborations Grant (Grant No. C23-2422436283), the State Key Laboratory of Radio Frequency Heterogeneous Integration (Independent Scientific Research Program No. 2024010), and the NTUT-SZU Joint Research Program.

Conflict of Interest

The authors declare no conflict of interest.

Keywords

flexible electronics, memory, MXenes, neuromorphic computing, synaptic devices

Received: November 15, 2024
Revised: January 21, 2025
Published online:

[1] X. Chen, B. Chen, P. Zhao, V. A. L. Roy, S.-T. Han, Y. Zhou, *Mater. Futures* **2023**, *2*, 023501.
[2] Q. Cao, W. Lü, X. R. Wang, X. Guan, L. Wang, S. Yan, T. Wu, X. Wang, *ACS Appl. Mater. Interfaces* **2020**, *12*, 42449.
[3] a) H. Zhang, X. Ju, H. Jiang, D. Yang, R. Wei, W. Hu, X. Lu, M. Zhu, *Sci. China Mater.* **2024**, *67*, 1907; b) R. Fang, W. Zhang, K. Ren, P. Zhang, X. Xu, Z. Wang, D. Shang, *Mater. Futures* **2023**, *2*, 022701.
[4] a) H. Seok, D. Lee, S. Son, H. Choi, G. Kim, T. Kim, *Adv. Electron. Mater.* **2024**, *10*, 2300839; b) X. Lian, X. Shen, J. Fu, Z. Gao, X. Wan, X. Liu, E. Hu, J. Xu, Y. Tong, *Electronics* **2020**, *9*, 2098.
[5] a) E. E. Schadt, M. D. Linderman, J. Sorenson, L. Lee, G. P. Nolan, *Nat. Rev. Genet.* **2010**, *11*, 647; b) Y. Wang, Q. Sun, J. Yu, N. Xu, Y. Wei, J. H. Cho, Z. L. Wang, *Adv. Funct. Mater.* **2023**, *33*, 2305791.
[6] a) T. Jin, J. Gao, Y. Wang, W. Chen, *Sci. China Mater.* **2022**, *65*, 2154; b) J. Pan, T. Wu, W. Yang, Y. Li, J. Zhang, H. Kan, *Sci. China Mater.* **2024**, *67*, 2838.
[7] a) Y. Guo, X. Wei, S. Gao, W. Yue, Y. Li, G. Shen, *Adv. Funct. Mater.* **2021**, *31*, 2104288; b) W. Wang, S. Gao, Y. Li, W. Yue, H. Kan, C. Zhang, Z. Lou, L. Wang, G. Shen, *Adv. Funct. Mater.* **2021**, *31*, 2101201; c) C. Zang, B. Li, Y. Sun, S. Feng, X.-Z. Wang, X. Wang, D.-M. Sun, *Nanoscale Adv.* **2022**, *4*, 5062.
[8] a) C.-H. Kim, S. Lim, S. Y. Woo, W.-M. Kang, Y.-T. Seo, S.-T. Lee, S. Lee, D. Kwon, S. Oh, Y. Noh, H. Kim, J. Kim, J.-H. Bae, J.-H. Lee, *Nanotechnology* **2019**, *30*, 032001; b) N. Youngblood, C. A. Ríos Ocampo, W. H. P. Pernice, H. Bhaskaran, *Nat. Photonics* **2023**, *17*, 561.
[9] a) X. Qi, W. Yin, S. Jin, A. Zhou, X. He, G. Song, Y. Zheng, Y. Bai, *J. Adv. Ceram.* **2022**, *11*, 273; b) Y. Zhu, H. Mao, Y. Zhu, X. Wang, C. Fu, S. Ke, C. Wan, Q. Wan, *Int. J. Extreme Manuf.* **2023**, *5*, 042010.
[10] S. W. Cho, S. M. Kwon, Y.-H. Kim, S. K. Park, *Adv. Intell. Syst.* **2021**, *3*, 2000162.
[11] D. Kuzum, S. Yu, H. S. Philip Wong, *Nanotechnology* **2013**, *24*, 382001.
[12] W. S. Wang, L. Q. Zhu, *Sci. Technol. Adv. Mater.* **2023**, *24*, 2152290.
[13] S. Wang, D. W. Zhang, P. Zhou, *Sci. Bull.* **2019**, *64*, 1056.
[14] Z. Zhang, G. Tian, J. Huo, F. Zhang, Q. Zhang, G. Xu, Z. Wu, Y. Cheng, Y. Liu, H. Yin, *Sci. China Inf. Sci.* **2023**, *66*, 200405.
[15] C. Choi, J. Leem, M. Kim, A. Taqieddin, C. Cho, K. W. Cho, G. J. Lee, H. Seung, H. J. Bae, Y. M. Song, T. Hyeon, N. R. Aluru, S. Nam, D.-H. Kim, *Nat. Commun.* **2020**, *11*, 5934.
[16] Y. Xie, S. C. Kundu, S. Fan, Y. Zhang, *Sci. China Mater.* **2024**, *67*, 3675.
[17] C. Yang, X. Hou, L. Zhang, *Mater. Futures* **2024**, *3*, 032401.
[18] a) A. Rani, J.-M. Song, M. Jung Lee, J.-S. Lee, *Appl. Phys. Lett.* **2012**, *101*, 233308; b) C. Wang, C. Wang, Z. Huang, S. Xu, *Adv. Mater.* **2018**, *30*, 1801368.
[19] J. Y. Lee, J. E. Ju, C. Lee, S. M. Won, K. J. Yu, *Int. J. Extreme Manuf.* **2024**, *6*, 042005.
[20] M.-K. Kim, J.-S. Lee, *ACS Appl. Mater. Interfaces* **2018**, *10*, 10280.
[21] a) G. Nagasarvari, N. M. Nair, S. D. Ranade, L. Neelakantan, P. Swaminathan, *Flex. Print. Electron.* **2023**, *8*, 045004; b) C. Liu, D. Zhang, J. Sun, D. Li, Q. Xiong, B. Lyu, W. Guo, W. C. H. Choy, *Adv. Funct. Mater.* **2024**, *34*, 2404791; c) Q. Lin, Y. Zhu, Y. Wang, D. Li, Y. Zhao, Y. Liu, F. Li, W. Huang, *Adv. Mater.* **2023**, *35*, 2210385; d) S. Lim, J. W. Suk, *J. Phys. D Appl. Phys.* **2023**, *56*, 063001.
[22] a) M. Osada, T. Sasaki, *Adv. Mater.* **2012**, *24*, 210; b) G. Cao, P. Meng, J. Chen, H. Liu, R. Bian, C. Zhu, F. Liu, Z. Liu, *Adv. Funct. Mater.* **2021**, *31*, 2005443; c) Z. Zhou, F. Yang, S. Wang, L. Wang, X. Wang, C. Wang, Y. Xie, Q. Liu, *Front. Phys.* **2021**, *17*, 23204; d) H. Zhou, S. Li, K.-W. Ang, Y.-W. Zhang, *Nano-Micro Lett.* **2024**, *16*, 121.
[23] a) J. Xu, J. Shim, J.-H. Park, S. Lee, *Adv. Funct. Mater.* **2016**, *26*, 5328; b) M. Naguib, M. Kurtoglu, V. Presser, J. Lu, J. J. Niu, M. Heon, L. Hultman, Y. Gogotsi, M. W. Barsoum, *Adv. Mater.* **2011**, *23*, 4248.
[24] S. Ling, C. Zhang, C. Ma, Y. Li, Q. Zhang, *Adv. Funct. Mater.* **2023**, *33*, 2208320.
[25] A. Shayesteh Zeraati, S. A. Mirkhani, P. Sun, M. Naguib, P. V. Braun, U. Sundararaj, *Nanoscale* **2021**, *13*, 3572.

[26] A. Lipatov, M. Alhabeb, H. Lu, S. Zhao, M. J. Loes, N. S. Vorobeva, Y. Dall'Agnese, Y. Gao, A. Gruverman, Y. Gogotsi, A. Sinitskii, *Adv. Electron. Mater.* **2020**, *6*, 1901382.
[27] K. Maleski, C. E. Shuck, A. T. Fafarman, Y. Gogotsi, *Adv. Opt. Mater.* **2021**, *9*, 2001563.
[28] S. Han, Y. Chen, Y. Hao, Y. Xie, D. Xie, Y. Chen, Y. Xiong, Z. He, F. Hu, L. Li, J. Zhu, S. Peng, *Sci. China Mater.* **2021**, *64*, 1127.
[29] a) Z. Zhao, K. Xia, Y. Hou, Q. Zhang, Z. Ye, J. Lu, *Chem. Soc. Rev.* **2021**, *50*, 12702; b) M. Z. Zhang, D. G. Jiang, F. H. Jin, Y. S. Sun, J. H. Wang, M. Y. Jiang, J. Y. Cao, B. Zhang, J. Q. Liu, *J. Colloid Interface Sci.* **2023**, *636*, 204; c) W. Liu, C. Hu, L. Li, G. Shen, *ACS Appl. Energy Mater.* **2023**, *6*, 7387; d) W. Luo, Y. Wei, Z. Zhuang, Z. Lin, X. Li, C. Hou, T. Li, Y. Ma, *Electrochim. Acta* **2022**, *406*, 139871; e) C. Zhang, B. Anasori, A. Seral-Ascaso, S.-H. Park, N. McEvoy, A. Shmeliov, G. S. Duesberg, J. N. Coleman, Y. Gogotsi, V. Nicolosi, *Adv. Mater.* **2017**, *29*, 1702678.
[30] a) T. T. He, W. Liu, T. Lv, M. S. Ma, Z. F. Liu, A. Vasiliev, X. G. Li, *Sens. Actuators, B* **2021**, *329*, 129275; b) H. Riazi, G. Taghizadeh, M. Soroush, *ACS Omega* **2021**, *6*, 11103; c) R. Bhardwaj, A. Hazra, *J. Mater. Chem. C* **2021**, *9*, 15735; d) B. Xu, M. Zhu, W. Zhang, X. Zhen, Z. Pei, Q. Xue, C. Zhi, P. Shi, *Adv. Mater.* **2016**, *28*, 3333; e) L. Wang, M. Zhang, B. Yang, J. Tan, X. Ding, W. Li, *Small Methods* **2021**, *5*, 2100409.
[31] a) X. Ming, A. K. Guo, Q. Zhang, Z. Z. Guo, F. Yu, B. F. Hou, Y. Wang, K. P. Homewood, X. B. Wang, *Carbon* **2020**, *167*, 285; b) X. Q. Xie, C. Chen, N. Zhang, Z. R. Tang, J. J. Jiang, Y. J. Xu, *Nat. Sustain.* **2019**, *2*, 856.
[32] W. Kong, J. X. Deng, L. H. Li, *J. Mater. Chem. A* **2022**, *10*, 14674.
[33] a) X. Meng, L. Wang, X. Wang, M. Zhen, Z. Hu, S.-Q. Guo, B. Shen, *Chemosphere* **2023**, *338*, 139550; b) X.-Q. Tan, W. Mo, X. Lin, J. Y. Loh, A. R. Mohamed, W.-J. Ong, *Nanoscale* **2023**, *15*, 6536; c) N. Kitchamsetti, A. L. F. de Barros, *ChemCatChem* **2023**, *15*, 202300690; d) P. Kuang, J. Low, B. Cheng, J. Yu, J. Fan, *J. Mater. Sci. Technol.* **2020**, *56*, 18.
[34] a) J. Li, L. H. Xu, H. Pan, L. M. Wang, Y. Shen, *Nano* **2023**, *18*, 2350051; b) T. Yun, H. Kim, A. Iqbal, Y. S. Cho, G. S. Lee, M. K. Kim, S. J. Kim, D. Kim, Y. Gogotsi, S. O. Kim, C. M. Koo, *Adv. Mater.* **2020**, *32*, 1906769; c) N. Wu, B. Li, F. Pan, R. Zhang, J. Liu, Z. Zeng, *Sci. China Mater.* **2023**, *66*, 1597.
[35] a) X. Lian, Y. Shi, X. Shen, X. Wan, Z. Cai, L. Wang, *Chin. J. Electron.* **2024**, *33*, 336; b) A. C. Khot, T. D. Dongale, J. H. Park, A. V. Kesavan, T. G. Kim, *ACS Appl. Mater. Interfaces* **2021**, *13*, 5216.
[36] a) G. Ding, B. Yang, R.-S. Chen, K. Zhou, S.-T. Han, Y. Zhou, *Appl. Phys. Rev.* **2021**, *8*, 011316; b) L. Bharali, J. Kalita, S. S. Dhar, *ChemistrySelect* **2023**, *8*, 202301486; c) J. Xu, T. Peng, X. Qin, Q. Zhang, T. Liu, W. Dai, B. Chen, H. Yu, S. Shi, *J. Mater. Chem. A* **2021**, *9*, 14147; d) X. Lian, Y. Shi, S. Li, B. Ding, C. Hua, L. Wang, *Contemp. Phys.* **2023**, *63*, 87.
[37] C. Zhang, Y. Li, C. Ma, Q. Zhang, *Small Sci.* **2022**, *2*, 2100086.
[38] F. Gul, Y. Babacan, *Microelectron. Eng.* **2018**, *194*, 56.
[39] Y. Cao, S. Wang, R. Wang, Y. Xin, Y. Peng, J. Sun, M. Yang, X. Ma, L. Lv, H. Wang, Y. Hao, *Sci. China Mater.* **2023**, *66*, 1569.
[40] L. Lv, P. Zhang, X. Yang, H. Wan, G. Ma, H. Wang, *Surf. Interfaces* **2024**, *44*, 103678.
[41] F. Nie, J. Wang, H. Fang, S. Ma, F. Wu, W. Zhao, S. Wei, Y. Wang, L. Zhao, S. Yan, C. Ge, L. Zheng, *Mater. Futures* **2023**, *2*, 035302.
[42] X. Shan, Y. Lin, Z. Wang, X. Zhao, Y. Tao, H. Xu, Y. Liu, *Mater. Futures* **2024**, *3*, 012701.
[43] a) D. B. Strukov, G. S. Snider, D. R. Stewart, R. S. Williams, *Nature* **2008**, *453*, 80; b) R. Waser, R. Dittmann, G. Staikov, K. Szot, *Adv. Mater.* **2009**, *21*, 2632.
[44] a) M. Zhao, B. Gao, J. Tang, H. Qian, H. Wu, *Appl. Phys. Rev.* **2020**, *7*, 011301; b) Z. Wang, H. Wu, G. W. Burr, C. S. Hwang, K. L. Wang, Q. Xia, J. J. Yang, *Nat. Rev. Mater.* **2020**, *5*, 173.
[45] D. Kim, I.-J. Kim, J.-S. Lee, *Adv. Intell. Syst.* **2021**, *3*, 2000206.
[46] J. Bian, Z. Liu, Y. Tao, Z. Wang, X. Zhao, Y. Lin, H. Xu, Y. Liu, *Int. J. Extreme Manuf.* **2024**, *6*, 012002.
[47] F. Pan, S. Gao, C. Chen, C. Song, F. Zeng, *Mater. Sci. Eng. R Rep.* **2014**, *83*, 1.
[48] W. Deng, X. Yan, L. Wang, N. Yu, W. Luo, L. Mai, *Nano Energy* **2024**, *128*, 109861.
[49] C. Gu, H.-W. Mao, W.-Q. Tao, Z. Zhou, X.-J. Wang, P. Tan, S. Cheng, W. Huang, L.-B. Sun, X.-Q. Liu, J.-Q. Liu, *ACS Appl. Mater. Interfaces* **2019**, *11*, 38061.
[50] J. Zhao, F. Liu, Q. Huang, T. Lu, M. Xi, L. Peng, X. Liang, *Nano Res.* **2021**, *14*, 4258.
[51] K. Lee, M. Weis, X. Chen, D. Taguchi, T. Manaka, M. Iwamoto, *Thin Solid Films* **2014**, *554*, 189.
[52] D. Li, B. Wu, X. Zhu, J. Wang, B. Ryu, W. D. Lu, W. Lu, X. Liang, *ACS Nano* **2018**, *12*, 9240.
[53] a) B. Hwang, J.-S. Lee, *Adv. Electron. Mater.* **2019**, *5*, 1800519; b) Q. Lin, W. Hu, Z. Zang, M. Zhou, J. Du, M. Wang, S. Han, X. Tang, *Adv. Electron. Mater.* **2018**, *4*, 1700596.
[54] T. Shi, R. Wang, Z. Wu, Y. Sun, J. An, Q. Liu, *Small Struct.* **2021**, *2*, 2000109.
[55] M. T. Sharbati, Y. Du, J. Torres, N. D. Ardolino, M. Yun, F. Xiong, *Adv. Mater.* **2018**, *30*, 1802353.
[56] X. Niu, B. Tian, Q. Zhu, B. Dkhil, C. Duan, *Appl. Phys. Rev.* **2022**, *9*, 021309.
[57] J. Hwang, Y. Goh, S. Jeon, *Small* **2024**, *20*, 2305271.
[58] Y. Liu, T. Wang, Z. Li, J. Yu, J. Meng, K. Xu, P. Liu, H. Zhu, Q. Sun, D. W. Zhang, L. Chen, *Adv. Funct. Mater.* **2023**, *9*, 2300208.
[59] Z. Wen, D. Wu, *Adv. Mater.* **2020**, *32*, 1904123.
[60] a) C. Ma, Z. Luo, W. Huang, L. Zhao, Q. Chen, Y. Lin, X. Liu, Z. Chen, C. Liu, H. Sun, X. Jin, Y. Yin, X. Li, *Nat. Commun.* **2020**, *11*, 1439; b) L. Bégon-Lours, M. Halter, F. M. Puglisi, L. Benatti, D. F. Falcone, Y. Popoff, D. D. Pineda, M. Sousa, B. J. Offrein, *Adv. Electron. Mater.* **2022**, *8*, 2101395; c) Y. S. Kuo, S. Y. Lee, C. C. Lee, S. W. Li, T. S. Chao, *IEEE Trans. Electron Devices* **2021**, *68*, 879.
[61] a) M. Wu, J. Li, *Proc. Natl. Acad. Sci. USA* **2021**, *118*, 2115703118; b) R. Athle, M. Borg, *IEEE Trans. Electron Devices* **2023**, *70*, 1412.
[62] B. Max, M. Hoffmann, H. Mulaosmanovic, S. Slesazeck, T. Mikolajick, *ACS Appl. Electron. Mater.* **2020**, *2*, 4023.
[63] Y. Q. Wang, W. X. Wang, C. W. Zhang, H. Kan, W. J. Yue, J. B. Pang, S. Gao, Y. Li, *ACS Appl. Electron. Mater.* **2022**, *4*, 3525.
[64] S.-B. Hua, T. Jin, X. Guo, *Int. J. Extreme Manuf.* **2024**, *6*, 032008.
[65] X. Lin, Z. Feng, Y. Xiong, W. Sun, W. Yao, Y. Wei, Z. L. Wang, Q. Sun, *Int. J. Extreme Manuf.* **2024**, *6*, 032011.
[66] a) W. Zhang, B. Gao, J. Tang, X. Li, W. Wu, H. Qian, H. Wu, *Phys. Status Solidi RRL* **2019**, *13*, 1900204; b) Y. Zhang, Z. Wang, J. Zhu, Y. Yang, M. Rao, W. Song, Y. Zhuo, X. Zhang, M. Cui, L. Shen, R. Huang, J. J. Yang, *Appl. Phys. Rev.* **2020**, *7*, 011308.
[67] P. Thakkar, J. Gosai, H. J. Gogoi, A. Solanki, *J. Mater. Chem. C* **2024**, *12*, 1583.
[68] G. Ding, H. Li, J. Zhao, K. Zhou, Y. Zhai, Z. Lv, M. Zhang, Y. Yan, S.-T. Han, Y. Zhou, *Chem. Rev.* **2024**, *124*, 12738.
[69] Y. Chen, Y. Wang, Y. Luo, X. Liu, Y. Wang, F. Gao, J. Xu, E. Hu, S. Samanta, X. Wan, X. Lian, J. Xiao, Y. Tong, *IEEE Electron Device Lett.* **2019**, *40*, 1686.
[70] N. He, Q. Zhang, L. Tao, X. Chen, Q. Qin, X. Liu, X. Lian, X. Wan, E. Hu, J. Xu, F. Xu, Y. Tong, *IEEE Electron Device Lett.* **2021**, *42*, 319.
[71] E. W. Lim, R. Ismail, *Electronics* **2015**, *4*, 586.
[72] Y. Li, S. Long, Q. Liu, H. Lü, S. Liu, M. Liu, *Chin. Sci. Bull.* **2011**, *56*, 3072.
[73] a) Q. Xia, J. J. Yang, *Nat. Mater.* **2019**, *18*, 309; b) K. He, C. Wang, Y. He, J. Su, X. Chen, *Chem. Rev.* **2023**, *123*, 13796.
[74] A. Nawaz, L. Merces, L. M. M. Ferro, P. Sonar, C. C. B. Bufon, *Adv. Mater.* **2023**, *35*, 2204804.

[75] Y. Wang, Y. Zheng, J. Gao, T. Jin, E. Li, X. Lian, X. Pan, C. Han, H. Chen, W. Chen, *InfoMat* **2021**, *3*, 917.
[76] S. Oh, J.-H. Lee, S. Seo, H. Choo, D. Lee, J.-I. Cho, J.-H. Park, *Adv. Sci.* **2022**, *9*, 2103808.
[77] Y. Choi, S. Oh, C. Qian, J.-H. Park, J. H. Cho, *Nat. Commun.* **2020**, *11*, 4595.
[78] H. Wang, Z. Ji, M. Liu, L. Shang, G. Liu, X. Liu, J. Liu, Y. Peng, *Sci. China Ser. E Technol. Sci.* **2009**, *52*, 3105.
[79] J. Liu, Z. Qin, H. Gao, H. Dong, J. Zhu, W. Hu, *Adv. Funct. Mater.* **2019**, *29*, 1808453.
[80] Z. Zhu, Y. Guo, Y. Liu, *Mater. Chem. Front.* **2020**, *4*, 2845.
[81] J.-S. Lee, *Electron. Mater. Lett.* **2011**, *7*, 175.
[82] Y. He, L. Zhu, Y. Zhu, C. Chen, S. Jiang, R. Liu, Y. Shi, Q. Wan, *Adv. Intell. Syst.* **2021**, *3*, 2000210.
[83] T. Mikolajick, M. H. Park, L. Begon-Lours, S. Slesazeck, *Adv. Mater.* **2023**, *35*, 2206042.
[84] Prateek, V. K. T., R. K. Gupta, *Chem. Rev.* **2016**, *116*, 4260.
[85] a) H. Huang, C. Ge, Z. Liu, H. Zhong, E. Guo, M. He, C. Wang, G. Yang, K. Jin, *J. Semicond.* **2021**, *42*, 013103; b) C. Sun, X. Liu, Q. Jiang, X. Ye, X. Zhu, R.-W. Li, *Sci. Technol. Adv. Mater.* **2023**, *24*, 2162325.
[86] G. Y. Wang, K. Lian, T. Y. Chu, *IEEE J. Electron Devices Soc.* **2021**, *9*, 939.
[87] K. Xu, S. K. Fullerton-Shirey, *J. Phys. Mater.* **2020**, *3*, 032001.
[88] J.-S. Ro, H.-M. An, H.-L. Park, *Jpn. J. Appl. Phys.* **2023**, 62, SE0801.
[89] R. Morais, D. H. Vieira, M. d. S. Klem, C. Gaspar, L. Pereira, R. Martins, N. Alves, *Semicond. Sci. Technol.* **2022**, *37*, 035007.
[90] J. Sun, Z. Wang, X. Wang, Y. Zhou, Y. Wang, Y. He, Y. Lei, H. Wang, X. Ma, *Sci. China Mater.* **2024**, *67*, 2856.
[91] A. Melianas, M.-A. Kang, A. VahidMohammadi, T. J. Quill, W. Tian, Y. Gogotsi, A. Salleo, M. M. Hamedi, *Adv. Funct. Mater.* **2022**, *32*, 2109970.
[92] Y. Yao, H. Cheng, B. Zhang, J. Yin, D. Zhu, W. Cai, S. Li, W. Zhao, *Mater. Futures* **2023**, *2*, 032302.
[93] J. Tang, F. Yuan, X. Shen, Z. Wang, M. Rao, Y. He, Y. Sun, X. Li, W. Zhang, Y. Li, B. Gao, H. Qian, G. Bi, S. Song, J. J. Yang, H. Wu, *Adv. Mater.* **2019**, *31*, 1902761.
[94] S. Ding, H. Li, C. Su, J. Yu, F. Jin, *Artif. Intell. Rev.* **2013**, *39*, 251.
[95] F. Sun, Q. Lu, L. Liu, L. Li, Y. Wang, M. Hao, Z. Cao, Z. Wang, S. Wang, T. Li, T. Zhang, *Adv. Mater. Technol.* **2020**, *5*, 1900888.
[96] S. H. Sung, T. J. Kim, H. Shin, T. H. Im, K. J. Lee, *Nat. Commun.* **2022**, *13*, 2811.
[97] S. Qin, F. Wang, Y. Liu, Q. Wan, X. Wang, Y. Xu, Y. Shi, X. Wang, R. Zhang, *2D Mater.* **2017**, *4*, 035022.
[98] a) Y. Xu, W. Liu, Y. Huang, C. Jin, B. Zhou, J. Sun, J. Yang, *Adv. Electron. Mater.* **2021**, *7*, 2100336; b) L.-a. Kong, J. Sun, C. Qian, Y. Fu, J. Wang, J. Yang, Y. Gao, *Org. Electron.* **2017**, *47*, 126; c) Z. Rotman, P.-Y. Deng, V. A. Klyachko, *J. Neurosci.* **2011**, *31*, 14800.
[99] S. Luo, K. Liao, P. Lei, T. Jiang, S. Chen, Q. Xie, W. Luo, W. Huang, S. Yuan, W. Jie, J. Hao, *Nanoscale* **2021**, *13*, 6654.
[100] X. Zhang, H. Chen, S. Cheng, F. Guo, W. Jie, J. Hao, *ACS Appl. Mater. Interfaces* **2022**, *14*, 44614.
[101] G. Rachmuth, H. Z. Shouval, M. F. Bear, C.-S. Poon, *Proc. Natl. Acad. Sci. USA* **2011**, *108*, E1266.
[102] Y. Wang, L. Yin, W. Huang, Y. Li, S. Huang, Y. Zhu, D. Yang, X. Pi, *Adv. Intell. Syst.* **2021**, *3*, 2000099.
[103] N. Caporale, Y. Dan, *Annu. Rev. Neurosci.* **2008**, *31*, 25.
[104] X. Wang, Y. Zong, D. Liu, J. Yang, Z. Wei, *Adv. Funct. Mater.* **2023**, *33*, 2213894.
[105] P. Huang, Z. Li, Z. Dong, R. Han, Z. Zhou, D. Zhu, L. Liu, X. Liu, J. Kang, *ACS Appl. Electron. Mater.* **2019**, *1*, 845.
[106] M. Gong, L. Zhang, P. Wan, *Prog. Polym. Sci.* **2020**, *107*, 101279.
[107] S. Jang, S. Jang, E.-H. Lee, M. Kang, G. Wang, T.-W. Kim, *ACS Appl. Mater. Interfaces* **2019**, *11*, 1071.
[108] A. Jedaa, M. Halik, *Appl. Phys. Lett.* **2009**, *95*, 103309.
[109] C. Hu, Z. Wei, L. Li, G. Shen, *Adv. Funct. Mater.* **2023**, *33*, 2302188.
[110] H. Gwon, J. Hong, H. Kim, D. H. Seo, S. Jeon, K. Kang, *Energy Environ. Sci.* **2014**, *7*, 538.
[111] S.-T. Han, Y. Zhou, V. A. L. Roy, *Adv. Mater.* **2013**, *25*, 5425.
[112] X. Chen, H. Lin, P. Chen, G. Guan, J. Deng, H. Peng, *Adv. Mater.* **2014**, *26*, 4444.
[113] K. Liu, B. Ouyang, X. Guo, Y. Guo, Y. Liu, *npj Flex. Electron.* **2022**, *6*, 1.
[114] a) W. Heng, S. Solomon, W. Gao, *Adv. Mater.* **2022**, *34*, 2107902; b) S. M. Won, E. Song, J. Zhao, J. Li, J. Rivnay, J. A. Rogers, *Adv. Mater.* **2018**, *30*, 1800534; c) L. Lan, J. Ping, J. Xiong, Y. Ying, *Adv. Sci.* **2022**, *9*, 2200560.
[115] a) M. Morales-Masis, S. De Wolf, R. Woods-Robinson, J. W. Ager, C. Ballif, *Adv. Electron. Mater.* **2017**, *3*, 1600529; b) H.-G. Im, S.-H. Jung, J. Jin, D. Lee, J. Lee, D. Lee, J.-Y. Lee, I.-D. Kim, B.-S. Bae, *ACS Nano* **2014**, *8*, 10973.
[116] D. Won, J. Bang, S. H. Choi, K. R. Pyun, S. Jeong, Y. Lee, S. H. Ko, *Chem. Rev.* **2023**, *123*, 9982.
[117] L. Gao, M. Wu, X. Yu, J. Yu, *Int. J. Extreme Manuf.* **2024**, *6*, 012005.
[118] Y. Ni, Y. Wang, W. Xu, *Small* **2021**, *17*, 1905332.
[119] P. Subudhi, D. Punetha, *Prog. Photovolt. Res. Appl.* **2023**, *31*, 753.
[120] M. Hassan, G. Abbas, N. Li, A. Afzal, Z. Haider, S. Ahmed, X. Xu, C. Pan, Z. Peng, *Adv. Mater. Technol.* **2022**, *7*, 2100773.
[121] a) K. Kinoshita, T. Okutani, H. Tanaka, T. Hinoki, H. Agura, K. Yazawa, K. Ohmi, S. Kishida, *Solid State Electron* **2011**, *58*, 48; b) S. J. Kim, M. J. Park, D. J. Yun, W. H. Lee, G. H. Kim, S. M. Yoon, *IEEE Trans. Electron Devices* **2016**, *63*, 1557; c) H.-C. Chang, C.-L. Liu, W.-C. Chen, *Adv. Funct. Mater.* **2013**, *23*, 4960.
[122] a) B. Sun, X. Zhang, G. Zhou, T. Yu, S. Mao, S. Zhu, Y. Zhao, Y. Xia, *J. Colloid Interface Sci.* **2018**, *520*, 19; b) B. Zhang, D. Li, Y. Wu, F. Fan, Y. Chen, *Org. Electron.* **2017**, *49*, 269; c) B. Liu, Y. Zhang, L. Zhang, Q. Yuan, W. Zhang, Y. Li, *J. Alloys Compd.* **2022**, *919*, 165872.
[123] a) Y. Chen, Y. Yang, P. Yuan, P. Jiang, Y. Wang, Y. Xu, S. Lv, Y. Ding, Z. Dang, Z. Gao, T. Gong, Y. Wang, Q. Luo, *Nano Res.* **2022**, *15*, 2913; b) J. Jang, Y. Song, D. Yoo, T.-Y. Kim, S.-H. Jung, S. Hong, J.-K. Lee, T. Lee, *Org. Electron.* **2014**, *15*, 2822.
[124] a) S.-W. Jung, J.-S. Choi, J. B. Koo, C. W. Park, B. S. Na, J.-Y. Oh, S. C. Lim, S. S. Lee, H. Y. Chu, S.-M. Yoon, *Org. Electron.* **2015**, *16*, 46; b) H. Wang, C. Gao, K. Sun, C. Shi, X. Yan, *IEEE Trans. Electron Devices* **2021**, *68*, 510.
[125] H.-M. Seung, K.-C. Kwon, G.-S. Lee, J.-G. Park, *Nanotechnology* **2014**, *25*, 435204.
[126] D. Thuau, M. Abbas, G. Wantz, L. Hirsch, I. Dufour, C. Ayela, *Sci. Rep.* **2016**, *6*, 38672.
[127] Y. Zhu, G. Liu, Z. Xin, C. Fu, Q. Wan, F. Shan, *ACS Appl. Mater. Interfaces* **2020**, *12*, 1061.
[128] F. Chen, S. Zhang, L. Hu, J. Fan, C.-H. Lin, P. Guan, Y. Zhou, T. Wan, S. Peng, C.-H. Wang, L. Wu, T. M. Furlong, N. Valanoor, D. Chu, *Adv. Funct. Mater.* **2023**, *33*, 2300266.
[129] Z. Rao, X. Wang, S. Mao, J. Qin, Y. Yang, M. Liu, C. Ke, Y. Zhao, B. Sun, *ACS Appl. Nano Mater.* **2023**, *6*, 18645.
[130] a) Y. Ni, J. Zhou, Y. Hao, H. Yu, Y. Wang, P. Gan, S. Hu, *Semicond. Sci. Technol.* **2019**, *34*, 055003; b) L. Zhang, T. Gong, H. Wang, Z. Guo, H. Zhang, *Nanoscale* **2019**, *11*, 12413; c) R. Nag, R. K. Layek, A. Bera, *ACS Appl. Nano Mater.* **2022**, *5*, 17939.
[131] J. Shang, W. Xue, Z. Ji, G. Liu, X. Niu, X. Yi, L. Pan, Q. Zhan, X.-H. Xu, R.-W. Li, *Nanoscale* **2017**, *9*, 7037.
[132] H. Zhang, F. Sun, G. Cao, D. Zhou, G. Zhang, J. Feng, S. Wang, F. Su, Y. Tian, Y. J. Liu, Y. Tian, *Int. J. Extreme Manuf.* **2023**, *5*, 015503.
[133] J. Zou, C.-Z. Li, C.-Y. Chang, H.-L. Yip, A. K.-Y. Jen, *Adv. Mater.* **2014**, *26*, 3618.
[134] H. Zhang, X. Zhu, Y. Tai, J. Zhou, H. Li, Z. Li, R. Wang, J. Zhang, Y. Zhang, W. Ge, F. Zhang, L. Sun, G. Zhang, H. Lan, *Int. J. Extreme Manuf.* **2023**, *5*, 032005.

[135] a) L. Tang, Y. Huang, C. Wang, Z. Zhao, Y. Yang, J. Bian, H. Wu, Z. Zhang, D. W. Zhang, *J. Mater. Chem. C* **2022**, *10*, 14695; b) Y. Lin, J. Liu, J. Shi, T. Zeng, X. Shan, Z. Wang, X. Zhao, H. Xu, Y. Liu, *Appl. Phys. Lett.* **2021**, *118*, 103502; c) T. Paul, P. K. Sarkar, S. Maiti, K. K. Chattopadhyay, *ACS Appl. Electron. Mater.* **2020**, *2*, 3667.
[136] a) M. Wang, S. Cai, C. Pan, C. Wang, X. Lian, Y. Zhuo, K. Xu, T. Cao, X. Pan, B. Wang, S.-J. Liang, J. J. Yang, P. Wang, F. Miao, *Nat. Electron.* **2018**, *1*, 130; b) A. C. Khot, T. D. Dongale, K. A. Nirmal, J. K. Deepthi, S. S. Sutar, T. G. Kim, *J. Mater. Sci. Technol.* **2023**, *150*, 1.
[137] J. Yun, *Adv. Funct. Mater.* **2017**, *27*, 1606641.
[138] Y.-H. Hsu, H.-W. Liu, S.-Y. Lien, W.-Y. Wu, *Thin Solid Films* **2022**, *748*, 139158.
[139] a) Y. C. Xu, W. R. Liu, Y. L. Huang, C. X. Jin, B. S. Zhou, J. Sun, J. L. Yang, *Adv. Electron. Mater.* **2021**, *7*, 2100336; b) Y. Ni, J. Zhou, Y. Hao, H. Lin, H. Yu, P. Gan, S. Hu, Z. Lin, *Org. Electron.* **2019**, *74*, 237; c) S. Huang, Y. Liu, Y. Zhao, Z. Ren, C. F. Guo, *Adv. Funct. Mater.* **2019**, *29*, 1805924.
[140] a) Y. Wang, C. Zhu, R. Pfattner, H. Yan, L. Jin, S. Chen, F. Molina-Lopez, F. Lissel, J. Liu, N. I. Rabiah, Z. Chen, J. W. Chung, C. Linder, M. F. Toney, B. Murmann, Z. Bao, *Sci. Adv.* **2017**, *3*, 1602076; b) Q. Pei, G. Zuccarello, M. Ahlskog, O. Inganäs, *Polymer* **1994**, *35*, 1347; c) L. Groenendaal, F. Jonas, D. Freitag, H. Pielartzik, J. R. Reynolds, *Adv. Mater.* **2000**, *12*, 481.
[141] M. Vosgueritchian, D. J. Lipomi, Z. Bao, *Adv. Funct. Mater.* **2012**, *22*, 421.
[142] S. Lai, S. K. Jang, J. H. Cho, S. Lee, *Nanoscale* **2018**, *10*, 5191.
[143] a) H.-S. Lee, J.-S. Ro, G.-M. Ko, H.-L. Park, *Flex. Print. Electron.* **2023**, *8*, 043001; b) M. Y. Teo, N. Kim, S. Kee, B. S. Kim, G. Kim, S. Hong, S. Jung, K. Lee, *ACS Appl. Mater. Interfaces* **2017**, *9*, 819.
[144] a) M. Fikry, M. Abbas, A. Sayed, A. Nouh, A. Ibrahim, A. S. Mansour, *J. Mater. Sci. Mater. Electron.* **2022**, *33*, 3914; b) D. Chen, J. Liang, Q. Pei, *Sci. China Chem.* **2016**, *59*, 659.
[145] a) L. Hu, H. S. Kim, J.-Y. Lee, P. Peumans, Y. Cui, *ACS Nano* **2010**, *4*, 2955; b) L. G. S. Albano, M. H. Boratto, O. Nunes-Neto, C. F. O. Graeff, *Org. Electron.* **2017**, *50*, 311.
[146] E. Yang, S. Kang, S. Jeong, K. Shin, J. S. Wi, J. S. Park, S. Lee, C. H. Chung, *Electron. Mater. Lett.* **2024**, *20*, 254.
[147] Y. Weng, Z. Yu, T. Wu, L. Liang, S. Liu, *New J. Chem.* **2023**, *47*, 5086.
[148] R. J. T. Nicholl, H. J. Conley, N. V. Lavrik, I. Vlassiouk, Y. S. Puzyrev, V. P. Sreenivas, S. T. Pantelides, K. I. Bolotin, *Nat. Commun.* **2015**, *6*, 8789.
[149] a) J. Choi, H. Yoo, *Polymers* **2023**, *15*, 1395; b) L.-C. Hsu, C.-C. Shih, H.-C. Hsieh, Y.-C. Chiang, P.-H. Wu, C.-C. Chueh, W.-C. Chen, *Polym. Chem.* **2018**, *9*, 5145.
[150] K. Au, X. S. Gao, J. Wang, Z. Y. Bao, J. M. Liu, J. Y. Dai, *J.Appl. Phys.* **2013**, *114*, 027019.
[151] a) E. Fortunato, P. Barquinha, R. Martins, *Adv. Mater.* **2012**, *24*, 2945; b) S. Yang, K. Liu, Y. Xu, L. Liu, H. Li, T. Zhai, *Adv. Mater.* **2023**, *35*, 2207901.
[152] a) W. Huang, Y. Wang, Y. Zhang, J. Zhu, D. Liu, J. Wang, L. Fan, R. Qiu, M. Zhang, *Carbon* **2022**, *189*, 386; b) A. Chortos, G. I. Koleilat, R. Pfattner, D. Kong, P. Lin, R. Nur, T. Lei, H. Wang, N. Liu, Y.-C. Lai, M.-G. Kim, J. W. Chung, S. Lee, Z. Bao, *Adv. Mater.* **2016**, *28*, 4441; c) H. Shim, F. Ershad, S. Patel, Y. Zhang, B. Wang, Z. Chen, T. J. Marks, A. Facchetti, C. Yu, *Nat. Electron.* **2022**, *5*, 660.
[153] W. Huang, J. Chen, G. Wang, Y. Yao, X. Zhuang, R. M. Pankow, Y. Cheng, T. J. Marks, A. Facchetti, *J. Mater. Chem.C.*, *9*, 9348.
[154] C. Leighton, *Nat. Mater.* **2019**, *18*, 13.
[155] C. Lv, F. Zhang, C. Li, Z. Li, J. Zhao, *Mater. Futures* **2023**, *2*, 032301.
[156] a) S. Gao, X. Yi, J. Shang, G. Liu, R.-W. Li, *Chem. Soc. Rev.* **2019**, *48*, 1531; b) A. K. Chauhan, P. Jha, D. K. Aswal, J. V. Yakhmi, *J. Electron. Mater.* **2022**, *51*, 447; c) B. Li, S. Zhang, L. Xu, Q. Su, B. Du, *Polymers* **2023**, *15*, 4374.
[157] P. Tian, L. Tang, K.-S. Teng, S.-P. Lau, *Mater. Futures* **2024**, *3*, 022301.
[158] a) K. Wang, S. Dai, Y. Zhao, Y. Wang, C. Liu, J. Huang, *Small* **2019**, *15*, 1900010; b) X. Zhang, H. Xie, Z. Liu, C. Tan, Z. Luo, H. Li, J. Lin, L. Sun, W. Chen, Z. Xu, L. Xie, W. Huang, H. Zhang, *Angew. Chem., Int. Ed.* **2015**, *54*, 3653; c) X. Han, S. Li, Z. Peng, A. O. Al-Yuobi, A. S. Omar Bashammakh, M. S. El-Shahawi, R. M. Leblanc, *J. Oleo Sci.* **2016**, *65*, 1; d) T. Chen, S. Yang, J. Wang, W. Chen, L. Liu, Y. Wang, S. Cheng, X. Zhao, *Adv. Electron. Mater.* **2021**, *7*, 2000882; e) K. Liang, R. Wang, B. Huo, H. Ren, D. Li, Y. Wang, Y. Tang, Y. Chen, C. Song, F. Li, B. Ji, H. Wang, B. Zhu, *ACS Nano* **2022**, *16*, 8651; f) J.-L. Meng, T.-Y. Wang, L. Chen, Q.-Q. Sun, H. Zhu, L. Ji, S.-J. Ding, W.-Z. Bao, P. Zhou, D. W. Zhang, *Nano Energy* **2021**, *83*, 105815.
[159] a) K. Chen, W. Gao, S. Emaminejad, D. Kiriya, H. Ota, H. Y. Y. Nyein, K. Takei, A. Javey, *Adv. Mater.* **2016**, *28*, 4397; b) B. Zhao, M. Xiao, Y. N. Zhou, *Nanotechnology* **2019**, *30*, 425202.
[160] Y. Li, C. Zhang, Z. Shi, C. Ma, J. Wang, Q. Zhang, *Sci. China Mater.* **2022**, *65*, 2110.
[161] a) Y. Park, M.-K. Kim, J.-S. Lee, *Carbon* **2020**, *165*, 455; b) J. Jiang, W. Hu, D. Xie, J. Yang, J. He, Y. Gao, Q. Wan, *Nanoscale* **2019**, *11*, 1360; c) Y. Yoon, K. Ganapathi, S. Salahuddin, *Nano Lett.* **2011**, *11*, 3768; d) X. Zhu, D. Li, X. Liang, W. D. Lu, *Nat. Mater.* **2019**, *18*, 141; e) S. Bertolazzi, P. Bondavalli, S. Roche, T. San, S.-Y. Choi, L. Colombo, F. Bonaccorso, P. Samorì, *Adv. Mater.* **2019**, *31*, 1806663.
[162] W. Xue, C. Gao, Z. Zhang, T. Han, N. Hou, W. Yin, L. Shi, X. Wang, G. Liu, X. Xu, *Sci. China Mater.* **2023**, *66*, 764.
[163] a) Q. Lu, Y. Yu, Q. Ma, B. Chen, H. Zhang, *Adv. Mater.* **2016**, *28*, 1917; b) B. Radisavljevic, A. Radenovic, J. Brivio, V. Giacometti, A. Kis, *Nat. Nanotechnol.* **2011**, *6*, 147; c) A. K. Geim, *Science* **2009**, *324*, 1530; d) Y. Qi, N. T. Jafferis, K. Lyons, Jr., C. M. Lee, H. Ahmad, M. C. McAlpine, *Nano Lett.* **2010**, *10*, 524; e) M. M. Rehman, G. U. Siddiqui, J. Z. Gul, S.-W. Kim, J. H. Lim, K. H. Choi, *Sci. Rep.* **2016**, *6*, 36195; f) T. Carey, S. Cacovich, G. Divitini, J. Ren, A. Mansouri, J. M. Kim, C. Wang, C. Ducati, R. Sordan, F. Torrisi, *Nat. Commun.* **2017**, *8*, 1202.
[164] S. Deng, A. V. Sumant, V. Berry, *Nano Today* **2018**, *22*, 14.
[165] R. Frisenda, M. Drüppel, R. Schmidt, S. Michaelis de Vasconcellos, D. Perez de Lara, R. Bratschitsch, M. Rohlfing, A. Castellanos-Gomez, *npj 2D Mater. Appl.* **2017**, *1*, 10.
[166] Y. Zhu, S. Murali, W. Cai, X. Li, J. W. Suk, J. R. Potts, R. S. Ruoff, *Adv. Mater.* **2010**, *22*, 3906.
[167] S. Porro, C. Ricciardi, *RSC Adv.* **2015**, *5*, 68565.
[168] X. Zhao, J. Xuan, Q. Li, F. Gao, X. Xun, Q. Liao, Y. Zhang, *Adv. Mater.* **2023**, *35*, 2207437.
[169] a) K. Kanahashi, J. Pu, T. Takenobu, *Adv. Energy Mater.* **2020**, *10*, 1902842; b) T. Dong, J. Simões, Z. Yang, *Adv. Mater. Interfaces* **2020**, *7*, 1901657.
[170] V. Selamneni, V. Adepu, H. Raghavan, P. Sahatiya, *FlatChem* **2022**, *33*, 100363.
[171] a) R. E. Ustad, S. S. Kundale, K. A. Rokade, S. L. Patil, V. D. Chavan, K. D. Kadam, H. S. Patil, S. P. Patil, R. K. Kamat, D.-k. Kim, T. D. Dongale, *Nanoscale* **2023**, *15*, 9891; b) I. M. Chirica, A. G. Mirea, Ş. Neaţu, M. Florea, M. W. Barsoum, F. Neaţu, *J. Mater. Chem. A* **2021**, *9*, 19589.
[172] a) M. Soleymaniha, M.-A. Shahbazi, A. R. Rafieerad, A. Maleki, A. Amiri, *Adv. Healthcare Mater.* **2019**, *8*, 1801137; b) M. Naguib, V. N. Mochalin, M. W. Barsoum, Y. Gogotsi, *Adv. Mater.* **2014**, *26*, 992.
[173] K. Goc, W. Prendota, L. Chlubny, T. Strączek, W. Tokarz, P. Borowiak, K. Witulska, M. M. Bućko, J. Przewoźnik, J. Lis, *Ceram. Int.* **2018**, *44*, 18322.
[174] K. R. G. Lim, M. Shekhirev, B. C. Wyatt, B. Anasori, Y. Gogotsi, Z. W. Seh, *Nat. Synth.* **2022**, *1*, 601.
[175] H. Lin, S. Gao, C. Dai, Y. Chen, J. Shi, *J. Am. Chem. Soc.* **2017**, *139*, 16235.
[176] M. Patel, N. R. Hemanth, J. Gosai, R. Mohili, A. Solanki, M. Roy, B. Fang, N. K. Chaudhari, *Trends Chem.* **2022**, *4*, 835.

[177] J. A. Kumar, P. Prakash, T. Krithiga, D. J. Amarnath, J. Premkumar, N. Rajamohan, Y. Vasseghian, P. Saravanan, M. Rajasimman, *Chemosphere* **2022**, *286*, 131607.
[178] Z. Xiao, X. Xiao, L. B. Kong, H. Dong, X. Li, B. He, S. Ruan, J. Zhai, K. Zhou, Q. Huang, L. Chu, *Int. J. Extreme Manuf.* **2024**, *6*, 022006.
[179] J. Halim, M. R. Lukatskaya, K. M. Cook, J. Lu, C. R. Smith, L.-Å. Näslund, S. J. May, L. Hultman, Y. Gogotsi, P. Eklund, M. W. Barsoum, *Chem. Mater.* **2014**, *26*, 2374.
[180] F. Li, S. Zhao, H. Wang, G. Zhu, H. Li, *Chem. Asian J.* **2023**, *18*, 202300474.
[181] M. Naguib, M. Kurtoglu, V. Presser, J. Lu, J. Niu, M. Heon, L. Hultman, Y. Gogotsi, M. W. Barsoum, *Adv. Mater.* **2011**, *23*, 4248.
[182] M. Naguib, O. Mashtalir, J. Carle, V. Presser, J. Lu, L. Hultman, Y. Gogotsi, M. W. Barsoum, *ACS Nano* **2012**, *6*, 1322.
[183] M. Ghidiu, M. R. Lukatskaya, M.-Q. Zhao, Y. Gogotsi, M. W. Barsoum, *Nature* **2014**, *516*, 78.
[184] T. Li, L. Yao, Q. Liu, J. Gu, R. Luo, J. Li, X. Yan, W. Wang, P. Liu, B. Chen, W. Zhang, W. Abbas, R. Naz, D. Zhang, *Angew. Chem., Int. Ed.* **2018**, *57*, 6115.
[185] S. Yang, P. Zhang, F. Wang, A. G. Ricciardulli, M. R. Lohe, P. W. M. Blom, X. Feng, *Angew. Chem., Int. Ed.* **2018**, *57*, 15491.
[186] M. Öper, U. Yorulmaz, C. Sevik, F. Ay, N. K. Perkgöz, *J. Appl. Phys.* **2022**, *131*, 025304.
[187] D. Wang, C. Zhou, A. S. Filatov, W. Cho, F. Lagunas, M. Wang, S. Vaikuntanathan, C. Liu, R. F. Klie, D. V. Talapin, *Science* **2023**, *379*, 1242.
[188] T. Hu, M. Hu, B. Gao, W. Li, X. Wang, *J. Phys. Chem. C* **2018**, *122*, 18501.
[189] Y. Jiang, J. Lao, G. Dai, Z. Ye, *ACS Nano* **2024**, *18*, 14050.
[190] A. Rafieerad, W. Yan, K. N. Alagarsamy, A. Srivastava, N. Sareen, R. C. Arora, S. Dhingra, *Adv. Funct. Mater.* **2021**, *31*, 2106786.
[191] X. Zou, H. Liu, H. Xu, X. Wu, X. Han, J. Kang, K. M. Reddy, *Mater. Today Energy* **2021**, *20*, 100668.
[192] D. Gandla, Z. Zhuang, V. V. Jadhav, D. Q. Tan, *Energy Storage Mater.* **2023**, *63*, 102977.
[193] Z. Lin, X. Li, H. Zhang, B. B. Xu, P. Wasnik, H. Li, M. V. Singh, Y. Ma, T. Li, Z. Guo, *Inorg. Chem. Front.* **2023**, *10*, 4358.
[194] J. Jia, T. Xiong, L. Zhao, F. Wang, H. Liu, R. Hu, J. Zhou, W. Zhou, S. Chen, *ACS Nano* **2017**, *11*, 12509.
[195] a) C. Xu, L. Wang, Z. Liu, L. Chen, J. Guo, N. Kang, X.-L. Ma, H.-M. Cheng, W. Ren, *Nat. Mater.* **2015**, *14*, 1135; b) J. Jeon, Y. Park, S. Choi, J. Lee, S. S. Lim, B. H. Lee, Y. J. Song, J. H. Cho, Y. H. Jang, S. Lee, *ACS Nano* **2018**, *12*, 338.
[196] D. Geng, X. Zhao, Z. Chen, W. Sun, W. Fu, J. Chen, W. Liu, W. Zhou, K. P. Loh, *Adv. Mater.* **2017**, *29*, 1700072.
[197] C. An, D. Dong, S. Wu, L. Gao, X. Chen, P. Jiao, Q. Deng, J. Li, N. Hu, *Chem. Asian J.* **2023**, *18*, 202300429.
[198] X. Lin, Z. Li, J. Qiu, Q. Wang, J. Wang, H. Zhang, T. Chen, *Biomater. Sci.* **2021**, *9*, 5437.
[199] H. Bark, G. Thangavel, R. J. Liu, D. H. C. Chua, P. S. Lee, *Small Methods* **2023**, *7*, 2300077.
[200] F. Sun, X. Wang, D. Wu, M. El-Khouly, T. Zheng, B. Zhang, Y. Chen, *ACS Appl. Nano Mater* **2023**, *6*, 7186.
[201] K. Zhao, J. Liu, X. Wang, Q. Che, B. Zhang, H. He, K. Wang, Y. Chen, *Adv. Opt. Mater.* **2024**, *12*, 2301761.
[202] S. Jung, U. Zafar, L. S. K. Achary, C. M. Koo, *EcoMat* **2023**, *5*, e12395.
[203] Y. Yan, R. Yu, C. Gao, Y. Sui, Y. Deng, H. Chen, T. Guo, *Sci. China Mater.* **2022**, *65*, 3087.
[204] a) B. Lyu, M. Kim, H. Jing, J. Kang, C. Qian, S. Lee, J. H. Cho, *ACS Nano* **2019**, *13*, 11392; b) A. K. Worku, M. A. Alemu, D. W. Ayele, M. Z. Getie, M. A. Teshager, *Green Chem. Lett. Rev.* **2024**, *17*, 2325983.
[205] G. Murali, J. K. Reddy Modigunta, Y. H. Park, J.-H. Lee, J. Rawal, S.-Y. Lee, I. In, S.-J. Park, *ACS Nano* **2022**, *16*, 13370.
[206] V. D. Phadtare, V. G. Parale, K.-Y. Lee, H. Choi, Y.-S. Bae, H.-H. Park, *Polym. Rev.* **2024**, *64*, 761.
[207] C. Zhang, Y. Ma, X. Zhang, S. Abdolhosseinzadeh, H. Sheng, W. Lan, A. Pakdel, J. Heier, F. Nüesch, *Energy Environ. Mater.* **2020**, *3*, 29.
[208] H. Lashgari, M. R. Abolhassani, A. Boochani, S. M. Elahi, J. Khodadadi, *Solid State Commun.* **2014**, *195*, 61.
[209] M. Tang, J. Li, Y. Wang, W. Han, S. Xu, M. Lu, W. Zhang, H. Li, *Symmetry* **2022**, *14*, 2232.
[210] Y. Xie, P. R. C. Kent, *Phys. Rev. B* **2013**, *87*, 235441.
[211] S. Uzun, S. Seyedin, A. L. Stoltzfus, A. S. Levitt, M. Alhabeb, M. Anayee, C. J. Strobel, J. M. Razal, G. Dion, Y. Gogotsi, *Adv. Funct. Mater.* **2019**, *29*, 1905015.
[212] a) M. Khazaei, A. Ranjbar, M. Arai, T. Sasaki, S. Yunoki, *J. Mater. Chem. C* **2017**, *5*, 2488; b) B. Lyu, Y. Choi, H. Jing, C. Qian, H. Kang, S. Lee, J. H. Cho, *Adv. Mater.* **2020**, *32*, 1907633; c) S. Palei, G. Murali, C.-H. Kim, I. In, S.-Y. Lee, S.-J. Park, *Nano-Micro Lett.* **2023**, *15*, 123.
[213] a) M. Kurtoglu, M. Naguib, Y. Gogotsi, M. W. Barsoum, *MRS Commun.* **2012**, *2*, 133; b) H. Kim, Z. Wang, H. N. Alshareef, *Nano Energy* **2019**, *60*, 179.
[214] A. Lipatov, H. Lu, M. Alhabeb, B. Anasori, A. Gruverman, Y. Gogotsi, A. Sinitskii, *Sci. Adv* **2018**, *4*, eaat0491.
[215] a) T. Hu, J. Yang, W. Li, X. Wang, C. M. Li, *Phys. Chem. Chem. Phys.* **2020**, *22*, 2115; b) J. Hu, S. Li, J. Zhang, Q. Chang, W. Yu, Y. Zhou, *Chin. Chem. Lett.* **2020**, *31*, 996.
[216] V. N. Borysiuk, V. N. Mochalin, Y. Gogotsi, *Nanotechnology* **2015**, *26*, 265705.
[217] Y. Pan, L. Fu, Q. Zhou, Z. Wen, C.-T. Lin, J. Yu, W. Wang, H. Zhao, *Polym. Compos.* **2020**, *41*, 210.
[218] a) M. Seredych, C. E. Shuck, D. Pinto, M. Alhabeb, E. Precetti, G. Deysher, B. Anasori, N. Kurra, Y. Gogotsi, *Chem. Mater.* **2019**, *31*, 3324; b) Y. Guo, S. Jin, L. Wang, P. He, Q. Hu, L.-Z. Fan, A. Zhou, *Ceram. Int.* **2020**, *46*, 19550.
[219] G. Li, K. Jiang, S. Zaman, J. Xuan, Z. Wang, F. Geng, *Inorg. Chem.* **2019**, *58*, 9397.
[220] Y. Pei, X. Zhang, Z. Hui, J. Zhou, X. Huang, G. Sun, W. Huang, *ACS Nano* **2021**, *15*, 3996.
[221] a) Y. Lee, S. J. Kim, Y.-J. Kim, Y. Lim, Y. Chae, B.-J. Lee, Y.-T. Kim, H. Han, Y. Gogotsi, C. W. Ahn, *J. Mater. Chem. A* **2020**, *8*, 573; b) Y. Chae, S. J. Kim, S.-Y. Cho, J. Choi, K. Maleski, B.-J. Lee, H.-T. Jung, Y. Gogotsi, Y. Lee, C. W. Ahn, *Nanoscale* **2019**, *11*, 8387; c) F. Xia, J. Lao, R. Yu, X. Sang, J. Luo, Y. Li, J. Wu, *Nanoscale* **2019**, *11*, 23330.
[222] S. Jiang, L. Lu, Y. Song, *Chem.-Eur. J.* **2024**, *30*, 202304036.
[223] I. Persson, J. Halim, T. W. Hansen, J. B. Wagner, V. Darakchieva, J. Palisaitis, J. Rosen, P. O. Å. Persson, *Adv. Funct. Mater.* **2020**, *30*, 1909005.
[224] a) X. Jiang, A. V. Kuklin, A. Baev, Y. Ge, H. Ågren, H. Zhang, P. N. Prasad, *Phys. Rep.* **2020**, *848*, 1; b) L. Guo, B. Mu, M.-Z. Li, B. Yang, R.-S. Chen, G. Ding, K. Zhou, Y. Liu, C.-C. Kuo, S.-T. Han, Y. Zhou, *ACS Appl. Mater. Interfaces* **2021**, *13*, 39595; c) L. Yue, H. Sun, Y. Zhu, Y. Li, F. Yang, X. Dong, J. Chen, X. Zhang, J. Chen, Y. Zhao, K. Chen, B. Yang, Y. Li, *J. Phys. Chem. Lett.* **2024**, *15*, 8667; d) J. Fang, Z. Tang, X.-C. Lai, F. Qiu, Y.-P. Jiang, Q.-X. Liu, X.-G. Tang, Q.-J. Sun, Y.-C. Zhou, J.-M. Fan, J. Gao, *ACS Appl. Mater. Interfaces* **2024**, *16*, 31348.
[225] B. Kalidasan, A. K. Pandey, R. Saidur, T. K. Han, Y. N. Mishra, *Mater. Today Sustain.* **2024**, *25*, 100634.
[226] S. Ullah, T. Najam, A. u. Rehman, S. S. Alarfaji, M. A. Ahmad, S. Riaz, B. Akkinepally, S. S. A. Shah, M. A. Nazir, *J. Alloys Compd.* **2024**, *1001*, 175172.
[227] X. Gao, Z. Jia, B. Wang, X. Wu, T. Sun, X. Liu, Q. Chi, G. Wu, *Chem. Eng. J.* **2021**, *419*, 130019.
[228] a) K. Hantanasirisakul, M. Alhabeb, A. Lipatov, K. Maleski, B. Anasori, P. Salles, C. Ieosakulrat, P. Pakawatpanurut, A. Sinitskii, S.

J. May, Y. Gogotsi, *Chem. Mater.* **2019**, *31*, 2941; b) B. Fu, J. Sun, C. Wang, C. Shang, L. Xu, J. Li, H. Zhang, *Small* **2021**, *17*, 2006054.
[229] a) G. R. Berdiyorov, *AIP Adv.* **2016**, *6*, 055105; b) A. Sarycheva, T. Makaryan, K. Maleski, E. Satheeshkumar, A. Melikyan, H. Minassian, M. Yoshimura, Y. Gogotsi, *J. Phys. Chem. C* **2017**, *121*, 19983.
[230] X. Jiang, Q. Liu, J. Xing, N. Liu, Y. Guo, Z. Liu, J. Zhao, *Appl. Phys. Rev.* **2021**, *8*, 031305.
[231] a) S. G. Eswaran, M. Rashad, A. S. K. Kumar, A. F. M. EL-Mahdy, *Chem. Asian J.* **2025**, 202401181; b) D. Yu, W. Wei, M. Wei, F. Wang, X. Liang, S. Sun, M. Gao, Q. Zhu, *J. Solid State Electrochem.* **2022**, *26*, 1399; c) J. Li, X. Wang, W. Sun, K. Maleski, C. E. Shuck, K. Li, P. Urbankowski, K. Hantanasirisakul, X. Wang, P. Kent, H. Wang, Y. Gogotsi, *ChemElectroChem* **2021**, *8*, 151; d) B. Sahu, M. K. Singh, L. Bansal, D. K. Rath, D. K. Rai, R. Kumar, *Adv. Eng. Mater.* **2024**, *26*, 2401295.
[232] a) S. Chertopalov, V. N. Mochalin, *ACS Nano* **2018**, *12*, 6109; b) N. Khatun, S. Dey, G. C. Behera, S. C. Roy, *Mater. Chem. Phys.* **2022**, *278*, 125651.
[233] D. Wijethunge, L. Zhang, A. Du, *J. Mater. Chem. C* **2021**, *9*, 11343.
[234] A. Chandrasekaran, A. Mishra, A. K. Singh, *Nano Lett.* **2017**, *17*, 3290.
[235] a) L. Zhang, C. Tang, C. Zhang, A. Du, *Nanoscale* **2020**, *12*, 21291; b) Z. Wang, N. Ding, C. Gui, S.-S. Wang, M. An, S. Dong, *Phys. Rev. Mater.* **2021**, *5*, 074408; c) J.-J. Zhang, L. Lin, Y. Zhang, M. Wu, B. I. Yakobson, S. Dong, *J. Am. Chem. Soc.* **2018**, *140*, 9768.
[236] Y. Yu, L.-D. Wang, W.-L. Li, Y.-L. Qiao, Y. Zhao, Y. Feng, T.-D. Zhang, R.-X. Song, W.-D. Fei, *Acta Mater.* **2018**, *150*, 173.
[237] R. Tahir, S. A. Zahra, U. Naeem, D. Akinwande, S. Rizwan, *RSC Adv.* **2022**, *12*, 24571.
[238] R. Tahir, M. W. Hakim, A. Murtaza, M. F. Khan, S. Rizwan, *Adv. Electron. Mater.* **2023**, *9*, 2300299.
[239] a) Y. Cao, T. Zhao, C. Liu, C. Zhao, H. Gao, S. Huang, X. Li, C. Wang, Y. Liu, E. G. Lim, Z. Wen, *Nano Energy* **2023**, *112*, 108441; b) X. Lian, Y. Shi, S. Li, B. Ding, C. Hua, L. Wang, *Contemp. Phys.* **2022**, *63*, 87; c) J. Gosai, M. Patel, L. Liu, A. Lokhandwala, P. Thakkar, M. Y. Chee, M. Jain, W. S. Lew, N. Chaudhari, A. Solanki, *ACS Appl. Mater. Interfaces* **2024**, *16*, 17821.
[240] a) S. Fatima, R. Tahir, D. Akinwande, S. Rizwan, *Carbon* **2024**, *218*, 118656; b) L. Kindohoun, K. Sattar, R. Tahir, S. Irfan, S. Rizwan, *Ceram. Int.* **2024**, *50*, 29877.
[241] X. Xie, Q. Wang, C. Zhao, Q. Sun, H. Gu, J. Li, X. Tu, B. Nie, X. Sun, Y. Liu, E. G. Lim, Z. Wen, Z. L. Wang, *ACS Nano* **2024**, *18*, 17041.
[242] G. Ding, K. Zeng, K. Zhou, Z. Li, Y. Zhou, Y. Zhai, L. Zhou, X. Chen, S.-T. Han, *Nanoscale* **2019**, *11*, 7102.
[243] S. Ling, C. Zhang, C. Zhang, M. Teng, C. Ma, J. Gao, X. Yan, Y. Pan, Y. Jiang, Y. Wu, Y. Li, *J. Solid State Chem.* **2023**, *318*, 123731.
[244] W.-J. Sun, Y.-Y. Zhao, X.-F. Cheng, J.-H. He, J.-M. Lu, *ACS Appl. Mater. Interfaces* **2020**, *12*, 9865.
[245] S. Fatima, X. Bin, M. A. Mohammad, D. Akinwande, S. Rizwan, *Adv. Electron. Mater.* **2022**, *8*, 2100549.
[246] S. Fatima, M. W. Hakim, D. Akinwande, S. Rizwan, *Mater. Today Phys.* **2022**, *26*, 100730.
[247] K. A. Nirmal, W. Ren, A. C. Khot, D. Y. Kang, T. D. Dongale, T. G. Kim, *Adv. Sci.* **2023**, *10*, 2300433.
[248] S. Fatima, R. Tahir, S. Rizwan, *Appl. Phys. Lett.* **2023**, *123*, 013503.
[249] K. Sattar, R. Tahir, H. Huang, D. Akinwande, S. Rizwan, *Carbon* **2024**, *221*, 118931.
[250] M. Boota, B. Anasori, C. Voigt, M.-Q. Zhao, M. W. Barsoum, Y. Gogotsi, *Adv. Mater.* **2016**, *28*, 1517.
[251] a) J. Wen, X. Li, W. Liu, Y. Fang, J. Xie, Y. Xu, *Chin. J. Catal.* **2015**, *36*, 2049; b) G. Zeng, Y. Chen, *Acta Biomater.* **2020**, *118*, 1.
[252] a) W. Luo, Y. Ma, T. Li, H. K. Thabet, C. Hou, M. M. Ibrahim, S. M. El-Bahy, B. B. Xu, Z. Guo, *J. Energy Storage* **2022**, *52*, 105008; b) B. Shen, R. Hao, Y. Huang, Z. Guo, X. Zhu, *Crystals* **2022**, *12*, 1099.
[253] M. Zhang, Y. Wei, C. Liu, Z. Ding, X. Liang, S. Ming, Y. Wang, W. Shao, E. Hu, X. Wang, Y. Zhang, M. Zhang, J. Xu, Y. Tong, *Appl. Phys. Lett.* **2023**, *123*, 06050.
[254] a) M. Zhang, Q. Qin, X. Chen, R. Tang, A. Han, S. Yao, R. Dan, Q. Wang, Y. Wang, H. Gu, H. Zhang, E. Hu, L. Wang, J. Xu, Y. Tong, *Ceram. Int.* **2022**, *48*, 16263; b) R. Tahir, S. Fatima, S. A. Zahra, D. Akinwande, H. Li, S. H. M. Jafri, S. Rizwan, *npj 2D Mater. Appl.* **2023**, *7*, 7.
[255] J. Huang, S. Yang, X. Tang, L. Yang, W. Chen, Z. Chen, X. Li, Z. Zeng, Z. Tang, X. Gui, *Adv. Mater.* **2023**, *35*, 2303737.
[256] S. Zhao, W. Ran, Z. Lou, L. Li, S. Poddar, L. Wang, Z. Fan, G. Shen, *Natl. Sci. Rev.* **2022**, *9*, nwac158.
[257] a) K. Wang, Y. Jia, X. Yan, *Nano Energy* **2022**, *100*, 107486; b) S. Ren, K. Wang, Y. Jia, X. Yan, *Adv. Intell. Syst.* **2023**, *5*, 2300402.
[258] Y. Wang, Y. Gong, L. Yang, Z. Xiong, Z. Lv, X. Xing, Y. Zhou, B. Zhang, C. Su, Q. Liao, S.-T. Han, *Adv. Funct. Mater.* **2021**, *31*, 2100144.
[259] J. Huang, J. Feng, Z. Chen, Z. Dai, S. Yang, Z. Chen, H. Zhang, Z. Zhou, Z. Zeng, X. Li, X. Gui, *Nano Energy* **2024**, *126*, 109684.
[260] S. Kim, S. B. Jo, J. Kim, D. Rhee, Y. Y. Choi, D. H. Kim, J. Kang, J. H. Cho, *Adv. Funct. Mater.* **2022**, *32*, 2111956.
[261] J. Zhu, Z. Wang, D. Liu, Q. Liu, W. Wang, X. Wang, M. Zhang, *Adv. Funct. Mater.* **2024**, *34*, 2403842.
[262] X. Lian, X. Shen, M. Zhang, J. Xu, F. Gao, X. Wan, E. Hu, Y. Guo, J. Zhao, Y. Tong, *Appl. Phys. Lett.* **2019**, *115*, 063501.
[263] A. D. Dillon, M. J. Ghidiu, A. L. Krick, J. Griggs, S. J. May, Y. Gogotsi, M. W. Barsoum, A. T. Fafarman, *Adv. Funct. Mater.* **2016**, *26*, 4162.
[264] a) X. Zhang, Y. Zhuo, Q. Luo, Z. Wu, R. Midya, Z. Wang, W. Song, R. Wang, N. K. Upadhyay, Y. Fang, F. Kiani, M. Rao, Y. Yang, Q. Xia, Q. Liu, M. Liu, J. J. Yang, *Nat. Commun.* **2020**, *11*, 51; b) K. Wang, Y. Jia, X. Yan, *Adv. Funct. Mater.* **2021**, *31*, 2104304.
[265] a) S. Duan, X. Wei, F. Zhao, H. Yang, Y. Wang, P. Chen, J. Hong, S. Xiang, M. Luo, Q. Shi, G. Shen, J. Wu, *Adv. Sci.* **2023**, *10*, 2304121; b) Z. Yunlong, Y. Yangbo, Z. Haiyan, C. Zijian, Z. Haitao, W. Guirong, Z. Weihao, X. Chenyang, Y. Zongyou, G. Libo, *Int. J. Extreme Manuf.* **2024**, *6*, 065502.
[266] B. Zeng, X. Zhang, C. Gao, Y. Zou, X. Yu, Q. Yang, T. Guo, H. Chen, *IEEE Trans. Electron Devices* **2023**, *70*, 1359.
[267] a) H. Qiu, S. Lan, Q. Lin, H. Zhu, W. Liao, L. Yang, *Org. Electron.* **2024**, *131*, 107090; b) Y. Guo, K. Li, D. Zou, Y. Li, L. Yan, Z. He, T. Zou, B. Huang, P. K. L. Chan, *Adv. Electron. Mater.* **2024**, *10*, 2300570.
[268] Y. Cao, C. Zhao, T. Zhao, Y. Sun, Z. Liu, X. Li, L. Yin, J. Gu, H. Ren, X. Geng, J. Yao, L. Kang, *J. Mater. Chem. C* **2023**, *11*, 3468.
[269] Q. Xue, H. Zhang, M. Zhu, Z. Pei, H. Li, Z. Wang, Y. Huang, Y. Huang, Q. Deng, J. Zhou, S. Du, Q. Huang, C. Zhi, *Adv. Mater.* **2017**, *29*, 1604847.
[270] H. Mao, C. Gu, S. Yan, Q. Xin, S. Cheng, P. Tan, X. Wang, F. Xiu, X. Liu, J. Liu, W. Huang, L. Sun, *Adv. Electron. Mater.* **2020**, *6*, 1900493.
[271] T. D. Dongale, G. U. Kamble, D. Y. Kang, S. S. Kundale, H.-M. An, T. G. Kim, *Phys. Status Solidi RRL* **2021**, *15*, 2100199.
[272] G. Zhou, J. Ji, Z. Chen, J. Shuai, Q. Liang, Q. Zhang, *Mater. Futures* **2024**, *3*, 042701.
[273] M. Chen, J. Liu, Y. Hu, Y. Wu, C.-Y. Tang, K. Ke, W. Yang, *Mater. Futures* **2024**, *3*, 032501.

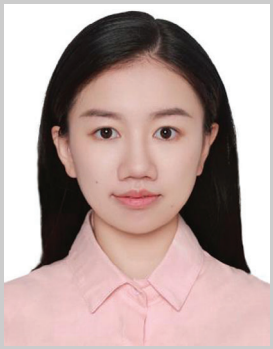

Yan Li was born in Xiamen, Fujian, China. She is currently studying at the Institute for Advanced Study, Shenzhen University, Shenzhen, China. She is major in physics and her main research interests focus on the two-dimensional function materials such as metal–organic framework and electronics devices like memristor and transistors.

Guanglong Ding is currently an Assistant Professor at the State Key Laboratory of Radio Frequency Heterogeneous Integration, College of Electronics and Information Engineering, Shenzhen University, Shenzhen, PR China. He received his Ph.D. degree from China Agricultural University. His research interests include optoelectronic neuromorphic devices and heterogeneous integration, involving data storage, artificial synapse, and intelligent sensors.

Ye Zhou is currently a Distinguished Professor at the Institute for Advanced Study, Shenzhen University. He is a Fellow of the Royal Society of Chemistry (FRSC), a Fellow of the Institute of Physics (FInstP), and a Fellow of the Institution of Engineering and Technology (FIET). His research interests include nanostructured materials and nano-scale devices for neuromorphic electronics.

Su-Ting Han is currently an Associate Professor at the Department of Applied Biology and Chemical Technology, The Hong Kong Polytechnic University. She received her Ph.D. degree in physics and materials science from the City University of Hong Kong, Hong Kong SAR in 2014. From 2014 to 2016, she was a Postdoctoral Research Fellow at City University of Hong Kong. She joined Shenzhen University in 2016 as an Associate Professor (tenure track) and was promoted to Full Professor (tenured) in 2021 and then Distinguished Professor in 2022. She was a Visiting Professor in the Department of Electrical Engineering and Computer Science at the University of Michigan, US, in 2019. Her research interest includes flash memory, memristor, neuromorphic computing and in-sensor computing systems.